APPENDIX 6A

NEGATIVE PRESSURE DESIGN EVALUATION

6A.1 Primary Containment Negative Pressure Evaluation Analysis

The primary containment has been designed for a negative pressure of 3 psig. The worst case for this consideration results from the inadvertent actuation of the drywell sprays. During such a transient, cold spray water is passed through the drywell atmosphere, resulting in a drop in gas region temperature and a corresponding drop in gas region pressure.

This condition has been analyzed for the Hope Creek Generating Station. A peak negative pressure of -2.83 psig is obtained in the drywell. The maximum drywell to suppression chamber pressure differential is 2.61 psid.

To determine the temporal pressure and temperature of the primary containment, the conservation equation of mass and energy, along with the state equations for steam and nitrogen (air) noncondensable, are written for the drywell and suppression chamber regions. A schematic of these regions is presented in Figure 6A-1. The various terms for the mass and energy transfer mechanisms are also presented in this figure. The system of equations that were solved are presented below.

6a.2 Nomenclature

A	Flow area, ft^2.
c	Flow coefficient (see equation (6A-43)).
C_v	Flow coefficient.
E	Energy content, BTU.

g_c	Standard acceleration due to gravity. 32.174 ft/s^2.
h	Specific enthalpy, BTU/lbm.
k	Ratio of the principle specific heats.
K	Loss coefficient, defined by the equation $144 g_c \Delta P = \frac{1}{2} K \rho v^2$.
M	Mass, lbm.
$\dot{M}_{cond}$	Condensation rate on a water surface, lbm/s.
$\dot{M}_{drop}$	Dropout rate of mist droplets from a vapor region, lbm/s.
$\dot{M}_{evap}$	Evaporation rate from a water surface, lbm/s.
P	Pressure or partial pressure, psia.
R	Gas constant, lbf-ft/lbm-°R.
Q	Transferred energy, BTU.
T	Temperature, °F.
T_{in}	Temperature of spray at inlet to drywell.
T_{out}	Temperature of spray water at outlet from drywell.
T^*	Absolute temperature, °R.
t	Time, s.
u	Specific internal energy, BTU/lbm.

V	Volume, ft^3.

GREEK SYMBOLS

α	Factor in temperature equation (see text).
β	Factor in temperature equation (see text).
ξ	Heat exchanger effectiveness.
ϵ	Spray efficiency.
ν	Specific volume, ft^3/lbm.
ρ	Density, lbm/ft^3.

SUBSCRIPTS

a	Air.
AT	Atmosphere.
D	Drywell region.
f	liquid.
g	saturated vapor.
PV	Purge valve flow (from the reactor building to the suppression pool vapor region).
S	Suppression vessel liquid region (or the "suppression pool").
SV	Suppression vessel vapor region.

sw Service water.

VB Vacuum breaker flow (from the suppression pool vapor region to the drywell region).

6A.3 Analytical Assumptions

Dalton's Law of Partial Pressures is assumed to hold, so that the total pressure in a volume is equal to the sum of the partial pressures. The gas regions are assumed to be saturated, so that the partial pressure of the steam is always equal to its saturation pressure.

The spray water is assumed to enter the drywell at temperature T_{in}, and to immediately exit to the suppression pool liquid region at a temperature of T_{out}. These temperatures are related by the spray efficiency, which is defined as

$$\epsilon = \frac{T_{in} - T_{out}}{T_{in} - T_D} \qquad (6A\text{-}1)$$

This functional correlation is determined in the work of Reference 1 and is illustrated in Figure 6A-2.

The spray suction is assumed to be aligned to the suppression pool liquid region.

The drywell region is assumed to remain saturated, and any liquid that condenses as a consequence of this (M_{cond}) is assumed to mix with the spray flow (and so immediately enter the suppression pool liquid region at a temperature of T_{out}).

The vacuum breaker flow of steam and air is determined from the pressures of the suppression vessel vapor region and the drywell region, using a flow coefficient that varies according to the valve position.

The suppression vessel vapor region is assumed to be saturated, and any liquid that condenses as a consequence of this (M_{drop}) is assumed to form as a mist in the vapor region (so that the vapor region receives the latent heat) and then to fall into the liquid region at a temperature of T_{SV}.

The interface between the liquid and vapor regions in the suppression vessel is assumed to transfer heat and mass through the simultaneous processes of evaporation (M_{evap}) and condensation (M_{cond}).

The energy required for evaporation is assumed to come entirely from the liquid region, and the steam is assumed to be formed and transferred to the vapor region at a temperature of T_S.

The energy liberated by condensation is assumed to go entirely to the liquid region, and the water is assumed to be formed and transferred to the liquid region at a temperature of T_{SV}.

The purge valve flow of steam and air is determined from the pressures of the atmosphere and the suppression vessel vapor region, using a flow coefficient that varies according to the valve position.

Any heat supplied from the equipment and structures in the drywell region as it is cooled is neglected.

6A.4 Analytical Models

6A.4.1 Drywell Region

A mass balance for the air in this region yields:

$$\frac{d(M_a)_D}{dt} = (\dot{M}_a)_{VB} \qquad \text{(6A-2)}$$

A mass balance for the water yields:

$$\frac{d(M_g)_D}{dt} = \left((\dot{M}_g)_{VB} + \dot{M}_{spray}\right)_{in} - \left(\dot{M}_{spray} + (\dot{M}_{cond})_D\right)_{out} \qquad \text{(6A-3)}$$

Also, the assumption of saturation implies that

$$(M_g)_D = \frac{V_D}{\nu_g(T_D)} \qquad \text{(6A-4)}$$

so that

$$\frac{d(M_g)_D}{dt} = -\frac{V_D}{\nu_g^2(T_D)}\frac{d\nu_g}{dT_D}\frac{dT_D}{dt} \qquad \text{(6A-5)}$$

From (6A-3) and (6A-5) we obtain the rate of condensation:

$$(\dot{M}_{cond})_D = (\dot{M}_g)_{VB} + \frac{V_D}{\nu_g^2(T_D)}\frac{d\nu_g}{dT_D}\frac{dT_D}{dt} \qquad \text{(6A-6)}$$

A balance of the total energy in the region yields:

$$\frac{dE_D}{dt} = \left(\dot{M}_{spray}h_f(T_{in}) + \dot{Q}_{VB}\right)_{in} - \left(\dot{M}_{spray}h_f(T_{out}) + \dot{M}_{cond}h_f(T_{out})\right)_{out} \qquad \text{(6A-7)}$$

Also,

$$E_D = (M_a)_D u_a(T_D) + (M_g)_D u_g(T_D) \tag{6A-8}$$

so that

$$\frac{dE_D}{dt} = (M_a)_D \frac{du_a}{dT_D}\frac{dT_D}{dt} + u_a(T_D)\frac{d(M_a)_D}{dt} + (M_g)_D \frac{du_g}{dT_D}\frac{dT_D}{dt} + u_g(T_D)\frac{d(M_g)_D}{dt} \tag{6A-9}$$

Hence the right hand side (RHS) of (6A-7) is equal to the RHS of (6A-9). Substituting from (6A-5) and (6A-6), and re-arranging gives

$$\alpha_D \frac{dT_D}{dt} = \beta_D \tag{6A-10}$$

where

$$\alpha_D = (M_a)_D \frac{du_a}{dT_D} + (M_g)_D \frac{du_g}{dT_D} + \frac{V_D}{v_g^2(T_D)}\frac{dv_g}{dT_D}\left(h_f(T_{out}) - u_g(T_D)\right) \tag{6A-11}$$

and

$$\beta_D = - u_a(T_D)\frac{d(M_a)_D}{dt} + \dot{M}_{spray}\left(h_f(T_{in}) - h_f(T_{out})\right) + \dot{Q}_{VB} - (\dot{M}_g)_{VB} h_f(T_{out}) \tag{6A-12}$$

6A.4.2 Suppression Vessel Vapor Region

Air mass balance:

$$\frac{d(M_a)_{SV}}{dt} = (\dot{M}_a)_{PV} - (\dot{M}_a)_{VB} \qquad \text{(6A-13)}$$

Steam mass balance:

$$\frac{d(M_g)_{SV}}{dt} = \left(\dot{M}_{evap} + (\dot{M}_g)_{PV}\right)_{in} - \left((\dot{M}_g)_{VB} + (\dot{M}_{cond})_{SV} + \dot{M}_{drop}\right)_{out} \qquad \text{(6A-14)}$$

Also

$$(M_g)_{SV} = \frac{V_{SV}}{\nu_g(T_{SV})} \qquad \text{(6A-15)}$$

so that

$$\frac{d(M_g)_{SV}}{dt} = \frac{-V_{SV}}{\nu_g^2(T_{SV})}\frac{d\nu_g}{dT_{SV}}\frac{dT_{SV}}{dt} + \frac{1}{\nu_g(T_{SV})}\frac{dV_{SV}}{dt} \qquad \text{(6A-16)}$$

Combining (6A-14) and (6A-16), and re-arranging gives:

$$\dot{M}_{drop} = \alpha_{drop}\frac{dT_{SV}}{dt} + \beta_{drop} \qquad \text{(6A-17)}$$

where

$$\alpha_{drop} = \frac{V_{SV}}{\nu_g^2(T_{SV})}\frac{d\nu_g}{dT_{SV}} \qquad \text{(6A-18)}$$

and

$$\beta_{drop} = \dot{M}_{evap} + (\dot{M}_g)_{PV} - (\dot{M}_g)_{VB} - (\dot{M}_{cond})_{SV} - \frac{1}{\nu_g(T_{SV})}\frac{dV_{SV}}{dt} \qquad \text{(6A-19)}$$

The energy balance for this region is

$$\frac{dE_{SV}}{dt} = \left(\dot{Q}_{PV} + \dot{M}_{evap}h_g(T_S)\right)_{in} - \left(\dot{Q}_{VB} + (\dot{M}_{cond})_{SV}h_g(T_{SV}) + \dot{M}_{drop}h_f(T_{SV})\right)_{out} \qquad \text{(6A-20)}$$

Also

$$E_{SV} = (M_a)_{SV}u_a(T_{SV}) + (M_g)_{SV}u_g(T_{SV}) \qquad \text{(6A-21)}$$

so that

$$\frac{dE_{SV}}{dt} = (M_a)_{SV}\frac{du_a}{dT_{SV}}\frac{dT_{SV}}{dt} + u_a(T_{SV})\frac{d(M_a)_{SV}}{dt} + (M_g)_{SV}\frac{du_g}{dT_{SV}}\frac{dT_{SV}}{dt} + u_g(T_{SV})\frac{d(M_g)_{SV}}{dt} \qquad \text{(6A-22)}$$

Combining (6A-20) and (6A-22), substituting from (6A-16) and (6A-17), and re-arranging gives, after some manipulation

$$\alpha_{SV}\frac{dT_{SV}}{dt} = \beta_{SV} \tag{6A-23}$$

where

$$\alpha_{SV} = (M_a)_{SV}\frac{du_a}{dT_{SV}} + (M_g)_{SV}\frac{du_g}{dT_{SV}} + \alpha_{drop}\left(h_f(T_{SV}) - u_g(T_{SV})\right) \tag{6A-24}$$

and

$$\begin{aligned}\beta_{SV} = {} & \dot{Q}_{PV} + \dot{M}_{evap}h_g(T_S) - \dot{Q}_{VB} - (\dot{M}_{cond})_{SV}h_g(T_{SV}) \\ & - \beta_{drop}h_f(T_{SV}) - u_a(T_{SV})\frac{d(M_a)_{SV}}{dt} - u_g(T_{SV})\frac{1}{v_g(T_{SV})}\frac{dV_{SV}}{dt}\end{aligned} \tag{6A-25}$$

6A.4.3 Suppression Vessel Liquid Region

The mass balance is

$$\begin{aligned}\frac{dM_S}{dt} &= \left((\dot{M}_{cond})_{SV} + (\dot{M}_{cond})_D + \dot{M}_{spray} + \dot{M}_{drop}\right)_{in} - \left(\dot{M}_{evap} + \dot{M}_{spray}\right)_{out} \\ &= (\dot{M}_{cond})_{SV} + (\dot{M}_{cond})_D + \dot{M}_{drop} - \dot{M}_{evap}\end{aligned} \tag{6A-26}$$

The volume of the region is

$$V_S = M_s v_f(T_S) \tag{6A-27}$$

so that

$$\frac{dV_S}{dt} = M_S \frac{dv_f}{dT_S}\frac{dT_S}{dt} + v_f(T_S)\frac{dM_S}{dt} \tag{6A-28}$$

and, because the liquid and vapor regions share a constant volume,

$$\frac{dV_{SV}}{dt} = -\frac{dV_S}{dt} \tag{6A-29}$$

The energy balance is

$$\frac{dE_S}{dt} = (\dot{M}_{cond})_{SV} h_g(T_{SV}) + (\dot{M}_{cond})_D h_f(T_{out}) + \dot{M}_{spray}\left(h_f(T_{out}) - h_f(T_S)\right) + \dot{M}_{drop} h_f(T_{SV}) - \dot{M}_{evap} h_g(T_S) \tag{6A-30}$$

Also

$$E_S = M_s u_f(T_S) \tag{6A-31}$$

so

$$\frac{dE_S}{dt} = M_S \frac{du_f}{dT_S}\frac{dT_S}{dt} + u_f(T_S)\frac{dM_S}{dt} \qquad \text{(6A-32)}$$

Combining (6A-30) and (6A-32) gives

$$\alpha_S \frac{dT_S}{dt} = \beta_S \qquad \text{(6A-33)}$$

where

$$\alpha_S = M_S \frac{du_f}{dT_S} \qquad \text{(6A-34)}$$

and

$$\beta_S = (\dot{M}_{cond})_{SV} h_g(T_{SV}) + (\dot{M}_{cond})_D h_f(T_{out}) + \dot{M}_{spray}\left(h_f(T_{out}) - h_f(T_S)\right) + \dot{M}_{drop} h_f(T_{SV}) - \dot{M}_{evap} h_g(T_S) - u_f(T_S)\frac{dM_S}{dt} \qquad \text{(6A-35)}$$

6A.4.4 Evaporation and Condensation

The evaporation and condensation rates in the suppression vessel are modelled using the kinetic theory of condensation from Reference 2. This results in the following expressions

$$(\dot{M}_{cond})_{SV} = 144\,\Gamma\,A_{cond}\sqrt{\frac{g_c}{2\pi R_g}}\,\frac{(P_g)_{SV}}{\sqrt{T^*_{SV}}} \qquad \text{(6A-36)}$$

$$\dot{M}_{evap} = 144\,A_{cond}\sqrt{\frac{g_c}{2\pi R_g}}\,\frac{(P_g)_S}{\sqrt{T^*_S}} \qquad \text{(6A-37)}$$

where

$$\Gamma = -w\sqrt{\pi}\,[1+erf(w)] - e^{-w^2} \qquad \text{(6A-38)}$$

$$w = \frac{-v_g(T_S)\left(\dot{M}_{evap} + (\dot{M}_{cond})_{SV}\right)}{A_{cond}\sqrt{2\,g_c\,R_g\,T^*_{SV}}} \qquad \text{(6A-39)}$$

and the erf function is defined as

$$erf(w) = \frac{2}{\sqrt{\pi}}\int_0^w e^{-z^2}dz \qquad \text{(6A-40)}$$

6A.4.5 Vacuum Breaker and Purge Valve Flows

The flow coefficients of these flow paths depend on the degree to which the valves are open. This, in turn, depends on the differential pressure across them, and their opening characteristics.

Given the flow coefficient for the vacuum breaker, the flow rate from the suppression vessel vapor region to the drywell is calculated using the non-choked adiabatic flow equations for a perfect gas (Ref 3) as follows.

$$\dot{M}_{VB} = c_{VB} A_{VB} 144 P_D \sqrt{2 g_c \frac{\rho_{SV}}{144 P_{SV}} \frac{k_{SV}}{k_{SV}-1} \left(\frac{P_{SV}}{P_D}\right)^{\frac{k_{SV}-1}{k_{SV}}} \left\{ \left(\frac{P_{SV}}{P_D}\right)^{\frac{k_{SV}-1}{k_{SV}}} - 1 \right\}} \qquad (6A\text{-}41)$$

(Compared to the equation in Ref 3 the denominator, which has a value less than one, has been neglected. This results in conservatively lower flow rates).

The flows are never expected to become choked, because choked flow requires a pressure ratio of less than about 0.57 (Ref 3). The smallest pressure ratios expected are of order (14.7-3)/14.7 = 0.79. Despite this expectation, a check has been included in the coding to make sure that choked conditions are never calculated to exist.

For a small pressure drop, equation (6A-41) can be manipulated into the form

$$144 g_c \Delta P = \left(\frac{1}{c_{VB}^2}\right) \frac{1}{2} \rho_{SV} \left(\frac{\dot{M}_{VB}}{\rho_{SV} A_{VB}}\right)^2 \qquad (6A\text{-}42)$$

which serves to define the flow coefficient c_{VB}. In terms of the usual loss coefficient K, it can be seen that

$$c_{VB} = \frac{1}{\sqrt{K_{VB}}} \qquad \text{(6A-43)}$$

The mass fractions of air and steam in this flow are assumed to be the same as the mass fractions in the suppression vessel vapor region.

The energy transferred by this flow is

$$\dot{Q}_{VB} = (\dot{M}_a)_{VB} h_a(T_{SV}) + (\dot{M}_g)_{VB} h_g(T_{SV}) \qquad \text{(6A-44)}$$

Exactly the same equations are used for the flow from the atmosphere to the suppression vessel through the purge valves. The mass fraction of steam in the atmosphere is required, and this is obtained from the specified value for the relative humidity, which is defined as

$$RH = \frac{(P_g)_{AT}}{(P_g)_{sat}} \qquad \text{(6A-45)}$$

For any given volume of the atmosphere, the mass of vapor in that volume is

$$(M_g)_{AT} = RH\, \rho_g(T_{AT})\, V_{AT} \qquad \text{(6A-46)}$$

Hence the mass fraction of steam is

$$\frac{(M_g)_{AT}}{M_{AT}} = RH \frac{\rho_g(T_{AT})}{\rho_{AT}} \qquad (6A\text{-}47)$$

6A.4.6 RHR Heat Exchanger

The water for the spray is drawn from the suppression vessel pool and passed through a heat exchanger. The spray temperature is modelled as

$$T_{spray} = T_S - \xi \frac{\min(\dot{M}_{spray}, \dot{M}_{sw})}{\dot{M}_{spray}} (T_S - T_{sw}) \qquad (6A\text{-}48)$$

where ξ is a specified efficiency for the heat exchanger.

6A.5 Solution Technique

Equations (6A-2), (6A-10), (6A-13), (6A-23), (6A-26), (6A-28), and (6A-33) specify the derivatives of the mass of air in the drywell, the temperature of the drywell, the mass of air in the suppression vessel, the temperature of the vapor in the suppression vessel, the mass of water in the suppression vessel, and the temperature of the water in the suppression vessel. Together, these quantities completely define the conditions in the containment. Given a suitable set of initial conditions, these differential equations can be integrated to give a transient solution.

A fourth order Runge-Kutta algorithm was used to perform the integration.

6A.6 Assumptions and Initial Conditions

The concern is that the primary containment pressure will become too low. Therefore the following assumptions, which tend to reduce the containment pressure, are conservatisms.

- The transfer of sensible heat from the equipment and structures to the drywell gas region is neglected, thereby reducing the energy (and so pressure) in this region.

- Re-evaporation of the condensed drywell steam is disallowed, thereby reducing the mass (and so pressure) in this region.

- A large volume for the drywell region is maintained by transferring condensed steam mass directly to the suppression pool.

- The cold leg of the residual heat removal (RHR) heat exchanger is from the hot leg of the Safety Auxiliaries Cooling System. Therefore, the minimum coolant temperature of 65 °F can be higher than the suppression pool temperature. Since it is conservative to neglect any possible heating of the containment spray due to the SACS flow, the RHR heat exchanger effectiveness is set to zero for this analysis.

Two sets of initial conditions will be examined. One set will be the nominal operating conditions of the containment. The other will be chosen to maximize the depressurization transient.

The presence of any noncondensables in the drywell tends to hold up the depressurization of this region following spray actuation. Thus, to maximize the depressurization, a condition is postulated wherein a small break occurs within the drywell, serving to pressurize this region and drive all the noncondensables to the suppression chamber gas space. This sets the initial pressure distribution (and, along with the assumptions regarding saturated conditions for

the steam phase, the temperature distribution) for all three regions: drywell, suppression chamber gas region, and suppression pool.

These conditions will be referred to as "post-break" conditions.

The following sections present both sets of initial conditions, and of the valve properties used. The results are presented in Table 6A-1.

6A.6.1 Nominal Conditions

At nominal conditions the primary containment is assumed to be at 14.2 psia, with a drywell temperature of 150°F and a suppression vessel temperature of 60°F. The drywell volume is 169,000 ft^3, and the water in the suppression vessel is assumed to occupy 122,000 ft^3 of the total 255,500 ft^3, leaving 133,500 ft^3 for the steam.

6A.6.2 Post-break Initial Conditions

It is postulated that a small break has driven all of the nitrogen from the drywell into the suppression vessel, which remains at 60°F.

6A.6.3 Valve Properties

Each suppression chamber to Reactor Building vacuum breaker is installed in series with a butterfly purge valve. Since the purge valves have a higher opening pressure, and take longer to open, the flow will be controlled by the purge valves and not the vacuum breakers. The following table compares these valve parameters to illustrate this.

	Vacuum breaker	Purge valve
Opening pressure (psid)	0.2 (assumed)	0.25
Opening time (s)	0.1 (assumed)	15

Once the opening pressure for the purge valve is exceeded, the valve disc angle is assumed to increase linearly to 90°. Once the pressure differential falls below 0.25 psid, the purge valve is assumed take 5 seconds to close. Closing times in excess of 5 seconds will not adversely affect the calculated peak differential pressures.

6A.7 Determination of Worst Case

The worst case of inadvertent spray actuation was determined by running a suite of cases based on a single valve failure. The suite included every combination of the following conditions.

- Failure of a single suppression chamber to drywell vacuum breaker valve *or* failure of a single suppression chamber to Reactor Building purge valve. (The failed valves are assumed to remain closed.)

- Activation of a single spray loop *or* activation of two spray loops.

- Nominal initial conditions *or* post-break initial conditions.

As a check that the time integration was not introducing errors, one transient was repeated with a timestep of 0.001 sec instead of 0.01 sec. The results were identical to the precision printed.

A tabulation of the main cases analyzed, and their maximum pressure differences, is presented in Table 6A-2.

The maximum negative drywell pressure achieved is predicted to be -2.83 psig. This is achieved in the case where two sprays are activated from nominal conditions, and one purge valve fails shut. Some graphical results from this case are presented in Figure 6A-3 and Figure 6A-4.

The maximum pressure differential between the drywell and the suppression vessel is predicted to be 2.61 psid. This is achieved in the case where two sprays are activated from post-break conditions, and one vacuum breaker fails shut. Some graphical results from this case are presented in Figure 6A-5 and Figure 6A-6.

6A.8 Conclusions

The conservative calculation methods presented here predict that the drywell pressure will not reach its design limit of -3 psig.

They also indicate that the drywell to suppression vessel pressure differential will not reach the design limit of 3 psid.

6A.9 References

6A-1 Takashi Tagami, "Interim Report on Safety Assessment and Facility Establishment (SAFE) Project,' February 28, 1966, Hitachi Ltd., Tokyo, Japan.

6A-2 Donal J. Wilhelm, "Condensation of Metal Vapor-Mercury and the Kinetic Theory of the Condensation", ANL-6984, October 1964.

6A-3 "Marks' Standard Handbook for Mechanical Engineers", Ninth Edition, Eugene A. Avallone and Theodore Baumeister III.

TABLE 6A-1

Initial and Boundary Conditions

	Nominal	Post-break
Drywell		
Volume (ft3)	169000	
Temperature (F)	150.000	244.257
Pressure (psia)	14.200	26.952
Steam partial pressure (psia)	3.719	26.952
Nitrogen partial pressure (psia)	10.481	0.000
Nitrogen mass (lb)	7578.835	0.000
Spray rate (gpm/train)	10000	
Spray rate (lb/s-train)	1391	
Suppression chamber		
Vapor volume (ft3)	133500	
Liquid volume (ft3)	122000	
Pressure (psia)	14.200	25.509
Temperature (F)	60.000	60.000
Steam partial pressure (psia)	0.258	0.258
Nitrogen partial pressure (psia)	13.942	25.251
Nitrogen mass (lb)	9343.573	16922.408
Liquid specific volume (ft3/lb)	0.016	
Depth of spargers (ft)	3.330	
Pressure to force water out of spargers (psi)	1.443	
Suppression pool free surface area (ft2)	10710	

TABLE 6A-1 (Cont)

Suppression Chamber to Drywell Vacuum Breakers	
Number of valve assemblies	7 or 8
Flow area per assembly (ft2)	1.85
Flow coefficient	0.63
Assumed lifting pressure (psid)	0.2
Assumed opening and closing time (s)	0.1
RHR System - Drywell Spray Mode	
Service water flow rate (gpm/train)	9000
Service water flow rate (lb/s-train)	1251
Heat exchanger effectiveness	0
Number of trains	1 or 2
Suppression chamber to Reactor Building Purge Valves	
Flow area per assembly (ft2)	1.85
Number of valve assemblies	1 or 2
Lifting pressure (psid)	0.25
Opening time (s)	15
Closing time (s)	5
Reactor Building Atmosphere	
Pressure (psia)	14.7
Temperature (°F)	60
Relative humidity (%)	50

TABLE 6A-2

Maximum Negative Pressure Inside Containment

	Largest Depressurization in Drywell (psig)	Largest Pressure Difference between Suppression Chamber and Drywell (psid)
1 Hx train		
7 Vacuum breakers	-1.72 (post-break)	0.70 (post-break)
2 Purge valves	-1.80 (from nominal)	0.28 (from nominal)
2 Hx train		
7 Vacuum breakers	-2.59 (post-break)	**2.61 (post-break)**
2 Purge valves	-2.60 (from nominal)	0.58 (from nominal)
2 Hx train		
8 Vacuum breakers	-2.79 (post-break)	2.05 (post-break)
1 Purge valves	**-2.83 (from nominal)**	0.42 (from nominal)
1 Hx train		
8 Vacuum breakers	-2.27 (post-break)	0.54 (post-break)
1 Purge valves	-2.34 (from nominal)	0.21 (from nominal)

TABLE 6A-3

COMPARISON OF SPRAY ACTUATION FOR SBA AND NORMAL OPERATION

Parameter	SBA	Normal Operation
Pressure, psia	14.696	14.696
Temperature, °F	163.3	150
Steam/Noncondensable Ratio	0.44	0.21

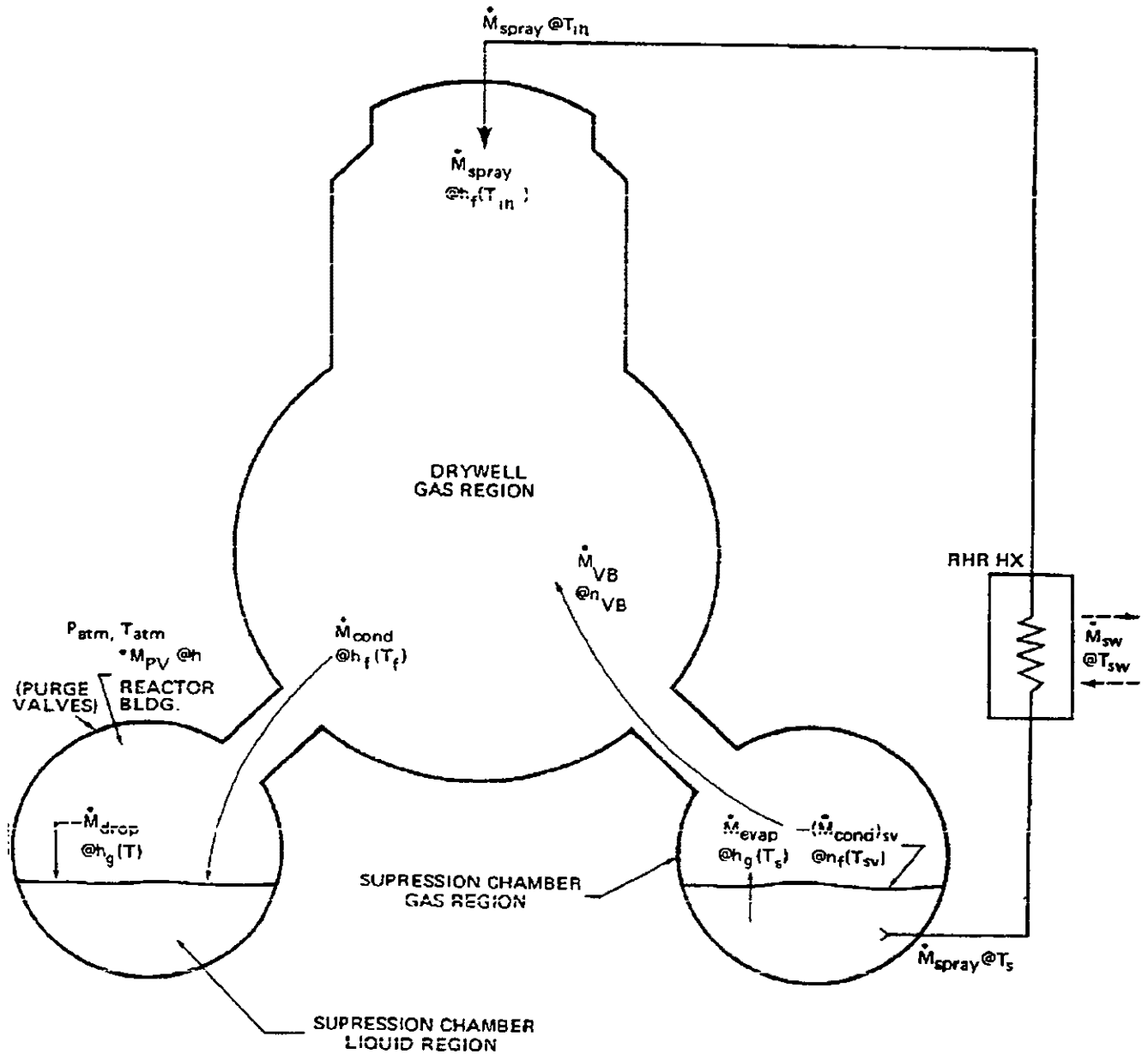

PUBLIC SERVICE ELECTRIC AND GAS COMPANY HOPE CREEK NUCLEAR GENERATING STATION	
SCHEMATIC FOR THE CALCULATION	
Updated FSAR Revision 7, December 29, 1995	Figure 6A-1

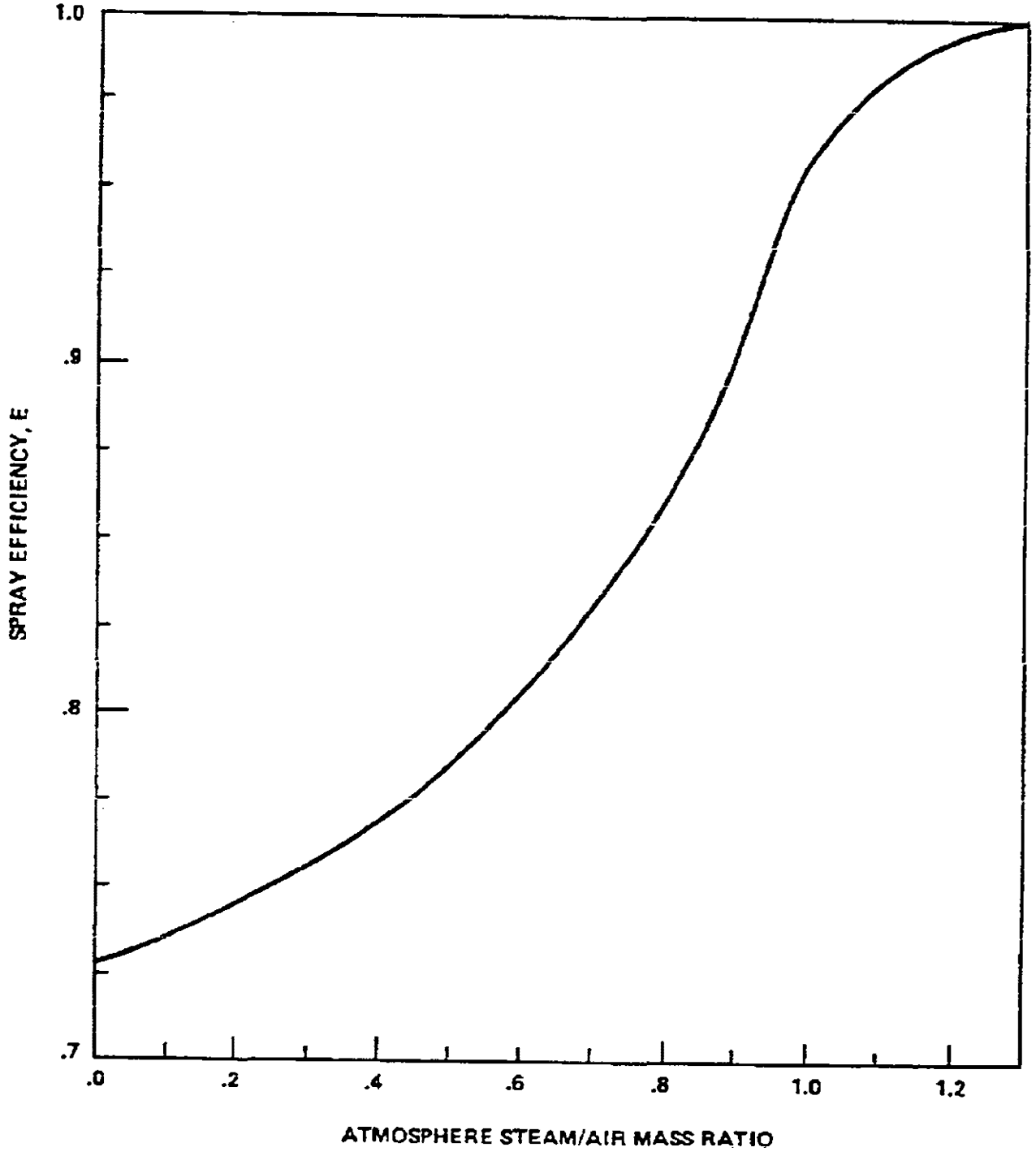

PUBLIC SERVICE ELECTRIC AND GAS COMPANY HOPE CREEK NUCLEAR GENERATING STATION
SPRAY EFFICIENCY CURVE
Updated FSAR Revision 7, December 29, 1995 — Figure 6A-2

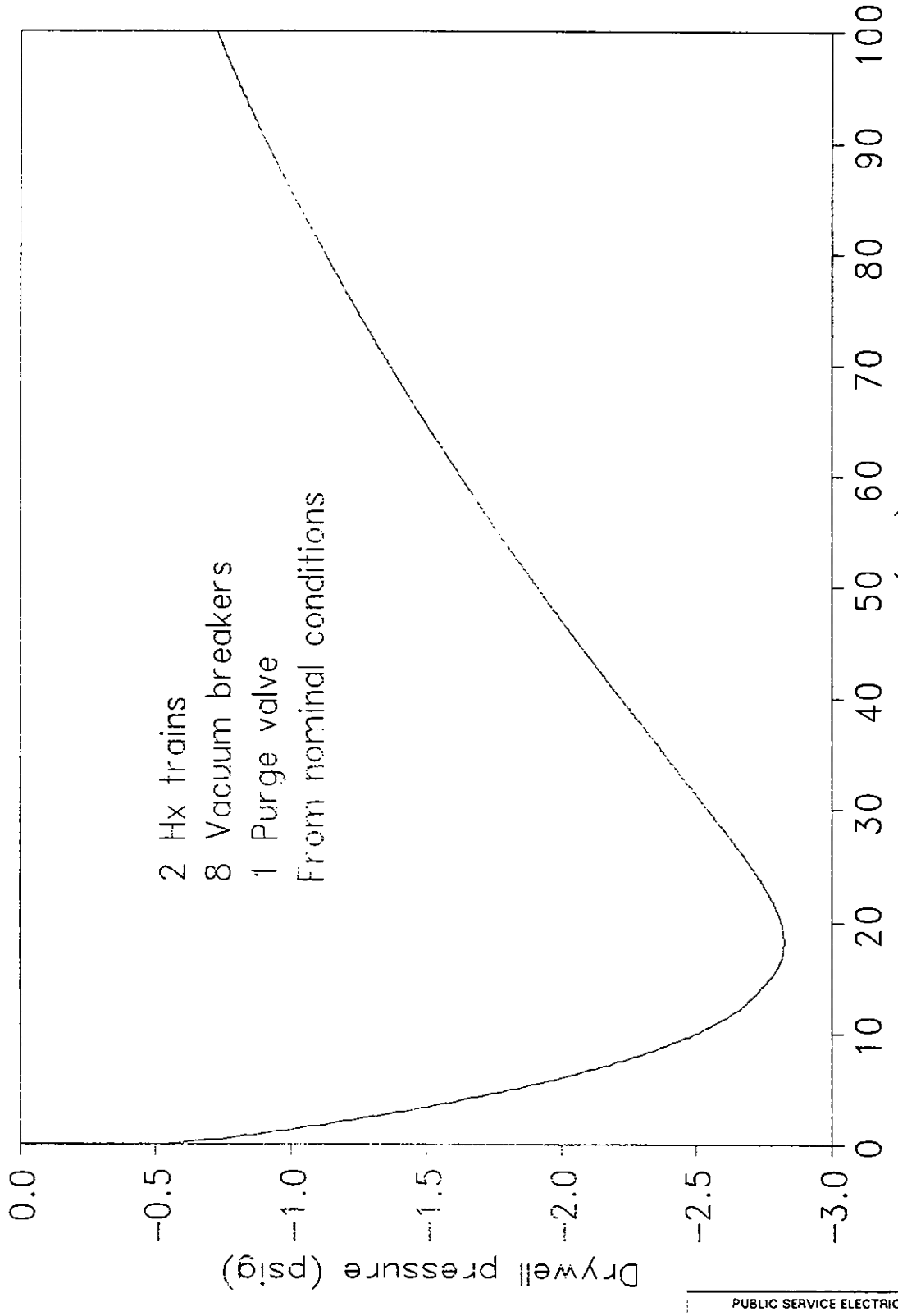

PUBLIC SERVICE ELECTRIC AND GAS COMPANY
HOPE CREEK NUCLEAR GENERATING STATION

DRYWELL PRESSURE WITH FAILED PURGE VALVE

Updated FSAR
Revision 7, December 29, 1995 Figure 6A-3

Figure 6A-3. Drywell pressure with failed purge valve.

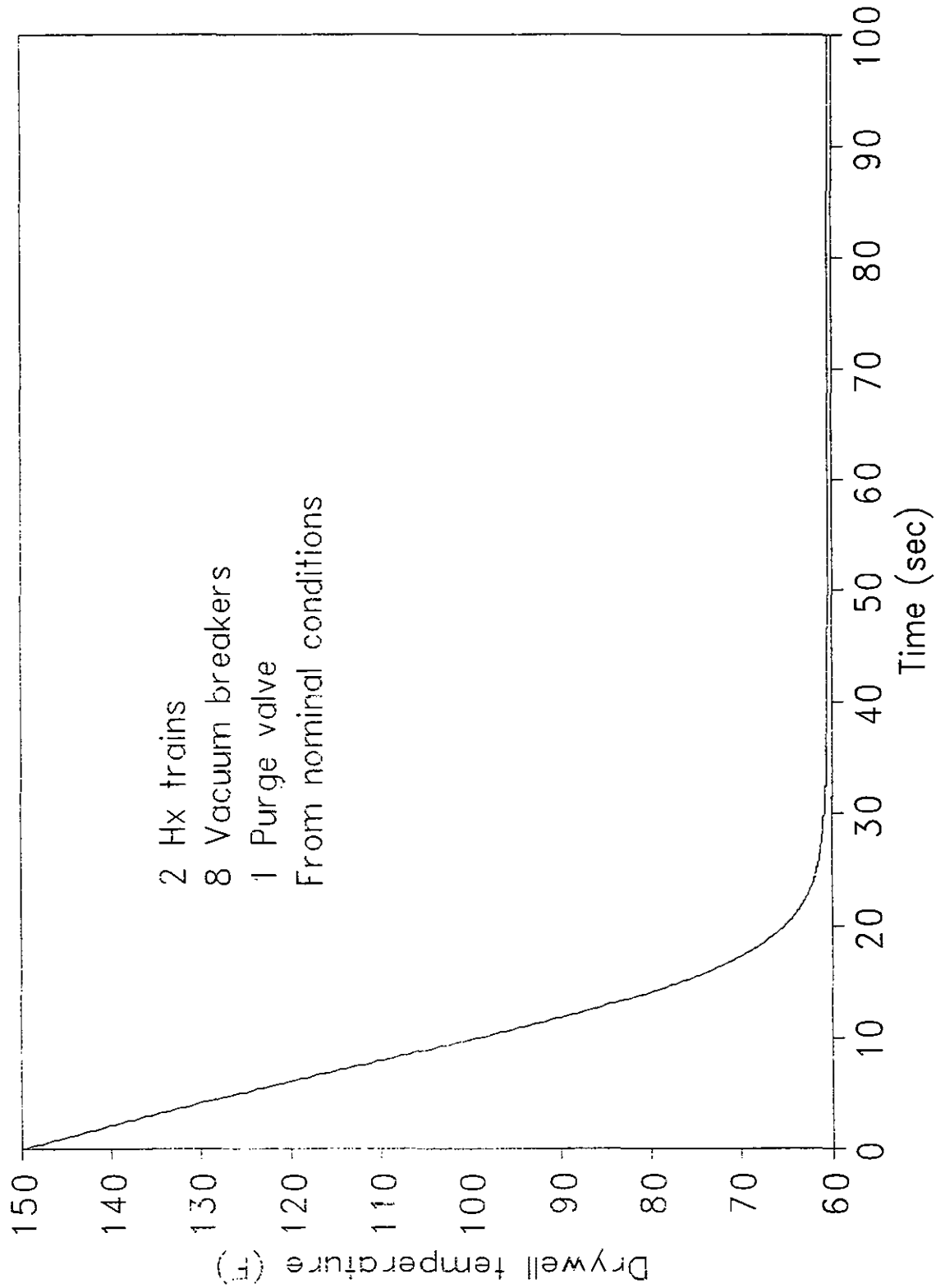

PUBLIC SERVICE ELECTRIC AND GAS COMPANY
HOPE CREEK NUCLEAR GENERATING STATION

DRYWELL TEMPERATURE WITH FAILED PURGE VALVE

Updated FSAR
Revision 7, December 29, 1995

Figure 6A-4

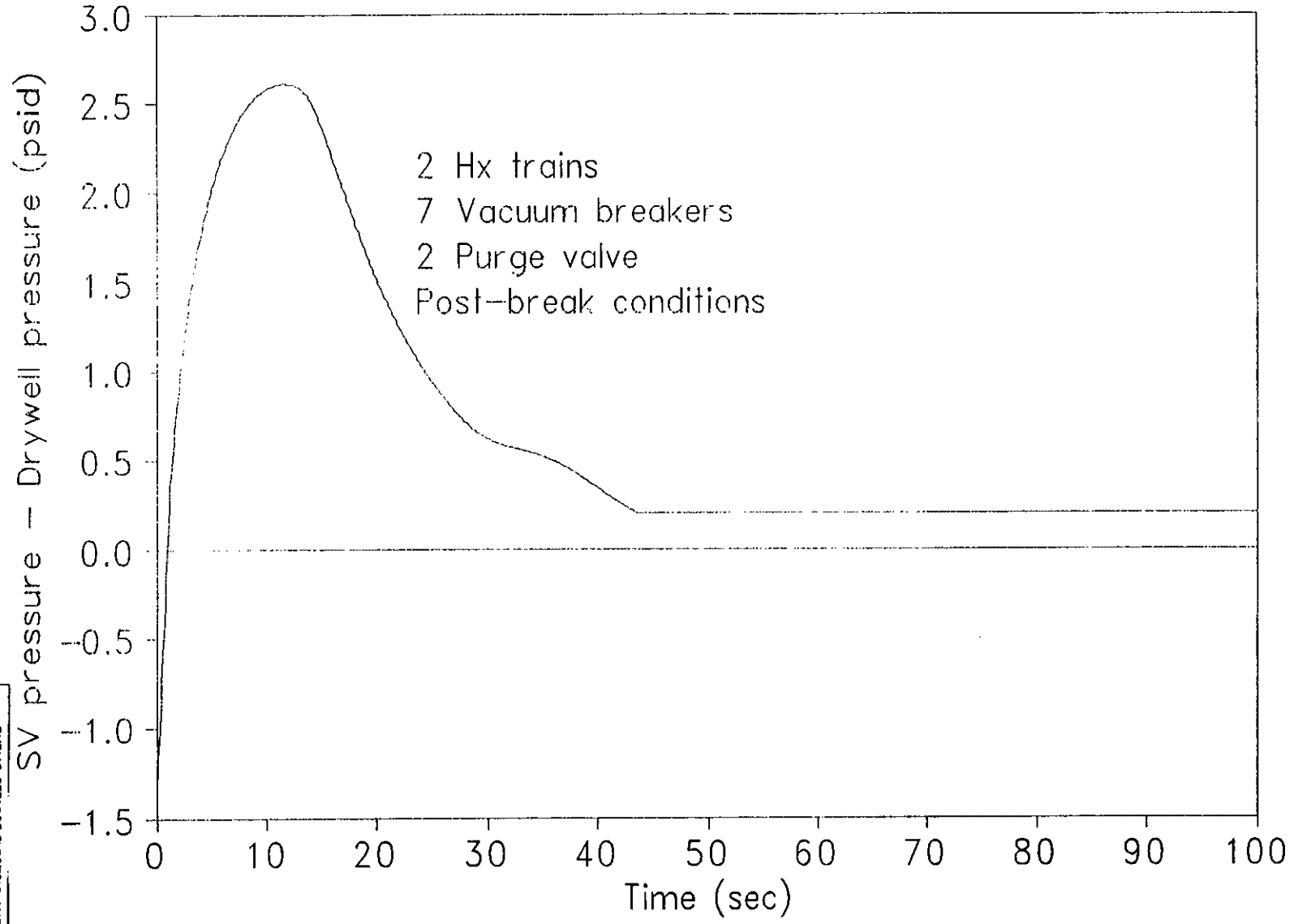

PUBLIC SERVICE ELECTRIC AND GAS COMPANY
HOPE CREEK NUCLEAR GENERATING STATION

DIFFERENTIAL PRESSURE WITH FAILED VACUUM BREAKER

Updated FSAR
Revision 7, December 29, 1995

Figure 6A-5

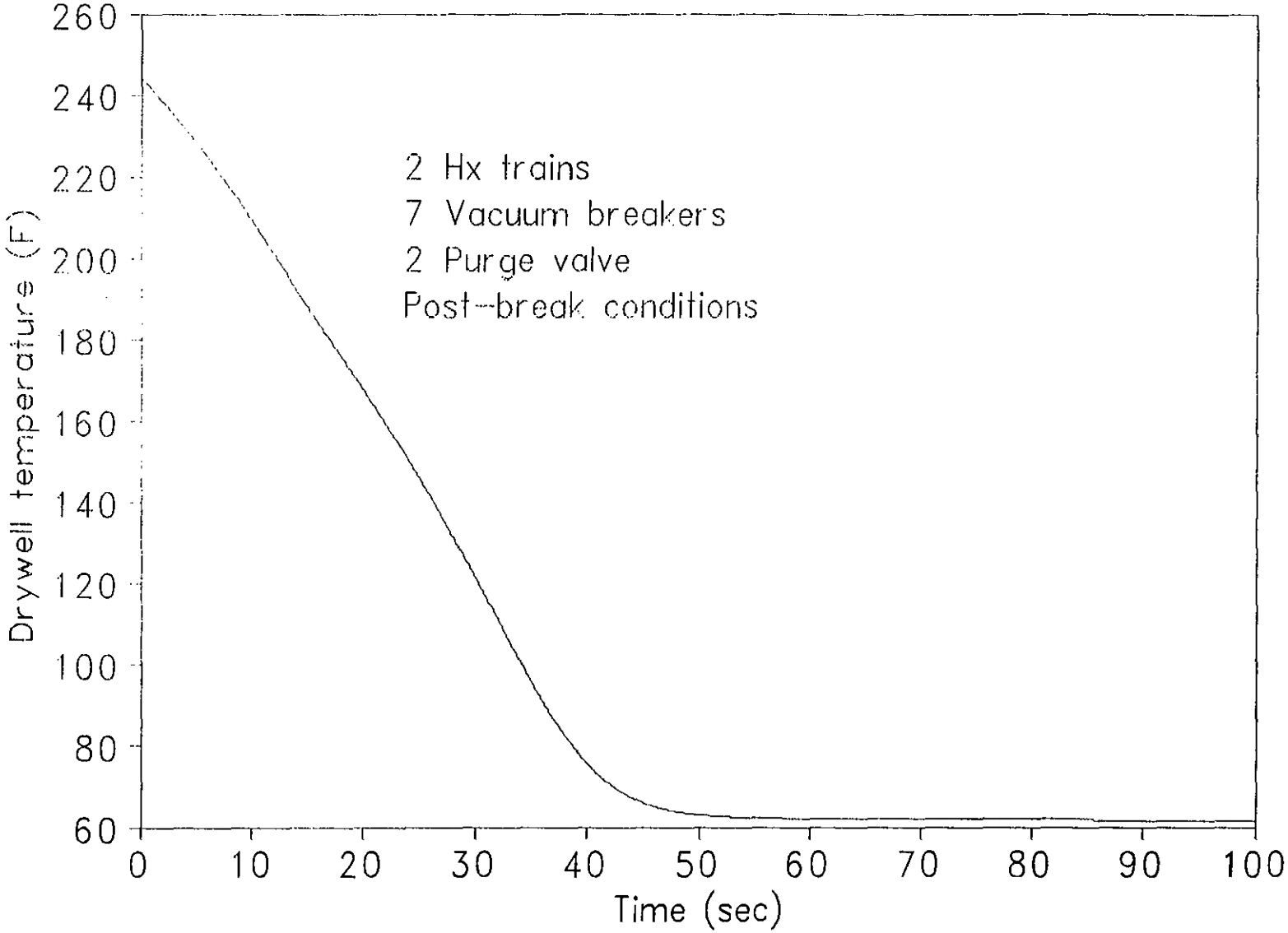

PUBLIC SERVICE ELECTRIC AND GAS COMPANY
HOPE CREEK NUCLEAR GENERATING STATION

DIFFERENTIAL TEMPERATURE WITH FAILED VACUUM BREAKER

Updated FSAR
Revision 7, December 29, 1995

Figure 6A-6

APPENDIX 6B *

SUBCOMPARTMENT DIFFERENTIAL PRESSURE CONSIDERATIONS

6B.1 INTRODUCTION

Differential pressure analyses were performed for the reactor pressure vessel (RPV) shield annulus and the drywell head region. The shield annulus analysis is done in two parts. The first part is a mechanistic analysis to determine the loads on the RPV and its supports, internals, and attached piping. The second part is a more conservative, nonmechanistic, analysis that is used only to check the adequacy of the structural design of the shield wall and its supports. The RPV shield annulus is 48.95-feet high and 1.833-feet wide at the top.

6B.1.1 Vessel Annulus Pressurization

The estimation of mass and energy release is based on the guidelines set forth in GE's Generic Annulus Pressurization Mass Energy Release Methodology (MFN178-78, transmitted as a letter from E. D. Fuller, GE, to D. F. Ross, NRC, on May 2, 1978), and Technical Description Annulus Pressurization Load Adequacy Evaluation (NEDO-24548/78 NED 302). Table 6B-1 presents the recirculation outlet line mass and energy release data estimated by applying the NEDO-24548 method of combining blowdown data calculated from finite and instantaneous break opening time approaches.

The mass flux and area, as functions of time, that are used for each side of the break are tabulated in Table 6B-2. In addition, pertinent physical parameters used in the blowdown estimation are also listed in the table. (Note that the nomenclature used here is the same as that in the previously mentioned GE documents). The break is postulated to occur at the nozzle safe end to pipe weld. Because the break is located within the shield wall

---

* See Appendix 3C for descriptions on the reactor asymmetric load evaluation for the MELLLA conditions.

penetration 50 percent of the blowdown is assumed to be released into the annulus with the remaining 50 percent to be vented to the containment atmosphere. Subsequent to this analysis, a flow diverter was added to the shield wall penetration, thus reducing the portion of the blowdown entering the annulus to 25 percent. Figure 6B-1 shows the flow obstruction and its location relative to the break. The subcompartment pressures calculated with the flow diverter in place are substantially less than the originally calculated pressures presented here.

In addition to the analysis for the recirculation outlet line break in the annulus, similar analyses using the same methodology for blowdown rate estimation are performed for a postulated feedwater line break in the annulus. Table 6B-3 presents the mass and energy release rates generated by applying only the very conservative instantaneous break opening time method. No credit is taken for the feedwater pipe whip restraint to limit the break opening area. Also, it is conservatively assumed in the analyses that the full blowdown is completely released into the annulus. Mass flux, as a function of time and areas used for each side of the break, is presented in Table 6B-4. Some pertinent physical parameters are also noted in the table.

6B.1.2 Shield Wall Structural Adequacy

For the shield wall analysis, a nonmechanistic break equal in area to a double ended rupture of a recirculation outlet line (4.1 square feet) is postulated. As an additional conservatism, the break is postulated to occur at three different locations in the annulus, one near the top (case A), one near the middle (case B), and one near the bottom (case C). The most severe loads on the shield wall and its supports resulted from cases B and C.

The mass and energy blowdown rates are calculated using the Moody Steady Slip Flow Model. For case B, this results in a constant mass release rate of 36,300 lbm/s at 514.24 Btu/lbm. For case C, the constant mass release rate is 37,000 lbm/s at 514.21 Btu/lbm.

6B.1.3 RHR Head Spray Line Break

The head spray pipe has been removed. However, the analysis of a postulated head spray line break discussed in Appendix 6B bounds the effects of an RPV head vent line break. Therefore, the discussion regarding a postulated head spray line break is still valid.

In considering the drywell head region, the maximum blowdown rate results from a break in the residual heat removal (RHR) head spray line. The blowdown mass and energy release rates for this line are calculated using Moody critical flow of 2060 lbm/s-ft^2 and an enthalpy of 1191.8 Btu/lbm. Table 6B-5 shows the blowdown rate for a 6-inch schedule 80S line break with an effective break area of 0.181 ft^2. Since this is the largest line that could pressurize the drywell head region, this postulated break is chosen for analysis.

The RPV shield annulus differential pressure calculation was performed by the computer code COPDA, whose computational procedure and analytical techniques are described in Reference 6B-1. These adjusted pressures are combined with the other appropriate loads, e.g., seismic and jet impingement to develop design loads for the affected structures and components. Subcompartment venting is used to ensure that the differential pressures developed will remain within the structural capability of component walls.

6B.2 BIOLOGICAL SHIELD ANNULUS SUBCOMPARTMENT MODELING PROCEDURES AND ANALYSIS

Two analyses of the pressure distribution around the reactor pressure vessel (RPV) after a feedwater line break and a recirculation outlet line break were performed. The general layout of the shield annulus is shown on Figure 6B-2. Figures 6B-3a and 6B-3b are schematics of the RPV shield annulus model. The model consists of six major levels. Each level was subdivided into 12 30° segments to form a total of 72 nodes inside the annulus plus an additional node for the remainder of the drywell.

In general, the arrangement of the pipes in the annulus determines the most representative level division, since the pipes constitute the only significant flow restrictions. This 73-pressure node

model is considered sufficiently detailed to conservatively predict the maximum pressures on the compartment structure. Therefore, a nodalization sensitivity study is not needed.

For the purpose of determining peak pressure in the reactor vessel shield annulus, all insulation was assumed to move flush against the biological shield wall while still maintaining its original thickness. The volume of the insulation was excluded from the net volume of each subcompartment, and the projected area of the insulation that blocks the venting path was also excluded from the free venting area used in the analysis.

The major vent path to the drywell atmosphere is through the top of the biological shield annulus. Venting through the shield wall is allowed only through the ventilation duct openings at the lower section of the shield wall.

Initial conditions used in this analysis were 15.45 psia, 135°F, and 30 percent relative humidity.

Tables 6B-6 and 6B-7 give the subcompartment volumes, flow areas, L/A ratio, and flow coefficients (including origins) used in this analysis.

The resultant pressure distributions are shown on Figure 6B-4 for the recirculation outlet line break, Figure 6B-5 for the feedwater line break, Figure 6B-6 for shield wall structure case B, and Figure 6B-7 for shield wall structure case C. Additionally, the load forcing functions, which include both peak and transient loadings on the RPV and the reactor shield wall, are presented on Figures 6B-8 and 6B-9 for the recirculation outlet line break, and on Figures 6B-10 and 6B-11 for the feedwater line break. This forcing function represents the time dependent resultant force on the structure, and originates from the vector sum of the product of compartment pressure and area for each of the 72 geometry nodes used to represent the surface.

The locations of the center of each node are given in Table 6B-8. The components of these nodal areas are calculated in the following manner:

$$(Ax) = R\ H\ (\mathrm{Sin}\theta_1 - \mathrm{Sin}\theta_2).$$

$$(Ay) = R\ H\ (\mathrm{Cos}\theta_2 - \mathrm{Cos}\theta_1).$$

where:

R = radius of the ith geometry node, in.
H = height of the ith geometry node, in.
θ_1 = starting angle (degrees) for ith geometry node
θ_2 = ending angle (degrees) for ith geometry node

Therefore, the force generated by a pressure, P, acting on a nodal area A has the following components:

$$(Fx) = P\ (Ax)$$

$$(Fy) = P\ (Ay)$$

The compartment pressure transients resulting from a break in the reactor shield annulus generate a nodal force distribution over exposed surfaces. The resultant of this nodal force distribution is presented on Figures 6B-8 through 6B-11. There are no external moments generated by this pressure response. Any moments would result from the application of the external force distribution to a structural model. This would generate shear stresses (leading to internal moments) due to bending of the elements used to represent the structure as a result of the nonuniform load distribution. Further discussion of this result is contained in Section 3, where the application of these annulus pressurization results is described in detail.

NOTE: The RHR head spray line has been removed from the RPV. However, this analysis is still valid as the postulated head spray line break bounds the effects of an RPV head vent line break in the drywell head region.

A pressure analysis of the drywell head region for a postulated head spray line break was performed. The effects of a 6-inch residual heat removal (RHR) head spray line break bound those of a 2-inch RPV head vent line, which is the only other line that runs through the drywell head region.

Figure 6B-12 illustrates the basic arrangement of the head region. Venting from the head region is accomplished through ventilation openings as shown on Figure 6B-12 and a manhole opening.

To determine the peak pressure in the drywell head, all insulation was assumed to remain in place. Initial conditions of 15.45 psia, 135°F, and 30 percent relative humidity were used in this analysis.

The maximum pressure in the drywell head region is 26.7 psia and occurs approximately 1.0 second after the head spray line break. Considering the containment pressure to be atmospheric (no drywell air displaced into the suppression chamber), a drywell head to containment pressure differential of 11.3 psid occurs at approximately 1.0 second after the break.

The manufacturer's design differential pressure (between the drywell head and containment region) for the water seal plate is conservatively defined as 20.0 psid. For the refueling bellows, the manufacturer's design differential pressure is defined as 15.0 psid.

6B.4 REFERENCES

6B-1 "Subcompartment Pressure Analyses," BN-TOP-4, Revision 1, November 1977, Bechtel Power Corporation, San Francisco, California.

TABLE 6B-1

MASS AND ENERGY BLOWDOWN RATE - RECIRCULATION LINE BREAK

Time, s	Mass Flow, lbm/s	Enthalpy, Btu/lbm
0.0	0.0	544.5
0.00255	1201.0	544.5
0.00390	2402.0	544.5
0.00496	3603.0	544.5
0.00586	4804.0	544.5
0.00804	8407.0	544.5
0.00868	9608.0	544.5
0.00924	10809.0	544.5
0.00980	12010.0	544.5
0.01180	16393.0	544.5
0.01380	20549.0	544.5
0.01580	24500.0	544.5
0.01780	28223.0	544.5
0.01880	30193.0	544.5
0.01910	30781.0	544.5
0.01911	11661.0	544.5
0.01980	12144.0	544.5
0.02180	13545.0	544.5
0.02580	16344.0	544.5
0.02980	19128.0	544.5
0.03380	21863.0	544.5
0.03780	24474.0	544.5
0.04180	26877.0	544.5
0.04680	29366.0	544.5
0.05480	31295.0	544.5
0.05890	32060.0	544.5
5.0	32060.0	544.5

TABLE 6B-2

RECIRCULATION OUTLET LINE BREAK BLOWDOWN MASS FLUX TIME HISTORY

Time, s	Mass Flux, $lbm/s/ft^2$	Effective Area, ft^2
Vessel Side		
0.0000	21260	0
0.00255	21260	0.02825
0.00390	21260	0.05649
0.00496	21260	0.08474
0.00586	21260	0.11298
0.00804	21260	0.19772
0.00868	21260	0.22596
0.00924	21260	0.25421
0.00980	21260	0.28246
0.01180	21260	0.38554
0.01380	21260	0.48328
0.01580	21260	0.57620
0.01780	21260	0.66376
0.01880	21260	0.71009
0.01910	21260	0.72392
0.01911	8055	0.72392
0.01980	8055	0.75382
0.02180	8055	0.84078
1.02580	8055	1.01453
1.02980	8055	1.18734
1.03380	8055	1.35711
1.03780	8055	1.51918
1.04180	8055	1.66834
1.04680	8055	1.82284

TABLE 6B-2 (Cont)

Time, s	Mass Flux, lbm/s/ft^2	Effective Area, ft^2
1.05480	8055	1.94258
0.05890	8055	1.99007
1.0	8055	3.538
Pipe Side		
0.0000	21260	0
0.00255	21260	0.02825
0.00390	21260	0.05649
0.00496	21260	0.08474
0.00586	21260	0.11298
0.00804	21260	0.19772
0.00868	21260	0.22596
0.00924	21260	0.25421
0.00980	21260	0.28246
0.01180	21260	0.38554
0.01380	21260	0.48328
0.01580	21260	0.57620
0.01780	21260	0.66376
0.01880	21260	0.71009
0.01910	21260	0.72392
0.01911	8055	0.72392
0.01980	8055	0.75382
0.02180	8055	0.84078
0.02580	8055	1.01453
0.02980	8055	1.18734
0.03380	8055	1.35711
0.03780	8055	1.51918
0.04180	8055	1.66834
0.04680	8055	1.82284

TABLE 6B-2 (Cont)

Time, s	Mass Flux, lbm/s/ft^2	Effective Area, ft^2
0.05480	8055	1.99007
0.05890	8055	0.442
1.0	8055	0.442

PERTINENT PHYSICAL PARAMETERS USED IN BLOWDOWN ESTIMATION

Minimum cross-sectional area between vessel and break = 3.538 ft^2
Minimum cross-sectional area between pipe and break = 0.442 ft^2
Pipe inside diameter at break location = 2.158 ft
Break area = 3.658 ft^2
Vessel pressure = 1053 psia
Vessel temperature = 546°F
Vessel enthalpy = 544.5 Btu/lbm
Saturation pressure = 1011.75 psia
Inventory length on vessel side = 3 ft
Inventory length on pipe side = 51 ft
Inventory volume on vessel side = 11 ft^3
Inventory volume on pipe side = 187 ft^3

TABLE 6B-3

REACTOR PRIMARY SYSTEM BLOWDOWN FLOW RATES AND FLUID ENTHALPY - FEEDWATER LINE BREAK

Time, s	Mass Flow, lbm/s	Enthalpy, Btu/lbm
0.0	0.0	403.5
0.0001	21180.0	403.5
0.0209	21180.0	403.5
0.0210	19480.0	403.5
5.0	19480.0	403.5

TABLE 6B-4

FEEDWATER LINE BREAK BLOWDOWN(1) MASS FLUX TIME HISTORY

Time, s	Mass Flux, lbm/s/ft^2	Effective Flow Area, ft^2
Vessel side		
0.0	0.0	0.00
	20000	0.3529
	20000	0.3529
	20000	0.2679
1.0	20000	0.2679
Supply pipe side		
0.0	0.0	0.00
	20000	0.7058
	20000	0.7058
	20000	0.7058
1.0	20000	0.7058

(1) Pertinent physical parameters used in blowdown estimation:
Maximum flow area = 1.0587 ft^2
Vessel pressure = 1155.3 psia
Vessel temperature = 425°F
Saturation pressure = 327 psia
Vessel enthalpy = 403.5 Btu/lbm
Feedwater specific volume = 0.01891 ft^3/lbm.

TABLE 6B-5

MASS AND ENERGY RELEASE RATE HEAD SPRAY LINE BREAK(1) (2)

Time, s	Steam Flow, lbm/s	Steam Enthalpy, Btu/lbm
0.0	746	1191.8
0.0030	746	1191.8
0.0031	373	1191.8
10.0	373	1191.8

(1) Head spray line break is based on a 6-inch schedule 80S pipe with Moody blowdown corresponding to 2060 lbm/s-ft^2; overall containment response is that of a "small break accident".

(2) Head spray line has been removed; however, head spray line break is still the bounding analysis for the drywell head region.

TABLE 6B-6

HCGS - COMPARTMENT VOLUMES USED IN REACTOR VESSEL SHIELD ANNULUS SUBCOMPARTMENT ANALYSIS

Compartment Number	Designation	Volume, ft^3
1	V1	72.0
2	V2	72.0
3	V3	72.0
4	V4	72.0
5	V5	72.0
6	V6	72.0
7	V7	72.0
8	V8	72.0
9	V9	72.0
10	V10	72.0
11	V11	72.0
12	V12	72.0
13	V13	95.0
14	V14	102.0
15	V15	101.0
16	V16	102.0
17	V17	102.0
18	V18	95.0
19	V19	95.0
20	V20	102.0
21	V21	101.0
22	V22	102.0
23	V23	102.0
24	V24	95.0
25	V25	79.0
26	V26	77.0
27	V27	77.0
28	V28	77.0

TABLE 6B-6 (Cont)

Compartment Number	Designation	Volume, ft^3
29	V29	77.0
30	V30	79.0
31	V31	79.0
32	V32	77.0
33	V33	77.0
34	V34	77.0
35	V35	77.0
36	V36	79.0
37	V37	80.0
38	V38	77.0
39	V39	80.0
40	V40	80.0
41	V41	77.0
42	V42	80.0
43	V43	80.0
44	V44	77.0
45	V45	80.0
46	V46	80.0
47	V47	77.0
48	V48	80.0
49	V49	103.0
50	V50	100.0
51	V51	103.0
52	V52	97.0
53	V53	95.0
54	V54	103.0
55	V55	103.0
56	V56	95.0
57	V57	97.0
58	V58	103.0
59	V59	100.0

TABLE 6B-6 (Cont)

Compartment Number	Designation	Volume, ft^3
60	V60	103.0
61	V61	46.0
62	V62	46.0
63	V63	46.0
64	V64	46.0
65	V65	46.0
66	V66	46.0
67	V67	46.0
68	V68	46.0
69	V69	46.0
70	V70	46.0
71	V71	46.0
72	V72	46.0
73	V73	169,000

TABLE 6B-7

HCGS - FLOW AREA AND COEFFICIENTS USED IN REACTOR VESSEL SHIELD ANNULUS SUBCOMPARTMENT ANALYSIS

Flow Paths	Flow Area, ft^2	K Factor	Description[1]	L/A ft^{-1}	Flow Coefficient
1-2	13.19	0.1008	30° turn	0.481	0.953
1-12	13.19	0.1008	30° turn	0.481	0.953
2-3	13.19	0.1008	30° turn	0.481	0.953
3-4	13.19	0.1008	30° turn	0.481	0.953
4-5	13.19	0.1008	30° turn	0.481	0.953
5-6	13.19	0.1008	30° turn	0.481	0.953
6-7	13.19	0.1008	30° turn	0.481	0.953
7-8	13.19	0.1008	30° turn	0.481	0.953
8-9	13.19	0.1008	30° turn	0.481	0.953
9-10	13.19	0.1008	30° turn	0.481	0.953
10-11	13.19	0.1008	30° turn	0.481	0.953
11-12	13.19	0.1008	30° turn	0.481	0.953
1-13	11.47	0.038	Friction	0.767	0.982
2-14	11.47	0.038	Friction	0.767	0.982

TABLE 6B-7 (Cont)

Flow Paths	Flow Area, ft^2	K Factor	Description(1)	L/A ft^{-1}	Flow Coefficient
3-15	11.47	0.038	Friction	0.767	0.982
4-16	11.47	0.038	Friction	0.767	0.982
5-17	11.47	0.038	Friction	0.767	0.982
6-18	11.47	0.038	Friction	0.767	0.982
7-19	11.47	0.038	Friction	0.767	0.982
8-20	11.47	0.038	Friction	0.767	0.982
9-21	11.47	0.038	Friction	0.767	0.982
10-22	11.47	0.038	Friction	0.767	0.982
11-23	11.47	0.038	Friction	0.767	0.982
12-24	11.47	0.038	Friction	0.767	0.982
1-73	0.85	0.41	Contraction	1.274	0.842
3-73	0.85	0.41	Contraction	1.274	0.842
4-73	0.85	0.41	Contraction	1.274	0.842
6-73	0.85	0.41	Contraction	1.274	0.842
7-73	0.85	0.41	Contraction	1.274	0.842
9-73	0.85	0.41	Contraction	1.274	0.842

TABLE 6B-7 (Cont)

Flow Paths	Flow Area, ft^2	K Factor	Description[1]	L/A ft^{-1}	Flow Coefficient
10-73	0.85	0.41	Contraction	1.274	0.842
12-73	0.85	0.41	Contraction	1.274	0.842
13-14	17.26	0.1008	30° turn	0.333	0.898
		0.14	Around pipe		
14-15	17.26	0.1008	30° turn	0.333	0.898
		0.14	Around pipe		
15-16	17.26	0.1008	30° turn	0.333	0.898
		0.14	Around pipe		
16-17	17.26	0.1008	30° turn	0.333	0.898
		0.14	Around pipe		
17-18	17.26	0.1008	30° turn	0.333	0.898
		0.14	Around pipe		
19-20	17.26	0.1008	30° turn	0.333	0.898
		0.14	Around pipe		
20-21	17.26	0.1008	30° turn	0.333	0.898
		0.14	Around pipe		
22-23	17.26	0.1008	30° turn	0.333	0.898
		0.14	Around pipe		
23-24	17.26	0.1008	30° turn	0.333	0.898
		0.14	Around pipe		

TABLE 6B-7 (Cont)

Flow Paths	Flow Area, ft^2	K Factor	Description(1)	L/A ft^{-1}	Flow Coefficient
21-22	17.26	0.1008	30° turn	0.333	0.898
		0.14	Around pipe		
13-24	12.67	0.1008	30° turn	0.421	0.671
		1.12	Around pipe		
18-19	12.67	0.1008	30° turn	0.421	0.671
		1.12	Around pipe		
13-25	6.434	1.3	Around pipe	1.177	0.624
		0.27	Around pipe		
18-30	6.434	1.3	Around pipe	1.177	0.624
		0.27	Around pipe		
19-31	6.434	1.3	Around pipe	1.177	0.624
		0.27	Around pipe		
24-36	6.434	1.3	Around pipe	1.177	0.624
		0.27	Around pipe		
14-26	7.81	0.27	Around pipe	0.968	0.806
		0.27	Around pipe		
16-28	7.81	0.27	Around pipe	0.968	0.806
		0.27	Around pipe		
17-29	7.81	0.27	Around pipe	0.968	0.806
		0.27	Around pipe		

TABLE 6B-7 (Cont)

Flow Paths	Flow Area, ft^2	K Factor	Description(1)	L/A ft^{-1}	Flow Coefficient
20-32	7.81	0.27	Around pipe	0.968	0.806
		0.27	Around pipe		
22-34	7.81	0.27	Around pipe	0.968	0.806
		0.27	Around pipe		
23-35	7.81	0.27	Around pipe	0.968	0.806
		0.27	Around pipe		
15-27	6.43	0.27	Around pipe	0.992	0.737
		0.27	Around pipe		
		0.30	Around pipe		
21-33	6.43	0.27	Around pipe	0.992	0.737
		0.27	Around pipe		
		0.30	Around pipe		
25-36	14.62	0.105	30° turn	0.429	0.951
30-31	14.62	0.105	30° turn	0.429	0.951
25-26	12.77	0.105	30° turn	0.451	0.889
		0.16	Around pipe		
26-27	12.77	0.105	30° turn	0.451	0.889
		0.16	Around pipe		
27-28	12.77	0.105	30° turn	0.451	0.889
		0.16	Around pipe		

TABLE 6B-7 (Cont)

Flow Paths	Flow Area, ft^2	K Factor	Description[1]	L/A ft^{-1}	Flow Coefficient
28-29	12.77	0.105 0.16	30° turn Around pipe	0.451	0.889
29-30	12.77	0.105 0.16	30° turn Around pipe	0.451	0.889
31-32	12.77	0.105 0.16	30° turn Around pipe	0.451	0.889
32-33	12.77	0.105 0.16	30° turn Around pipe	0.451	0.889
33-34	12.77	0.105 0.16	30° turn Around pipe	0.451	0.889
34-35	12.77	0.105 0.16	30° turn Around pipe	0.451	0.889
35-36	12.77	0.105 0.16	30° turn Around pipe	0.451	0.889
25-37	11.47	0.06	Friction	0.695	0.971
26-38	11.47	0.06	Friction	0.695	0.971
27-39	11.47	0.06	Friction	0.695	0.971
28-40	11.47	0.06	Friction	0.695	0.971
29-41	11.47	0.06	Friction	0.695	0.971

TABLE 6B-7 (Cont)

Flow Paths	Flow Area, ft^2	K Factor	Description(1)	L/A ft^{-1}	Flow Coefficient
30-42	11.47	0.06	Friction	0.695	0.971
31-43	11.47	0.06	Friction	0.695	0.971
32-44	11.47	0.06	Friction	0.695	0.971
33-45	11.47	0.06	Friction	0.695	0.971
34-46	11.47	0.006	Friction	0.695	0.971
35-47	11.47	0.06	Friction	0.695	0.971
36-48	11.47	0.06	Friction	0.695	0.971
37-38	13.02	0.105	30° turn	0.442	0.886
		0.16	Around LPCI		
		0.01	Around instrument		
41-42	13.02	0.105	30° turn	0.442	0.886
		0.16	Around LPCI		
		0.01	Around instrument		
43-44	13.02	0.105	30° turn	0.442	0.886
		0.16	Around LPCI		
		0.01	Around instrument		
47-48	13.02	0.105	30° turn	0.442	0.886
		0.16	Around LPCI		
		0.01	Around instrument		

TABLE 6B-7 (Cont)

Flow Paths	Flow Area, ft^2	K Factor	Description(1)	L/A ft^{-1}	Flow Coefficient
38-39	13.02	0.15	30° turn	0.442	0.951
40-41	13.02	0.15	30° turn	0.442	0.951
44-45	13.02	0.15	30° turn	0.442	0.951
46-47	13.02	0.15	30° turn	0.442	0.951
39-40	14.62	0.15	30° turn	0.429	0.951
45-46	14.62	0.15	30° turn	0.429	0.951
37-48	14.31	0.105 0.01	30° turn Around instrument	0.428	0.947
42-43	14.31	0.105 0.01	30° turn Around instrument	0.428	0.947
37-49	10.86	0.0788 0.06	Around instrument Friction	0.806	0.937
42-54	10.86	0.0788 0.06	Around instrument Friction	0.806	0.937
43-55	10.86	0.0788 0.06	Around instrument Friction	0.806	0.937
48-60	10.86	0.0788 0.06	Around instrument Friction	0.806	0.937
39-51	11.47	0.06	Friction	0.805	0.971

TABLE 6B-7 (Cont)

Flow Paths	Flow Area, ft^2	K Factor	Description(1)	L/A ft^{-1}	Flow Coefficient
40-52	11.47	0.06	Friction	0.805	0.971
45-57	11.47	0.06	Friction	0.805	0.971
46-58	11.47	0.06	Friction	0.805	0.971
38-50	8.27	1.075	Around LPCI	0.864	0.694
41-53	8.27	1.075	Around LPCI	0.864	0.694
44-56	8.27	1.075	Around LPCI	0.864	0.694
47-59	8.27	1.075	Around LPCI	0.864	0.694
49-61	9.18	0.468	Around pipe	0.724	0.804
		0.0788	Around instrument		
50-62	9.18	0.468	Around pipe	0.724	0.804
		0.0788	Around instrument		
51-63	9.18	0.468	Around pipe	0.724	0.804
		0.0788	Around instrument		
54-66	9.18	0.468	Around pipe	0.724	0.804
		0.0788	Around instrument		
55-67	9.18	0.468	Around pipe	0.724	0.804
		0.0788	Around instrument		
58-70	9.18	0.468	Around pipe	0.724	0.804
		0.0788	Around instrument		

TABLE 6B-7 (Cont)

Flow Paths	Flow Area, ft^2	K Factor	Description(1)	L/A ft^{-1}	Flow Coefficient
60-72	9.18	0.468	Around pipe	0.724	0.804
		0.0788	Around instrument		
59-71	9.18	0.468	Around pipe	0.724	0.804
		0.0788	Around instrument		
49-50	15.35	0.006	Around instrument	0.358	0.846
		0.1005	30° turn		
		0.146	Around LPCI		
		0.146	Around pipe		
53-54	15.35	0.1005	30° turn	0.358	0.846
		0.146	Around LPCI		
		0.146	Around pipe		
		0.006	Around instrument		
55-56	15.35	0.1005	30°turn	0.358	0.846
		0.146	Around LPCI		
		0.146	Around pipe		
		0.006	Around instrument		
59-60	15.35	0.1005	30° turn	0.358	0.846
		0.146	Around LPCI		
		0.146	Around pipe		
		0.006	Around instrument		
58-59	16.84	0.1005	30° turn	0.338	0.953
50-51	16.84	0.1005	30° turn	0.338	0.953

TABLE 6B-7 (Cont)

Flow Paths	Flow Area, ft^2	K Factor	Description(1)	L/A ft^{-1}	Flow Coefficient
52-53	14.66	0.1005	30° turn	0.365	0.798
		0.469	Around pipe		
56-57	14.66	0.1005	30° turn	0.365	0.798
		0.469	Around pipe		
49-60	19.21	0.1005	30° turn	0.326	0.953
54-55	19.21	0.1005	30° turn	0.326	0.953
51-52	16.95	0.1005	30° turn	0.342	0.896
		0.146	Around pipe		
57-58	16.95	0.1005	30° turn	0.342	0.896
		0.146	Around pipe		
52-64	6.89	0.468	Around pipe	0.959	0.718
		0.468	Around pipe		
53-65	6.89	0.468	Around pipe	0.959	0.718
		0.468	Around pipe		
56-68	6.89	0.468	Around pipe	0.959	0.718
		0.468	Around pipe		
57-69	6.89	0.468	Around pipe	0.959	0.718
		0.468	Around pipe		
61-62	6.03	0.53	Around pipe	0.853	0.761
		0.104	Around instrument		
		0.094	30° turn		

TABLE 6B-7 (Cont)

Flow Paths	Flow Area, ft^2	K Factor	Description[1]	L/A ft^{-1}	Flow Coefficient
67-68	6.03	0.53	Around pipe	0.853	0.761
		0.104	Around instrument		
		0.094	30° turn		
63-64	6.64	0.53	Around pipe	0.796	0.785
		0.094	30° turn		
65-66	6.64	0.53	Around pipe	0.796	0.785
		0.094	30° turn		
69-70	6.64	0.53	Around pipe	0.796	0.785
		0.094	30° turn		
71-72	6.64	0.53	Around pipe	0.796	0.785
		0.094	30° turn		
62-63	8.91	0.094	30° turn	0.703	0.956
66-67	8.91	0.094	30° turn	0.703	0.956
70-71	8.91	0.094	30° turn	0.703	0.956
61-72	8.91	0.094	30° turn	0.703	0.956
64-65	8.91	0.094	30° turn	0.703	0.956
68-69	8.91	0.094	30° turn	0.703	0.956
61-73	10.33	0.12	Contraction	0.212	0.945
62-73	10.33	0.12	Contraction	0.212	0.945

TABLE 6B-7 (Cont)

Flow Paths	Flow Area, ft^2	K Factor	Description(1)	L/A ft^{-1}	Flow Coefficient
63-73	10.33	0.12	Contraction	0.212	0.945
64-73	10.33	0.12	Contraction	0.212	0.945
65-73	10.33	0.12	Contraction	0.212	0.945
66-73	10.33	0.12	Contraction	0.212	0.945
67-73	10.33	0.12	Contraction	0.212	0.945
68-73	10.33	0.12	Contraction	0.212	0.945
69-73	10.33	0.12	Contraction	0.212	0.945
70-73	10.33	0.12	Contraction	0.212	0.945
71-73	10.33	0.12	Contraction	0.212	0.945
72-73	10.33	0.12	Contraction	0.212	0.945

(1) Factor for final expansion is included in the flow coefficient calculation.

TABLE 6B-8

GEOMETRY NODE LOCATIONS(1)

Elevation	Node Numbers
116' - 3.77"	1 - 12
125' - 1.48"	13 - 24
134' - 3.88"	25 - 36
142' - 3.63"	37 - 48
151' - 6.50"	49 - 60
159' - 2.75"	61 - 72

Node Angles	Node Numbers
345°	1, 13, 25, 37, 49, 61
315°	2, 14, 26, 38, 50, 62
285°	3, 14, 27, 39, 51, 63
255°	4, 15, 28, 40, 52, 64
225°	5, 16, 29, 41, 53, 65
195°	6, 17, 30, 42, 54, 66
165°	7, 18, 31, 43, 55, 67
135°	8, 19, 32, 44, 56, 68
105°	9, 20, 33, 45, 57, 69
75°	10, 21, 34, 46, 58, 70
45°	11, 22, 35, 47, 59, 71
15°	12, 23, 30, 48, 60, 72

(1) Elevations and node angles are for center of geometry nodes.

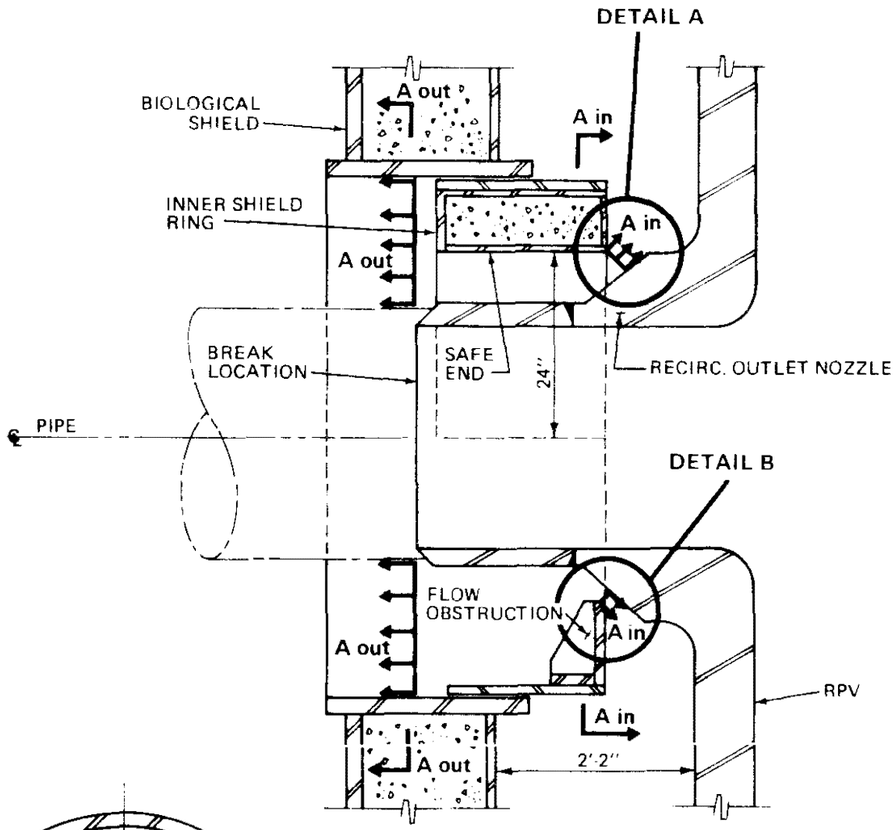

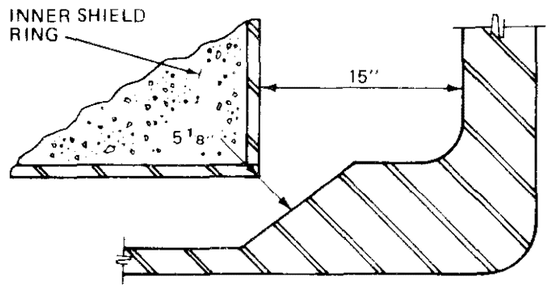

DETAIL **A**

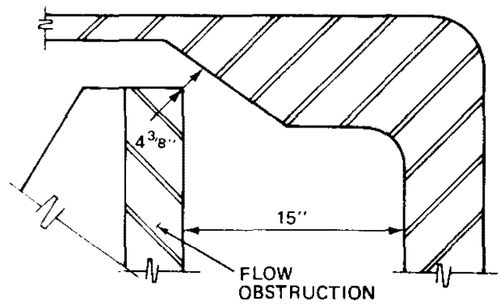

DETAIL **B**

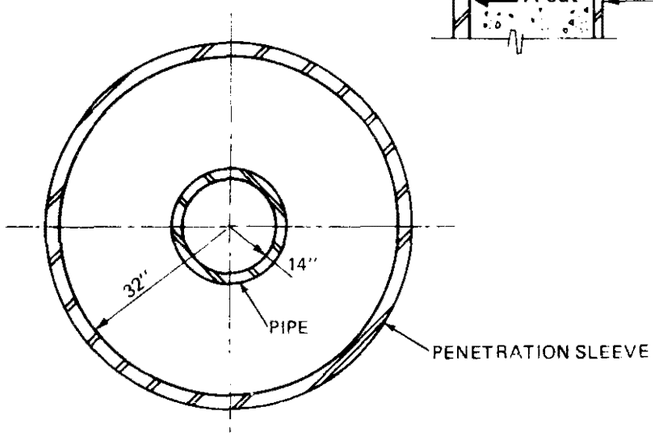

SECTION **A-A** (OUT)

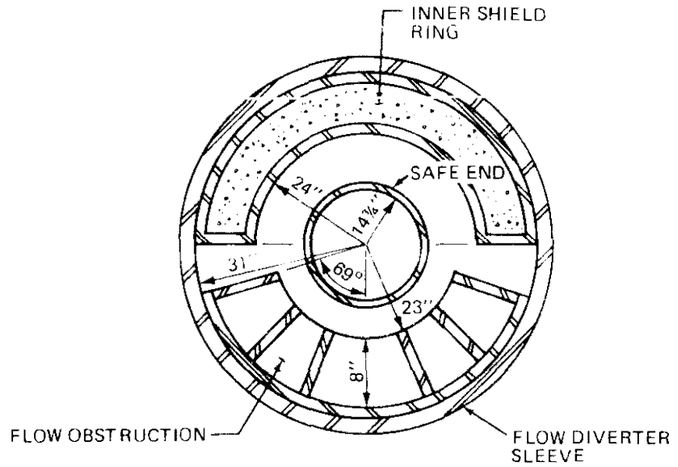

SECTION **A-A** (IN)

NOTE:
DIMENSIONS ARE NOMINAL.

REVISION 0
APRIL 11, 1988

PUBLIC SERVICE ELECTRIC AND GAS COMPANY
HOPE CREEK NUCLEAR GENERATING STATION

RECIRCULATION OUTLET NOZZLE
FLOW DIVERTER

UPDATED FSAR

FIGURE 6B-1

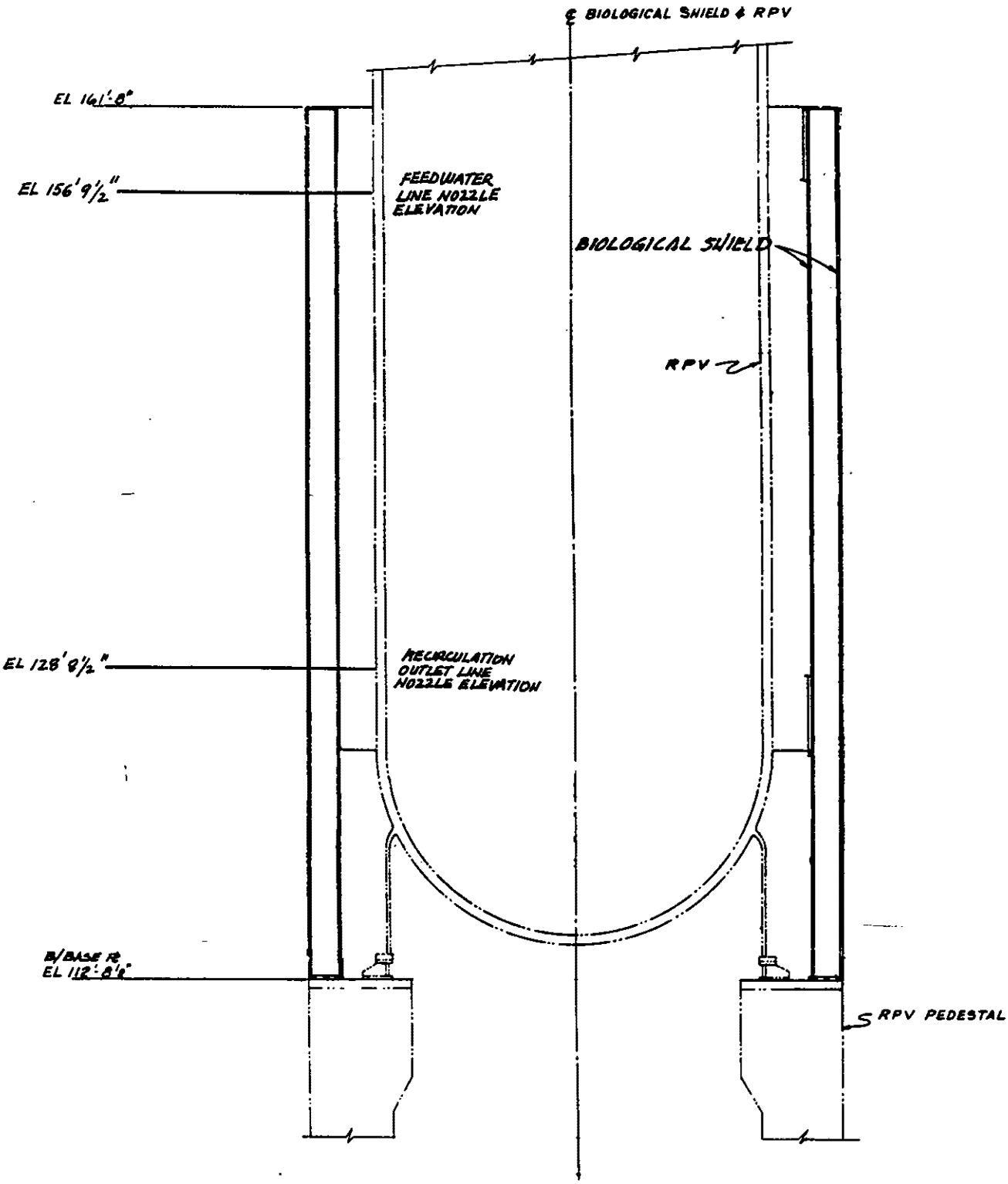

REVISION 0
APRIL 11, 1988

PUBLIC SERVICE ELECTRIC AND GAS COMPANY
HOPE CREEK NUCLEAR GENERATING STATION

REACTOR SHIELD ANNULUS ARRANGEMENT

UPDATED FSAR

FIGURE 6B-2

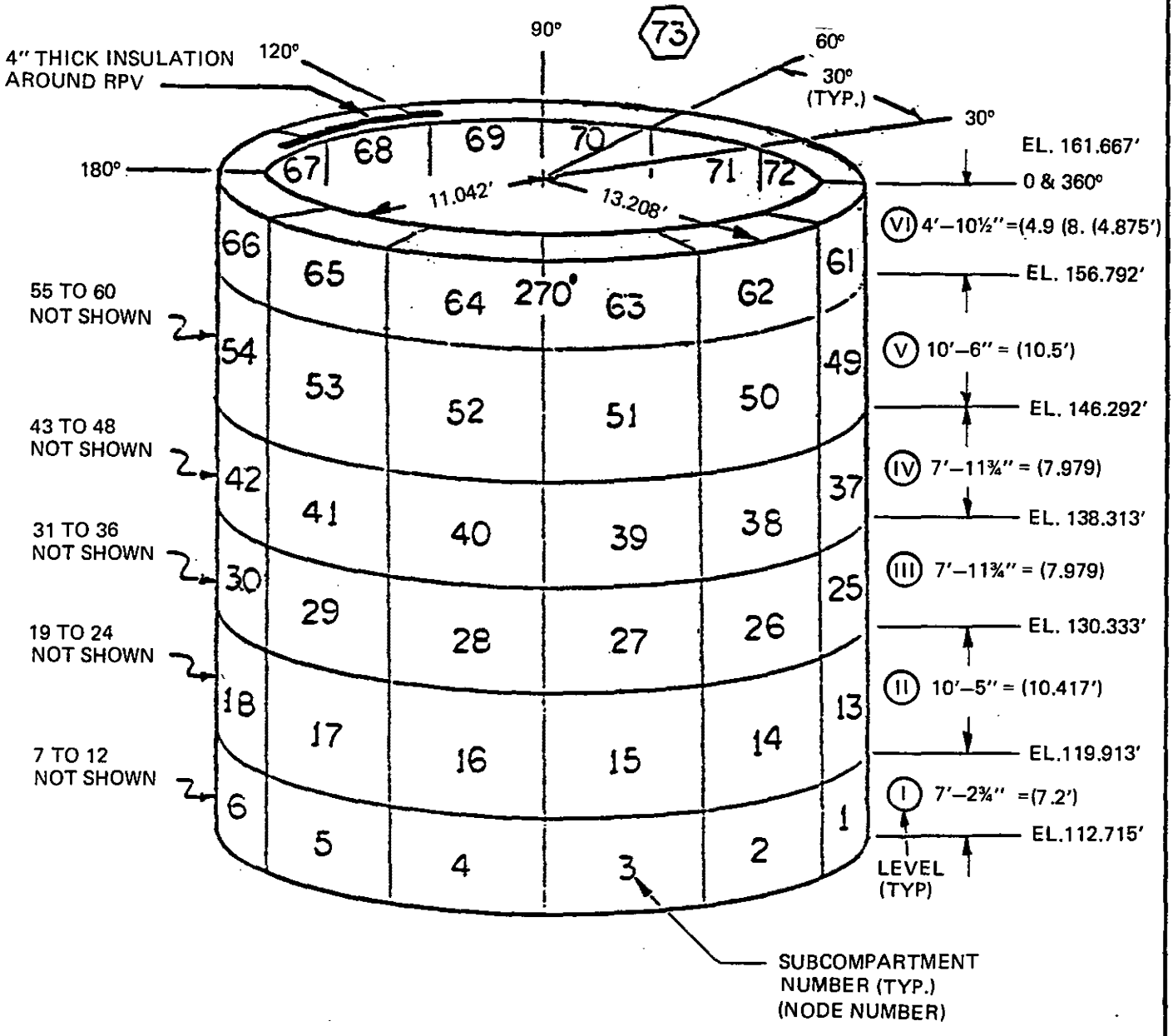

REVISION 0
APRIL 11, 1988

PUBLIC SERVICE ELECTRIC AND GAS COMPANY
HOPE CREEK NUCLEAR GENERATING STATION

SCHEMATIC OF THE RPV SHIELD ANNULUS MODEL

UPDATED FSAR

FIGURE 6B-3a

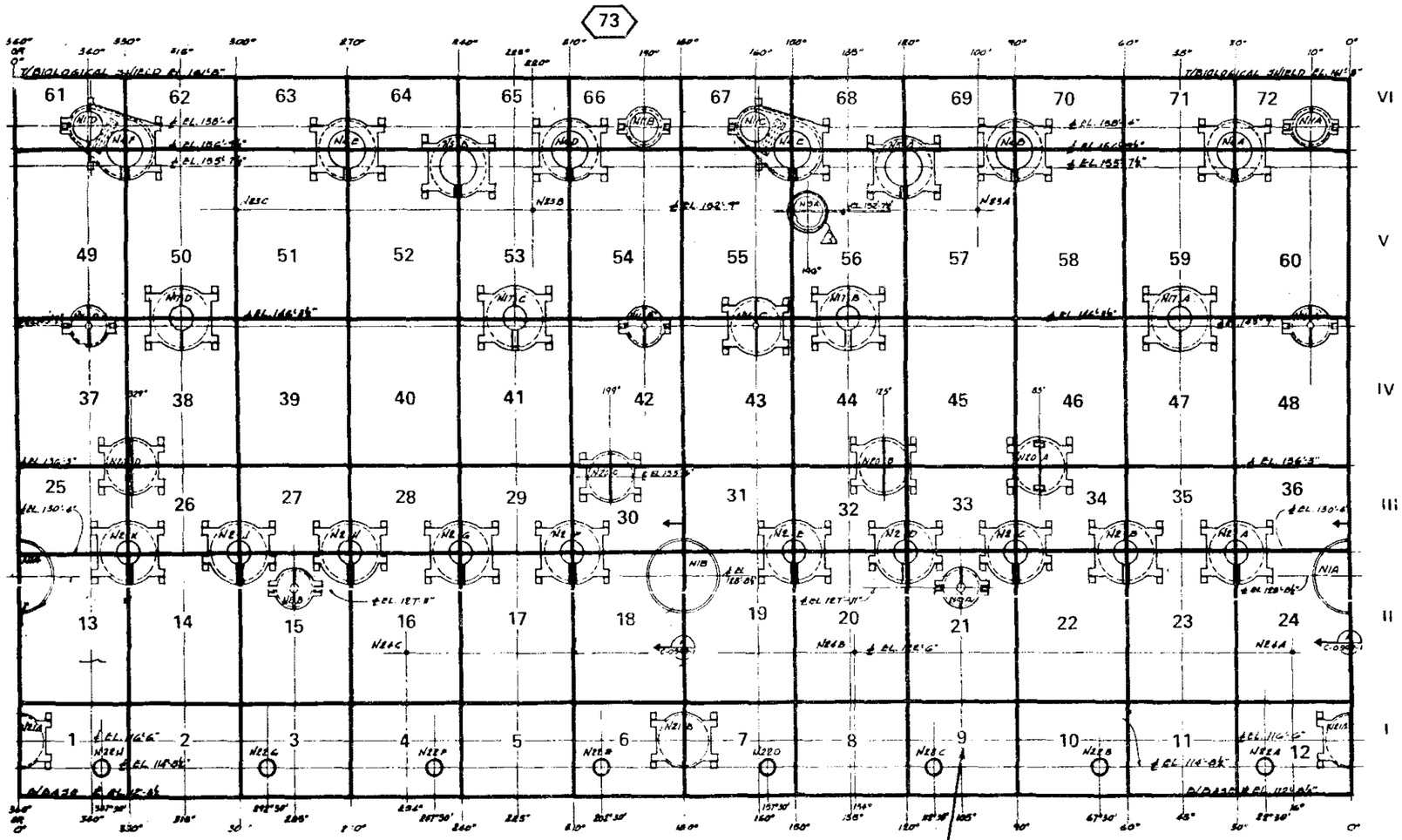

REVISION 0
APRIL 11, 1988

PUBLIC SERVICE ELECTRIC AND GAS COMPANY
HOPE CREEK NUCLEAR GENERATING STATION

SCHEMATIC OF RPV SHIELD
ANNULUS DEVELOPED MODEL

UPDATED FSAR — FIGURE 6B-3b

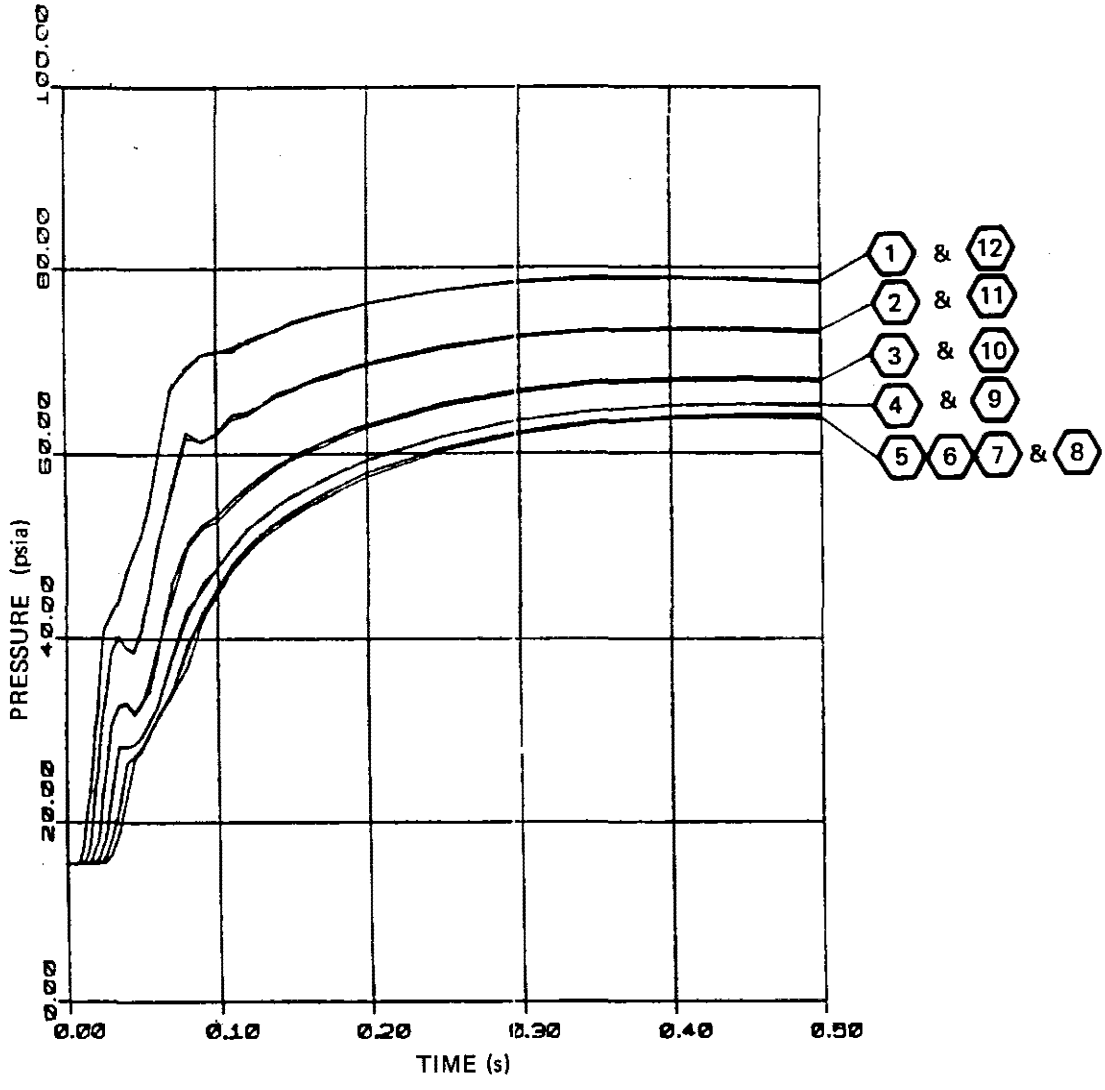

REVISION 0
APRIL 11, 1988

PUBLIC SERVICE ELECTRIC AND GAS COMPANY
HOPE CREEK NUCLEAR GENERATING STATION

PRESSURE TRANSIENT IN SHIELD ANNULUS FOLLOWING A RECIRCULATION LINE BREAK AT THE NOZZLE SAFE END

UPDATED FSAR

Sheet 1 of 6
FIGURE 6B-4

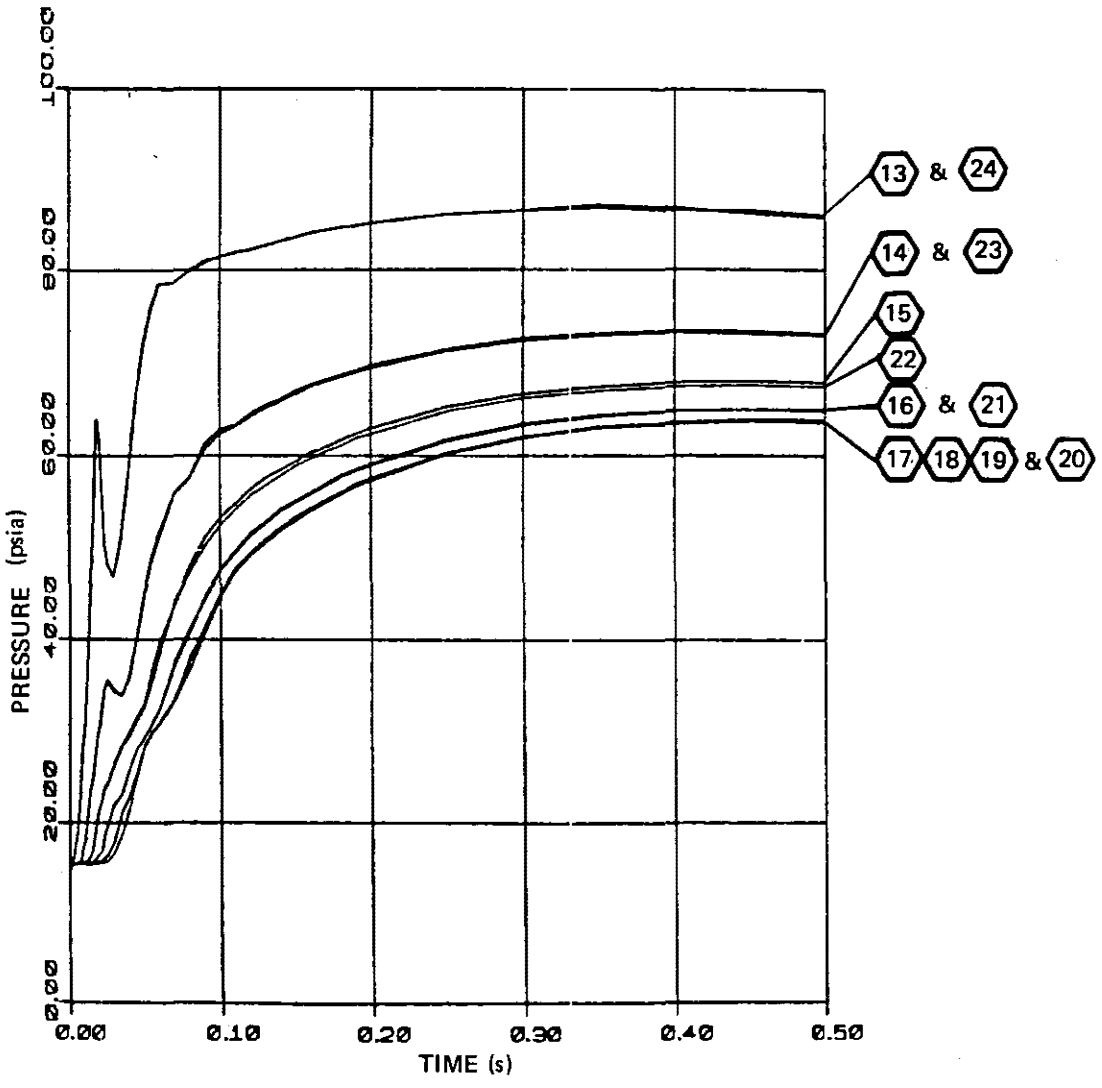

REVISION 0
APRIL 11, 1988

PUBLIC SERVICE ELECTRIC AND GAS COMPANY
HOPE CREEK NUCLEAR GENERATING STATION

PRESSURE TRANSIENT IN SHIELD ANNULUS FOLLOWING A RECIRCULATION LINE BREAK AT THE NOZZLE SAFE END

UPDATED FSAR

Sheet 2 of 6
FIGURE 6B-4

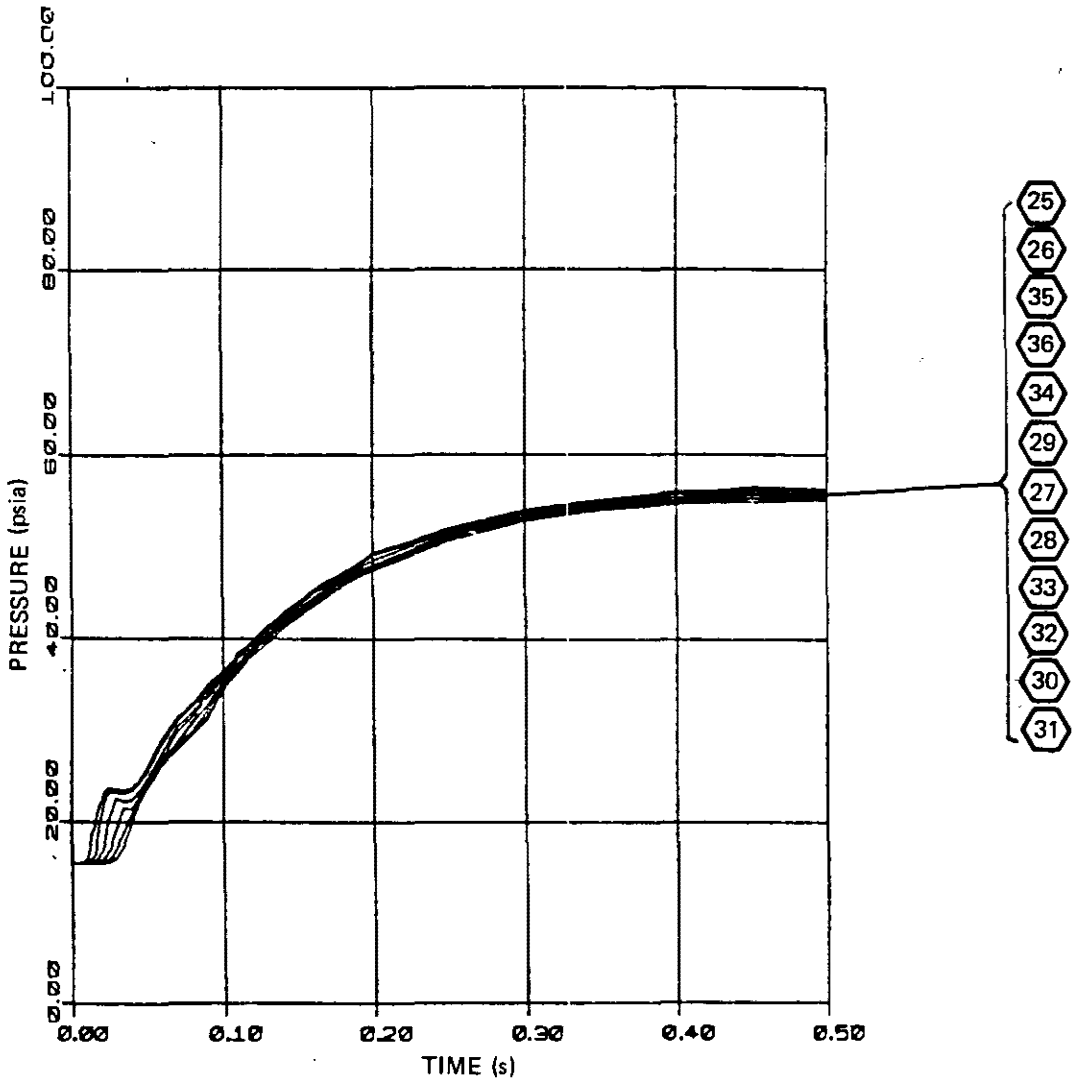

REVISION 0
APRIL 11, 1988

PUBLIC SERVICE ELECTRIC AND GAS COMPANY
HOPE CREEK NUCLEAR GENERATING STATION

PRESSURE TRANSIENT IN SHIELD ANNULUS FOLLOWING A RECIRCULATION LINE BREAK AT THE NOZZLE SAFE END

UPDATED FSAR

Sheet 3 of 6
FIGURE 6B-4

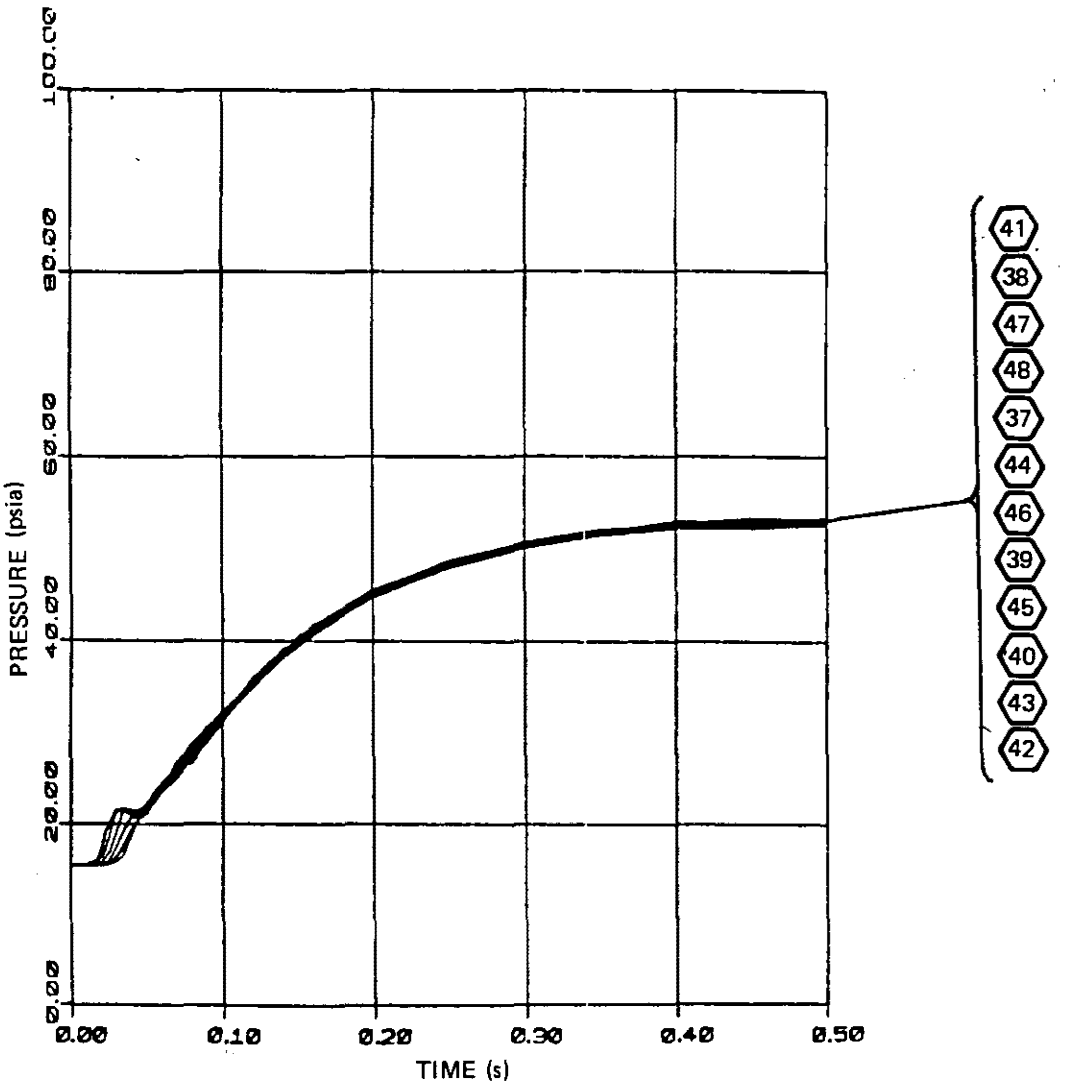

REVISION 0
APRIL 11, 1988

PUBLIC SERVICE ELECTRIC AND GAS COMPANY
HOPE CREEK NUCLEAR GENERATING STATION

PRESSURE TRANSIENT IN SHIELD ANNULUS FOLLOWING A RECIRCULATION LINE BREAK AT THE NOZZLE SAFE END

UPDATED FSAR

Sheet 4 of 6
FIGURE 6B-4

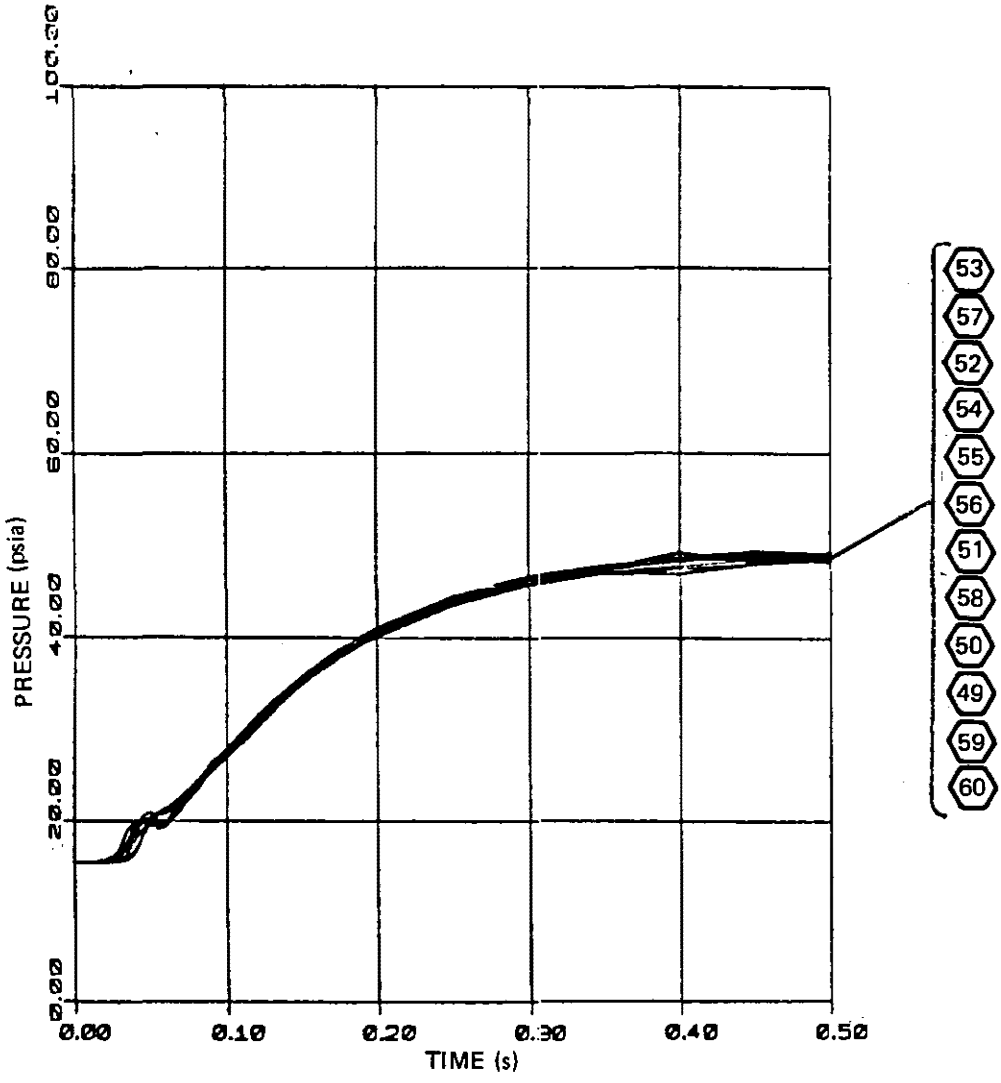

REVISION 0
APRIL 11, 1988

PUBLIC SERVICE ELECTRIC AND GAS COMPANY
HOPE CREEK NUCLEAR GENERATING STATION

PRESSURE TRANSIENT IN SHIELD ANNULUS FOLLOWING A RECIRCULATION LINE BREAK AT THE NOZZLE SAFE END

UPDATED FSAR

Sheet 5 of 6
FIGURE 6B-4

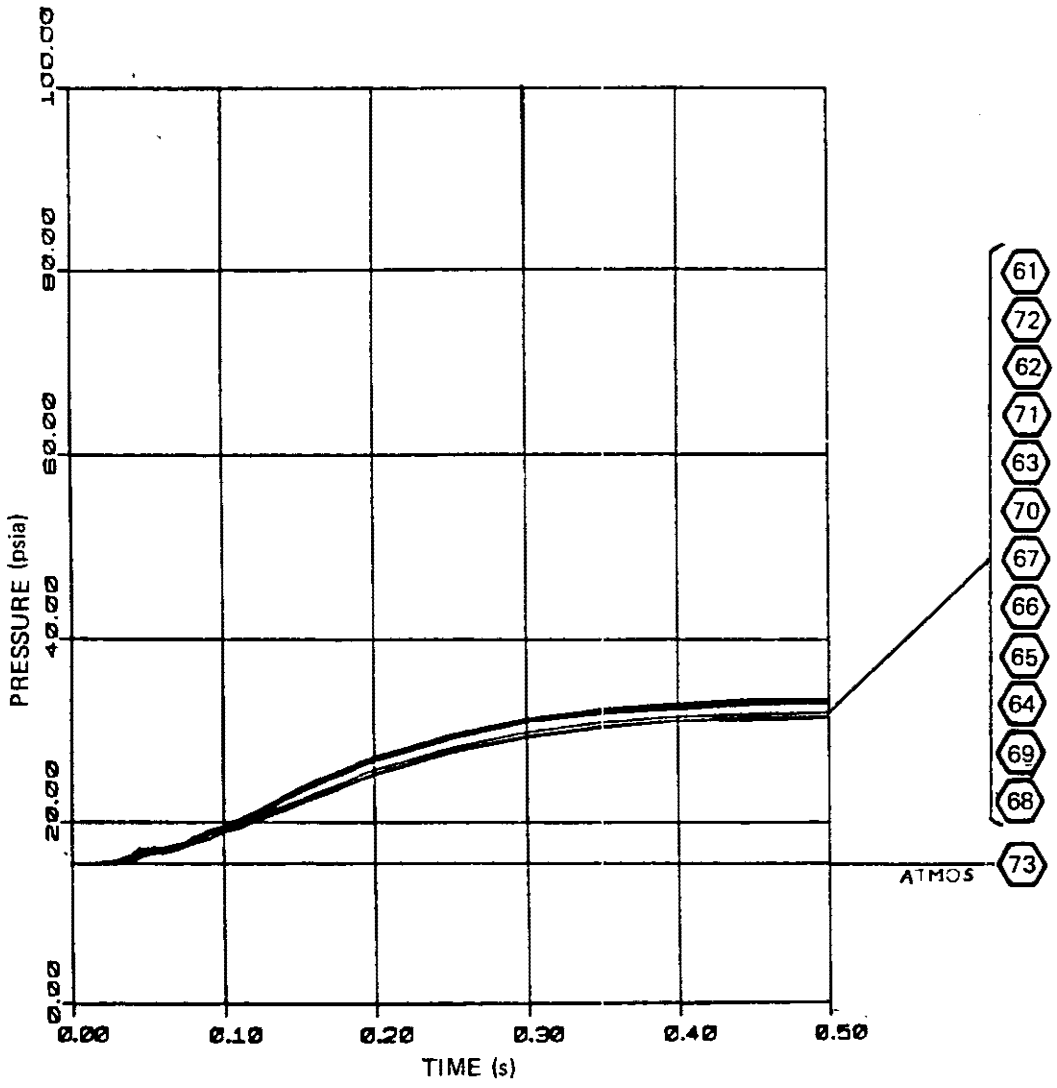

REVISION 0
APRIL 11, 1988

PUBLIC SERVICE ELECTRIC AND GAS COMPANY
HOPE CREEK NUCLEAR GENERATING STATION

PRESSURE TRANSIENT IN SHIELD ANNULUS FOLLOWING A RECIRCULATION LINE BREAK AT THE NOZZLE SAFE END

UPDATED FSAR

Sheet 6 of 6
FIGURE 6B-4

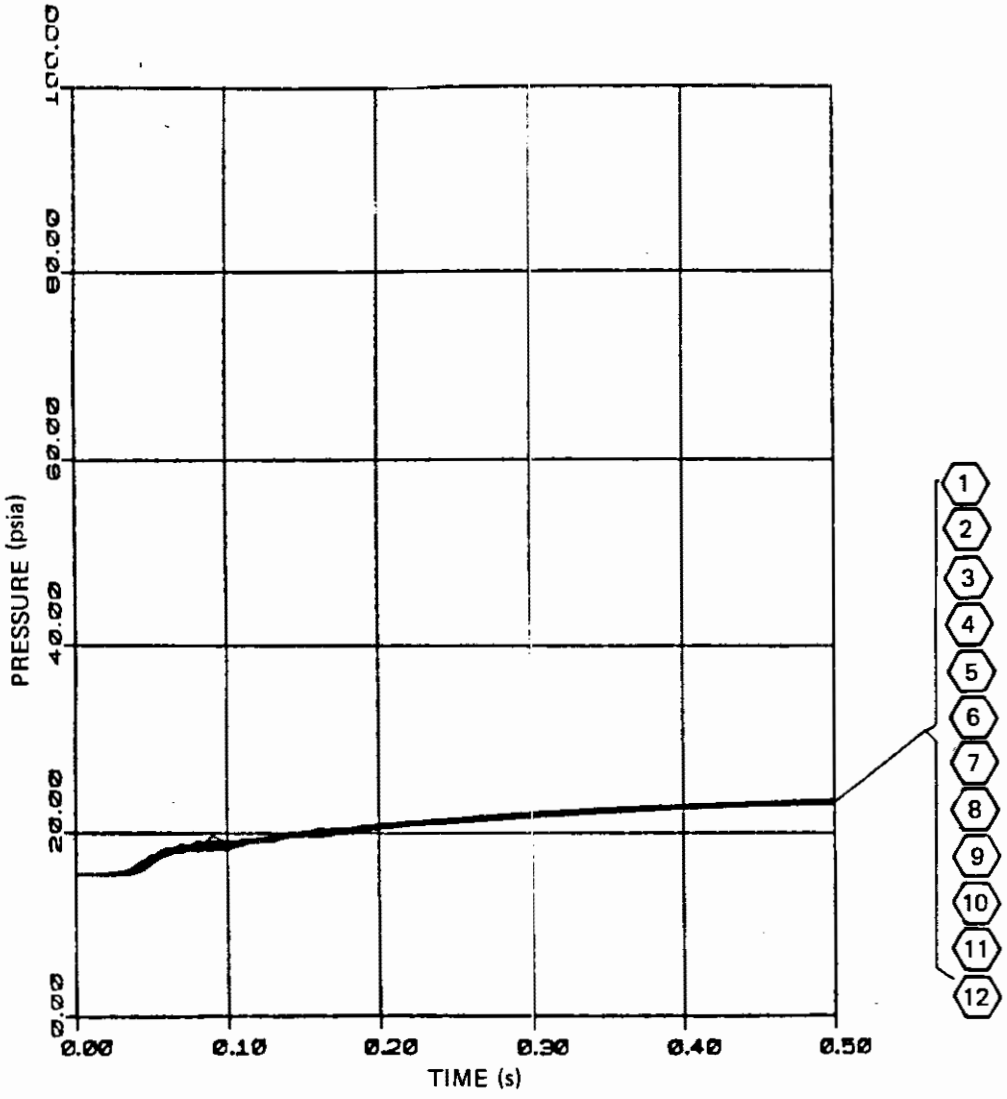

REVISION 0
APRIL 11, 1988

PUBLIC SERVICE ELECTRIC AND GAS COMPANY
HOPE CREEK NUCLEAR GENERATING STATION

PRESSURE TRANSIENT IN SHIELD ANNULUS FOLLOWING A FEEDWATER LINE BREAK

UPDATED FSAR

Sheet 1 of 6
FIGURE 6B-5

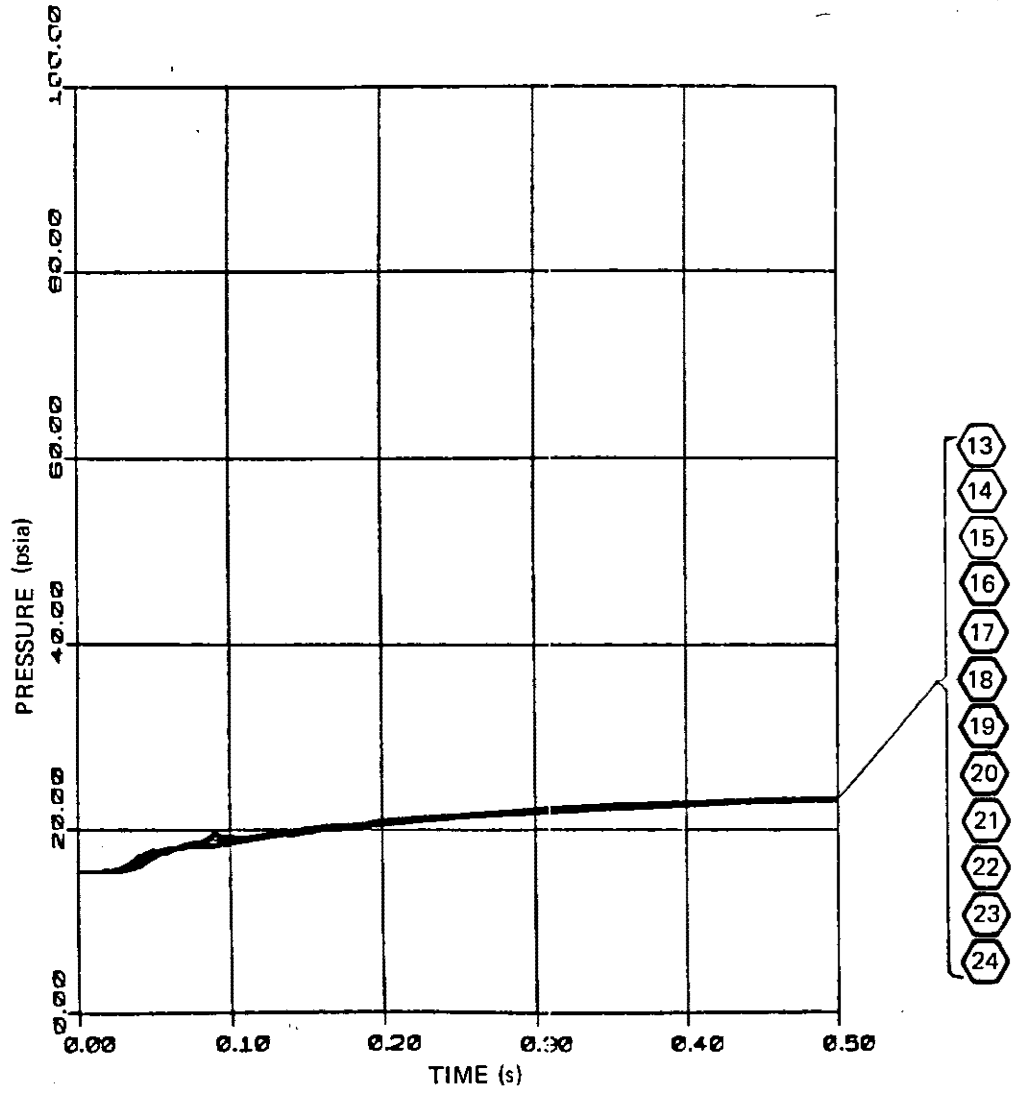

REVISION 0
APRIL 11, 1988

PUBLIC SERVICE ELECTRIC AND GAS COMPANY
HOPE CREEK NUCLEAR GENERATING STATION

PRESSURE TRANSIENT IN SHIELD ANNULUS FOLLOWING A FEEDWATER LINE BREAK

UPDATED FSAR

Sheet 2 of 6
FIGURE 6B-5

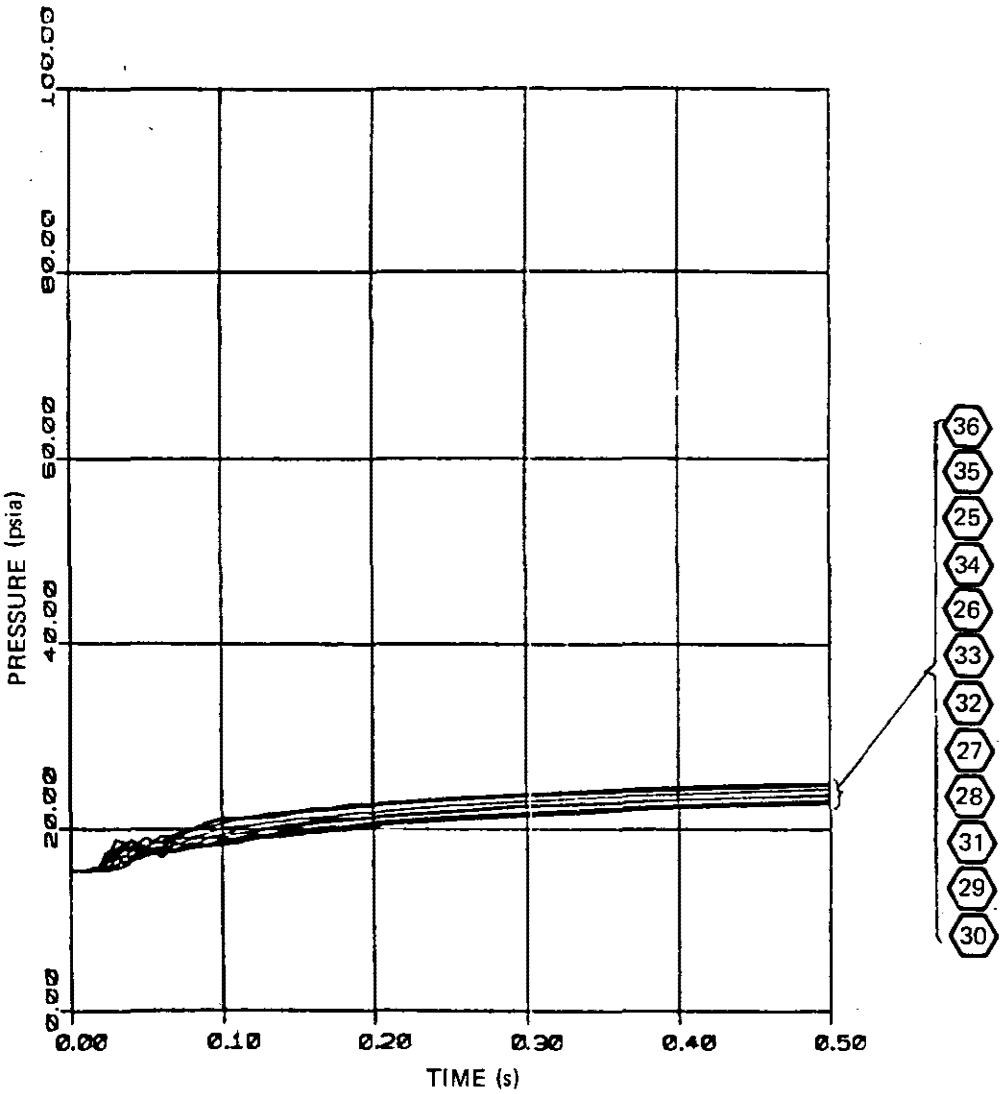

REVISION 0
APRIL 11, 1988

PUBLIC SERVICE ELECTRIC AND GAS COMPANY
HOPE CREEK NUCLEAR GENERATING STATION

PRESSURE TRANSIENT IN SHIELD ANNULUS FOLLOWING A FEEDWATER LINE BREAK

UPDATED FSAR

Sheet 3 of 6
FIGURE 6B-5

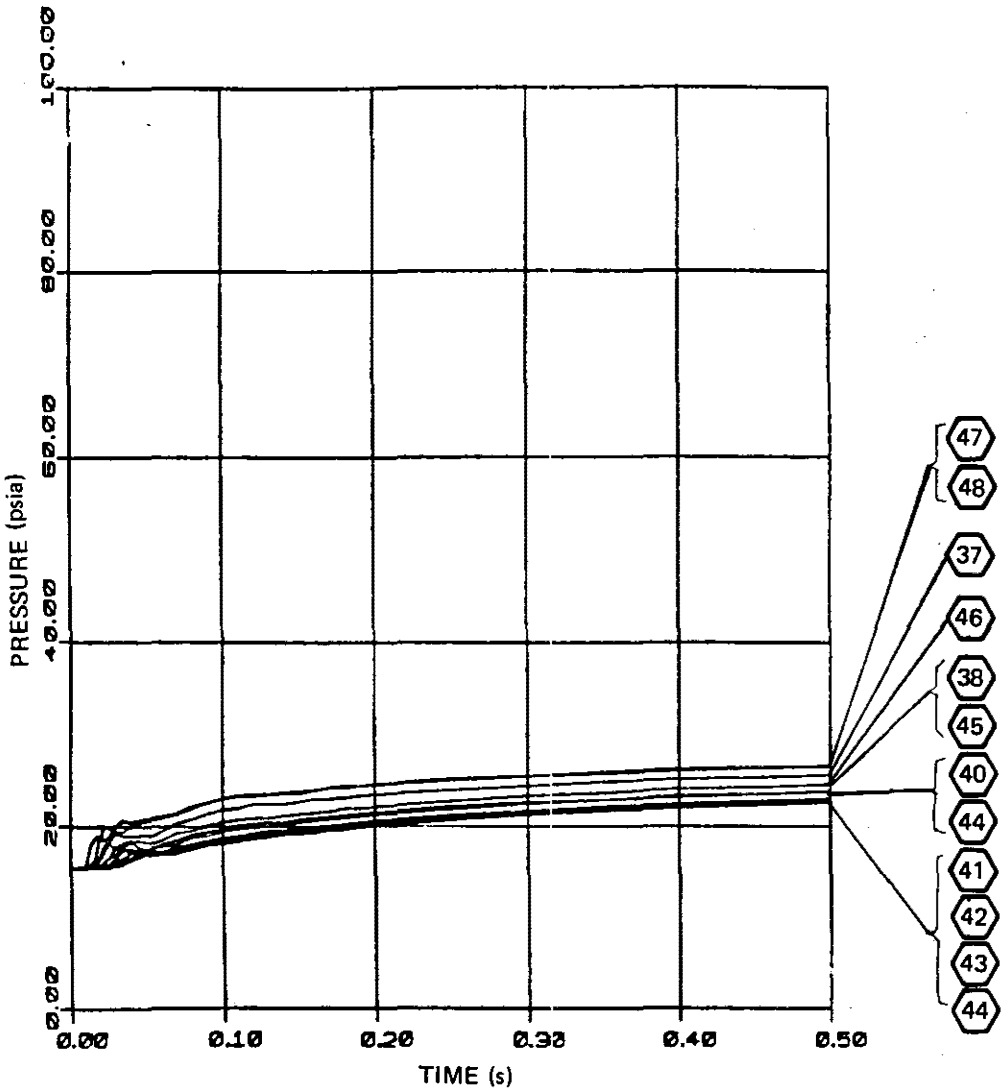

REVISION 0
APRIL 11, 1988

PUBLIC SERVICE ELECTRIC AND GAS COMPANY
HOPE CREEK NUCLEAR GENERATING STATION

PRESSURE TRANSIENT IN SHIELD ANNULUS FOLLOWING A FEEDWATER LINE BREAK

UPDATED FSAR

Sheet 4 of 6
FIGURE 6B-5

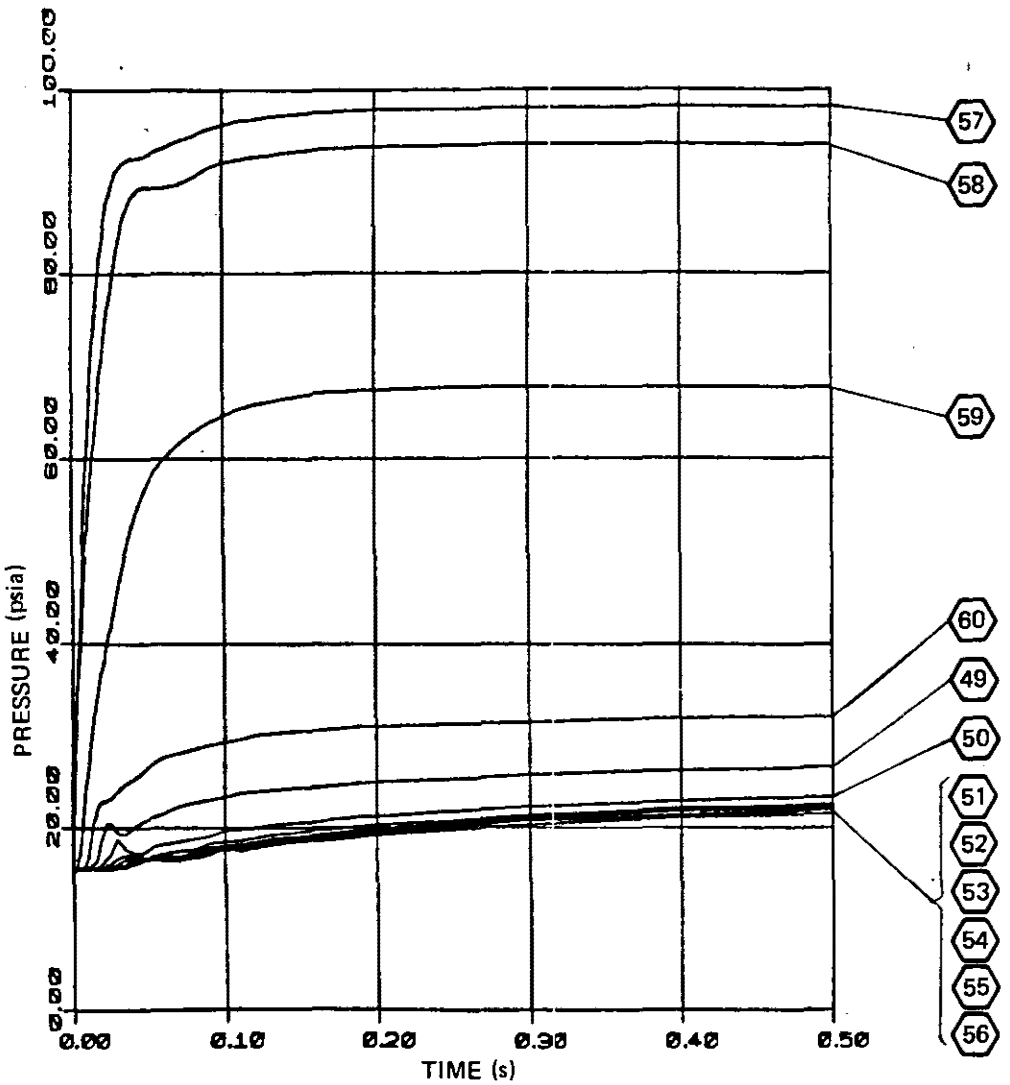

REVISION 0
APRIL 11, 1988

PUBLIC SERVICE ELECTRIC AND GAS COMPANY
HOPE CREEK NUCLEAR GENERATING STATION

PRESSURE TRANSIENT IN SHIELD ANNULUS FOLLOWING A FEEDWATER LINE BREAK

UPDATED FSAR

Sheet 5 of 6
FIGURE 6B-5

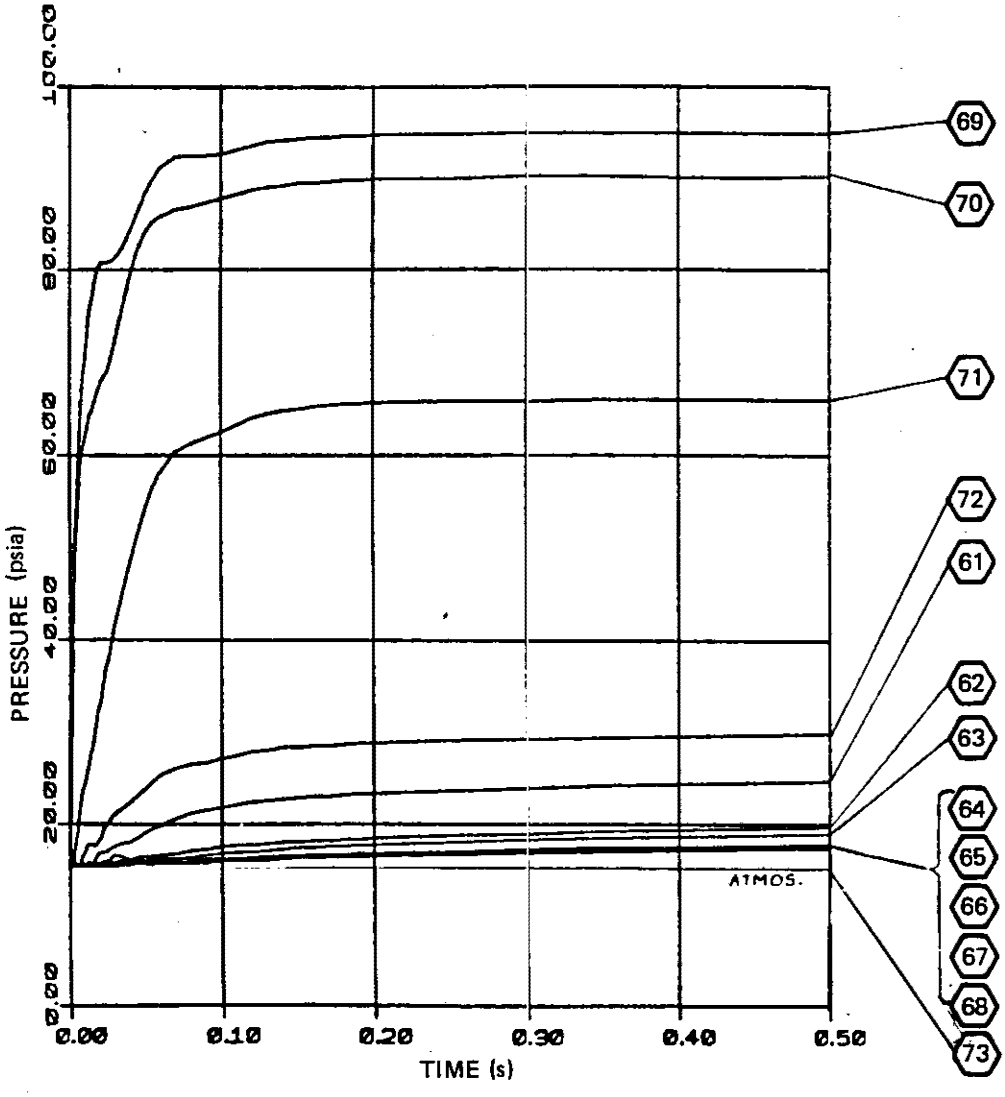

REVISION 0
APRIL 11, 1988

PUBLIC SERVICE ELECTRIC AND GAS COMPANY
HOPE CREEK NUCLEAR GENERATING STATION

PRESSURE TRANSIENT IN SHIELD ANNULUS FOLLOWING A FEEDWATER LINE BREAK

UPDATED FSAR

Sheet 6 of 6
FIGURE 6B-5

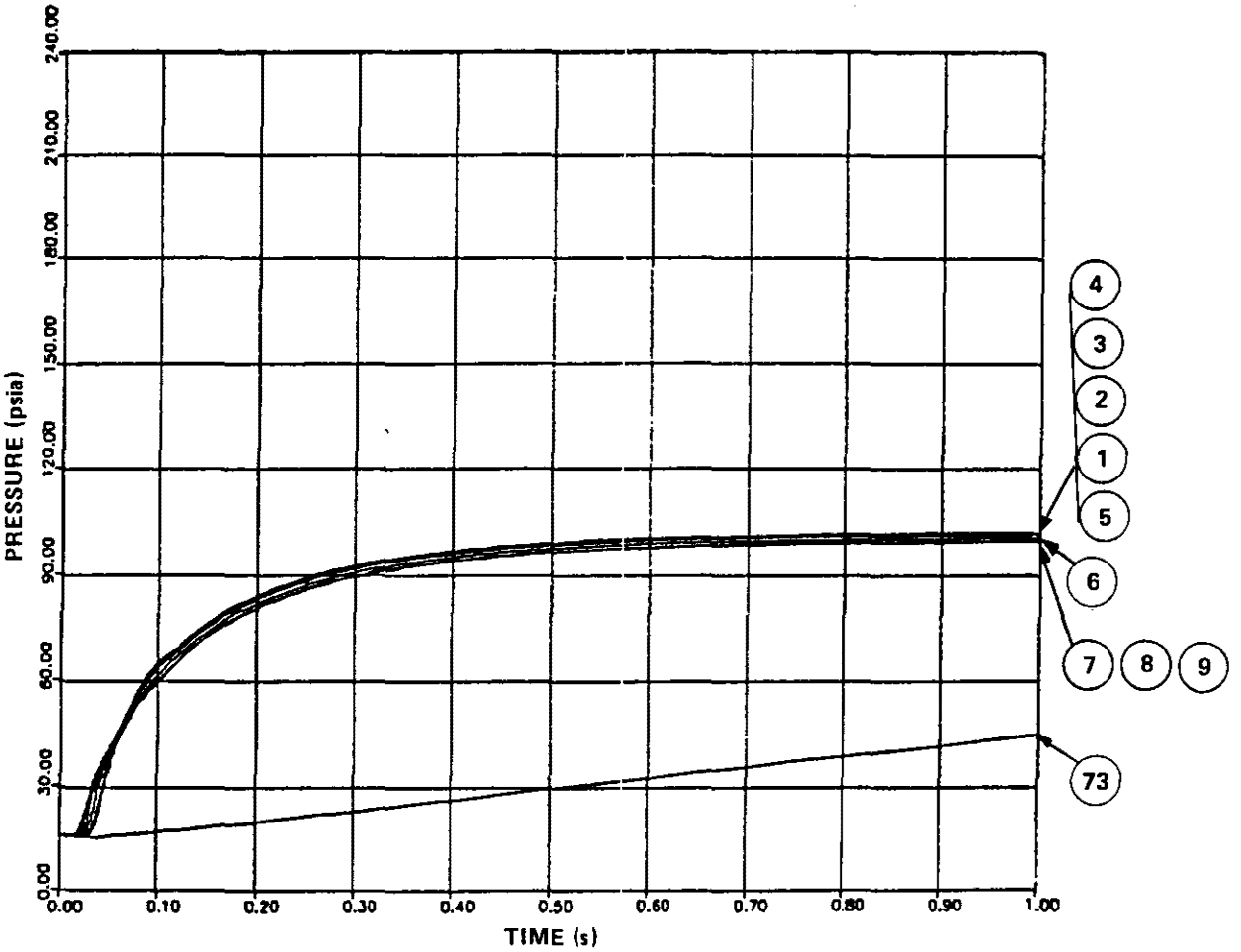

REVISION 0
APRIL 11, 1988

PUBLIC SERVICE ELECTRIC AND GAS COMPANY
HOPE CREEK NUCLEAR GENERATING STATION

PRESSURE TRANSIENT IN SHIELD ANNULUS FOR STRUCTURAL ANALYSIS CASE B

UPDATED FSAR

Sheet 1 of 8
FIGURE 6B-6

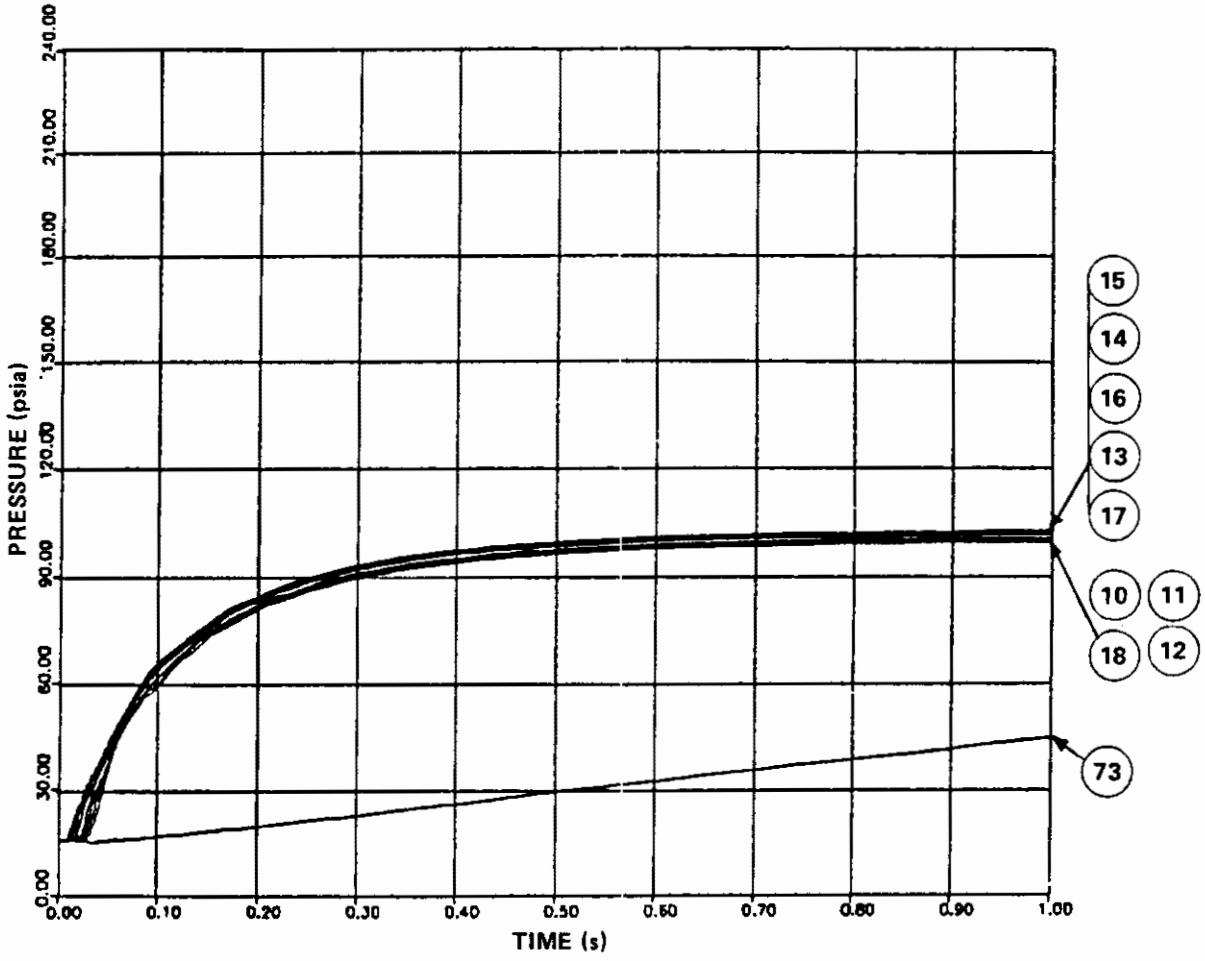

REVISION 0
APRIL 11, 1988

PUBLIC SERVICE ELECTRIC AND GAS COMPANY
HOPE CREEK NUCLEAR GENERATING STATION

PRESSURE TRANSIENT IN SHIELD ANNULUS FOR STRUCTURAL ANALYSIS CASE B

UPDATED FSAR

Sheet 2 of 8
FIGURE 6B-6

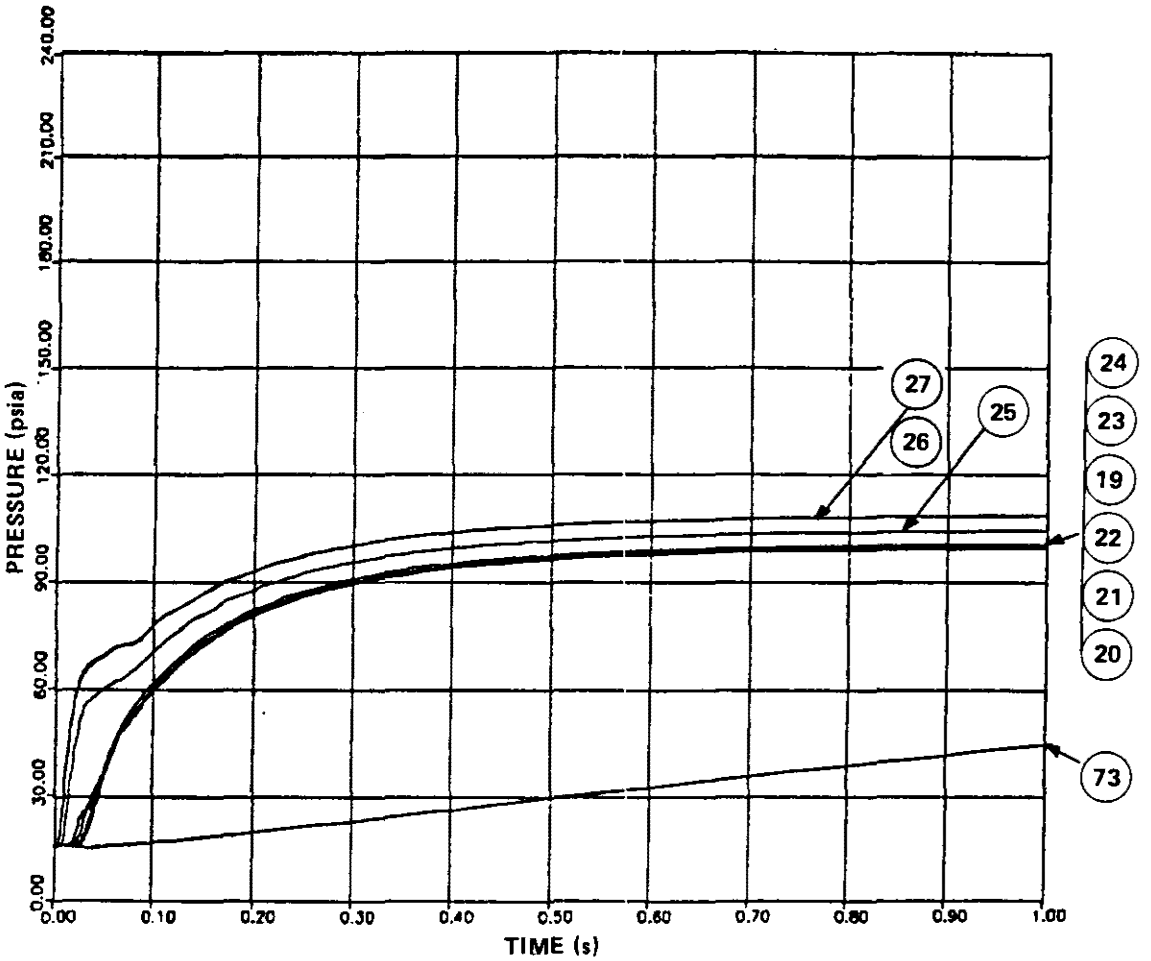

REVISION 0
APRIL 11, 1988

PUBLIC SERVICE ELECTRIC AND GAS COMPANY
HOPE CREEK NUCLEAR GENERATING STATION

PRESSURE TRANSIENT IN SHIELD ANNULUS FOR STRUCTURAL ANALYSIS CASE B

UPDATED FSAR

Sheet 3 of 8
FIGURE 6B-6

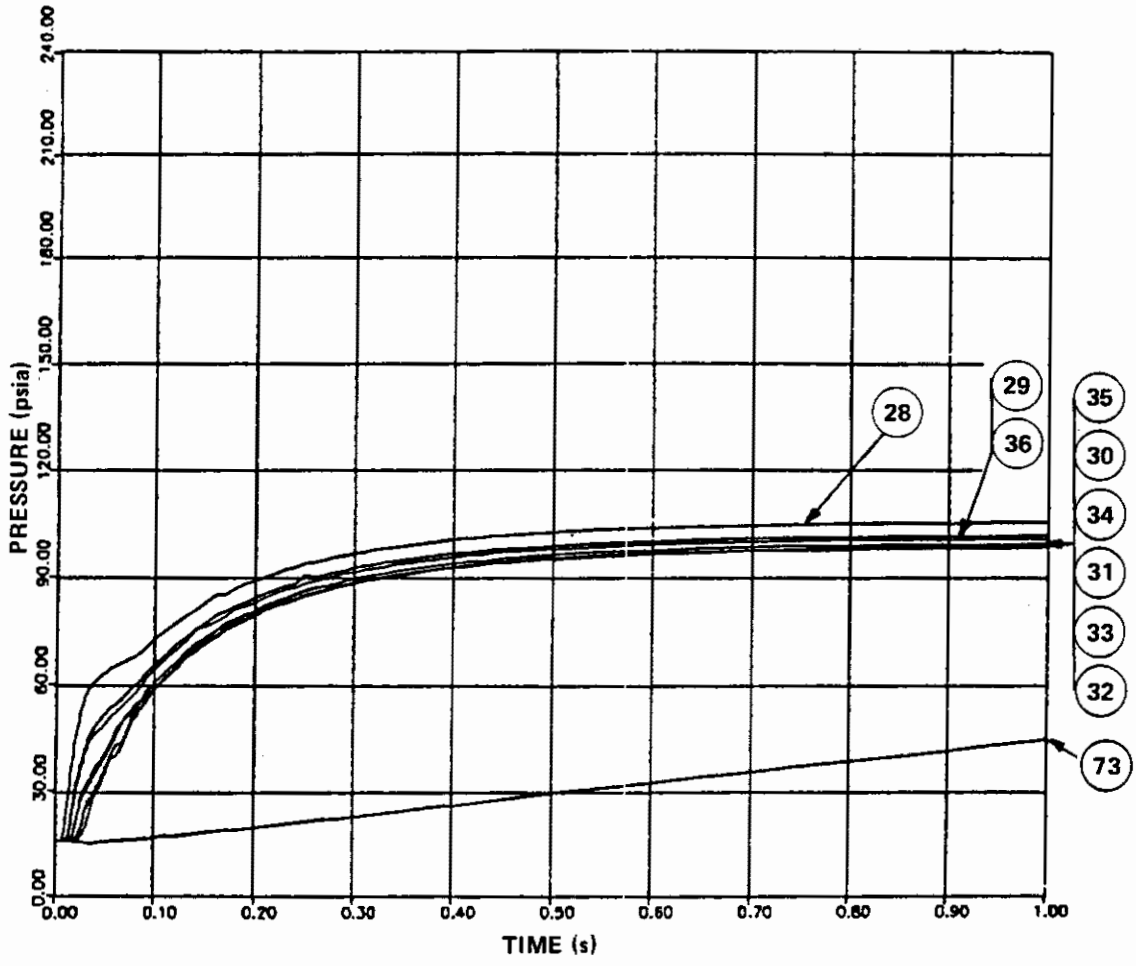

REVISION 0
APRIL 11, 1988

PUBLIC SERVICE ELECTRIC AND GAS COMPANY
HOPE CREEK NUCLEAR GENERATING STATION

PRESSURE TRANSIENT IN SHIELD ANNULUS FOR STRUCTURAL ANALYSIS CASE B

UPDATED FSAR

Sheet 4 of 8
FIGURE 6B-6

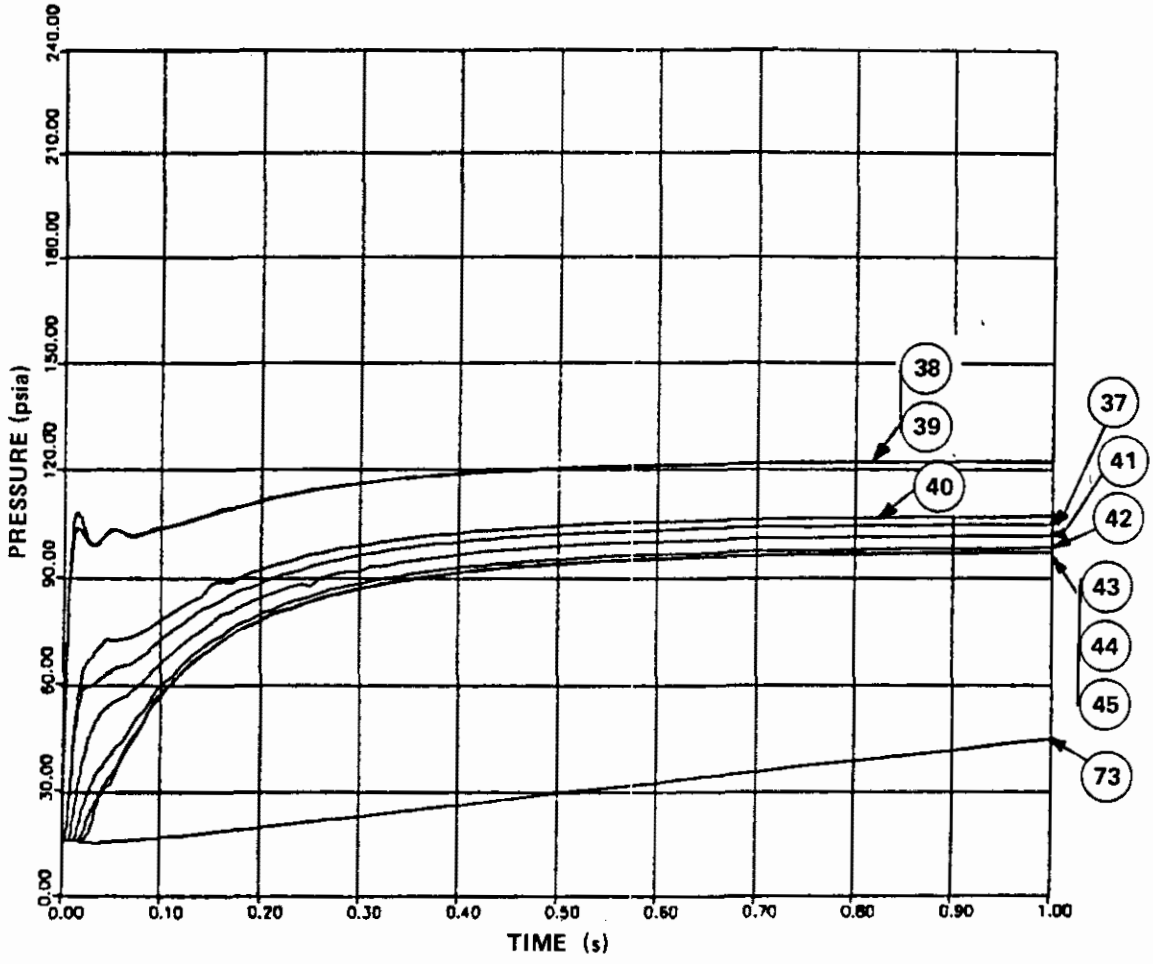

REVISION 0
APRIL 11, 1988

PUBLIC SERVICE ELECTRIC AND GAS COMPANY
HOPE CREEK NUCLEAR GENERATING STATION

PRESSURE TRANSIENT IN SHIELD ANNULUS FOR STRUCTURAL ANALYSIS CASE B

UPDATED FSAR

Sheet 5 of 8
FIGURE 6B-6

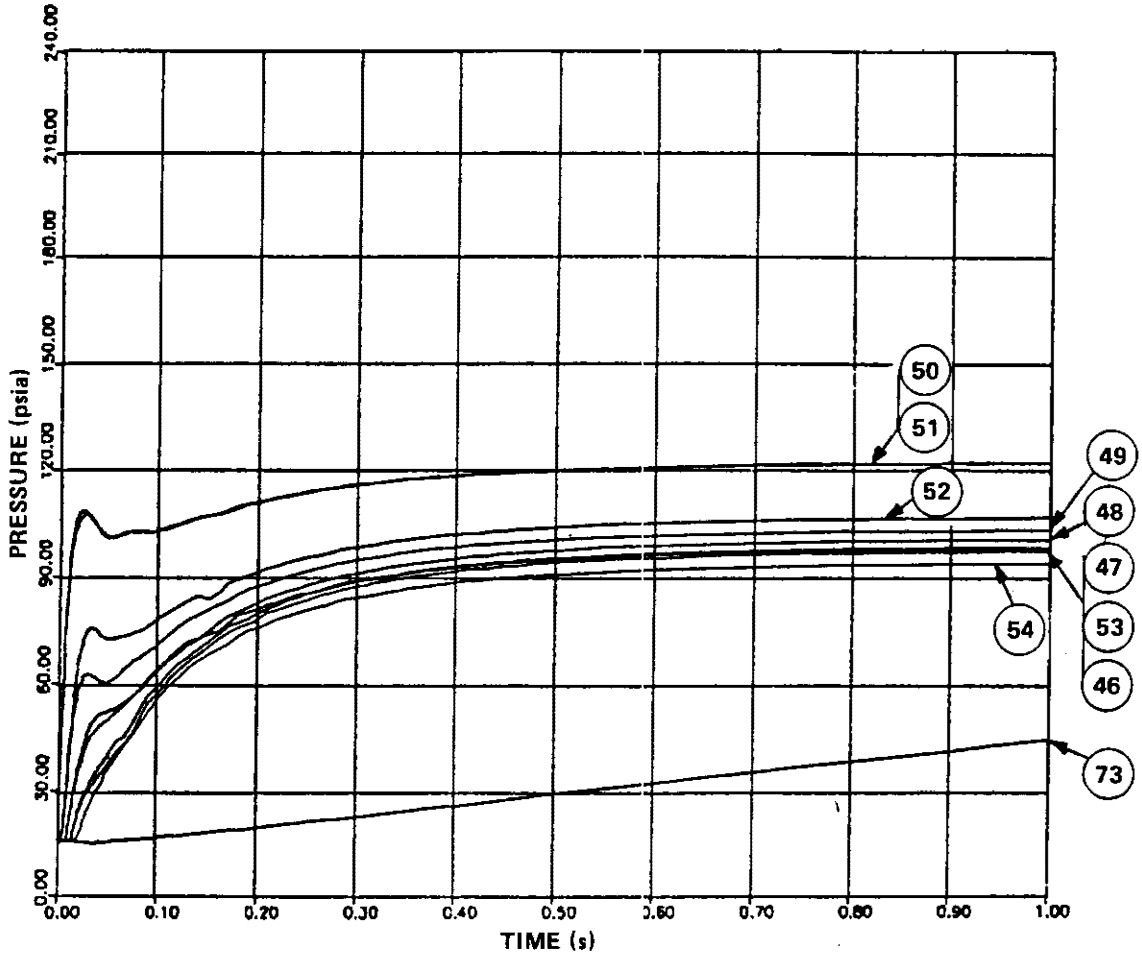

REVISION 0
APRIL 11, 1988

PUBLIC SERVICE ELECTRIC AND GAS COMPANY
HOPE CREEK NUCLEAR GENERATING STATION

PRESSURE TRANSIENT IN SHIELD ANNULUS FOR STRUCTURAL ANALYSIS CASE B

UPDATED FSAR

Sheet 6 of 8
FIGURE 6B-6

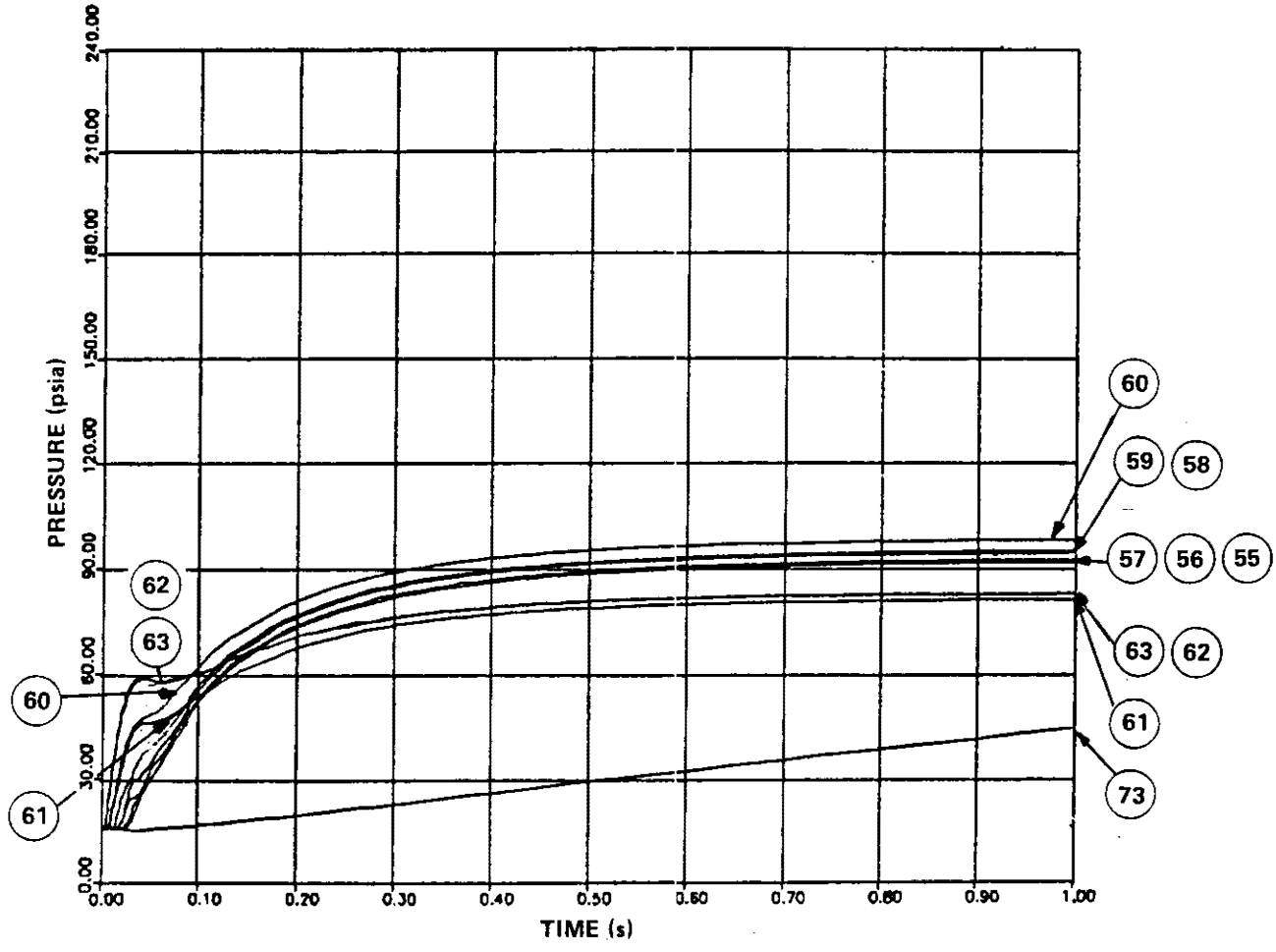

REVISION 0
APRIL 11, 1988

PUBLIC SERVICE ELECTRIC AND GAS COMPANY
HOPE CREEK NUCLEAR GENERATING STATION

PRESSURE TRANSIENT IN SHIELD ANNULUS FOR STRUCTURAL ANALYSIS CASE B

UPDATED FSAR

Sheet 7 of 8
FIGURE 6B-6

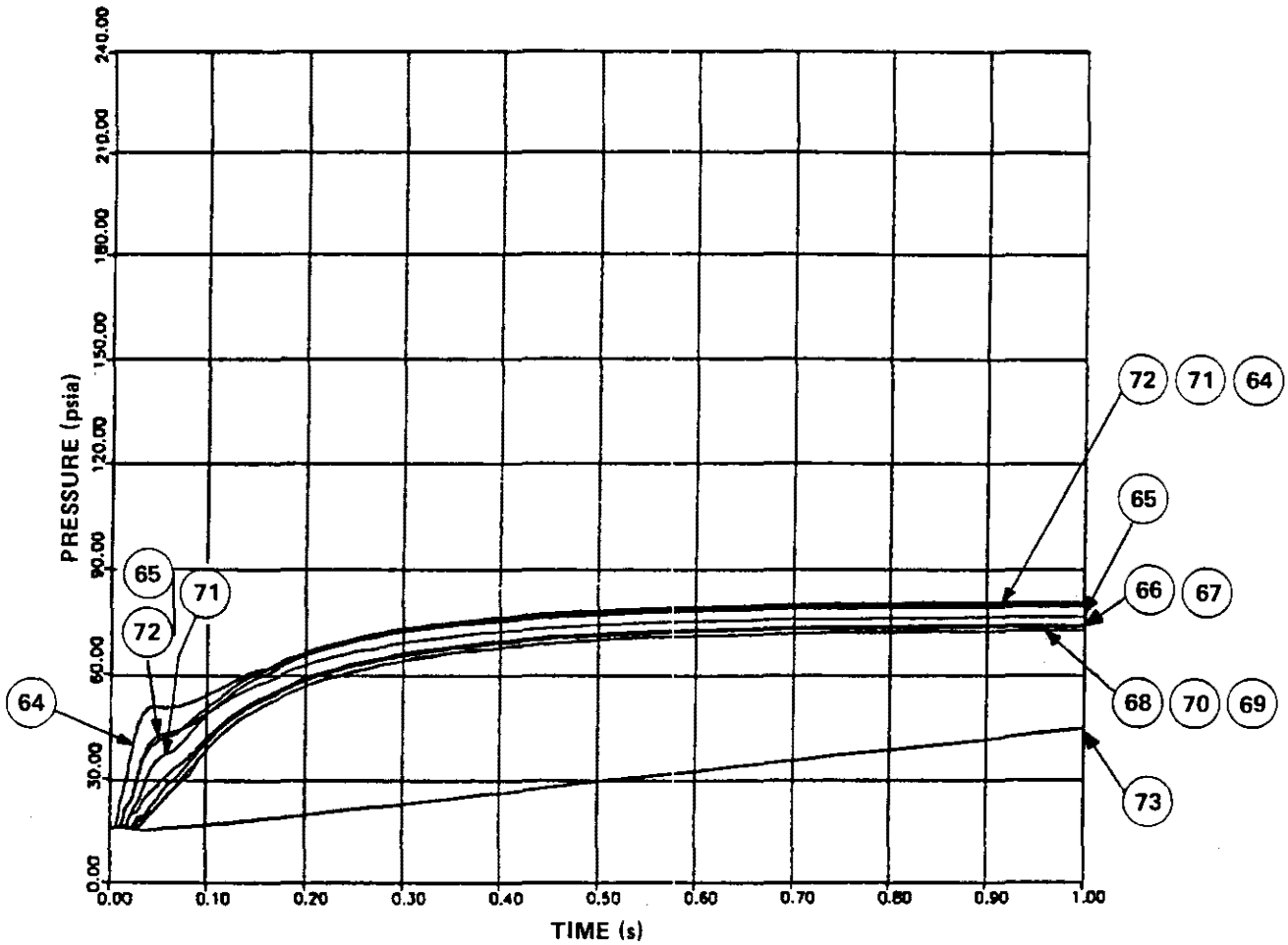

REVISION 0
APRIL 11, 1988

PUBLIC SERVICE ELECTRIC AND GAS COMPANY
HOPE CREEK NUCLEAR GENERATING STATION

PRESSURE TRANSIENT IN SHIELD ANNULUS FOR STRUCTURAL ANALYSIS CASE B

UPDATED FSAR

Sheet 8 of 8
FIGURE 6B-6

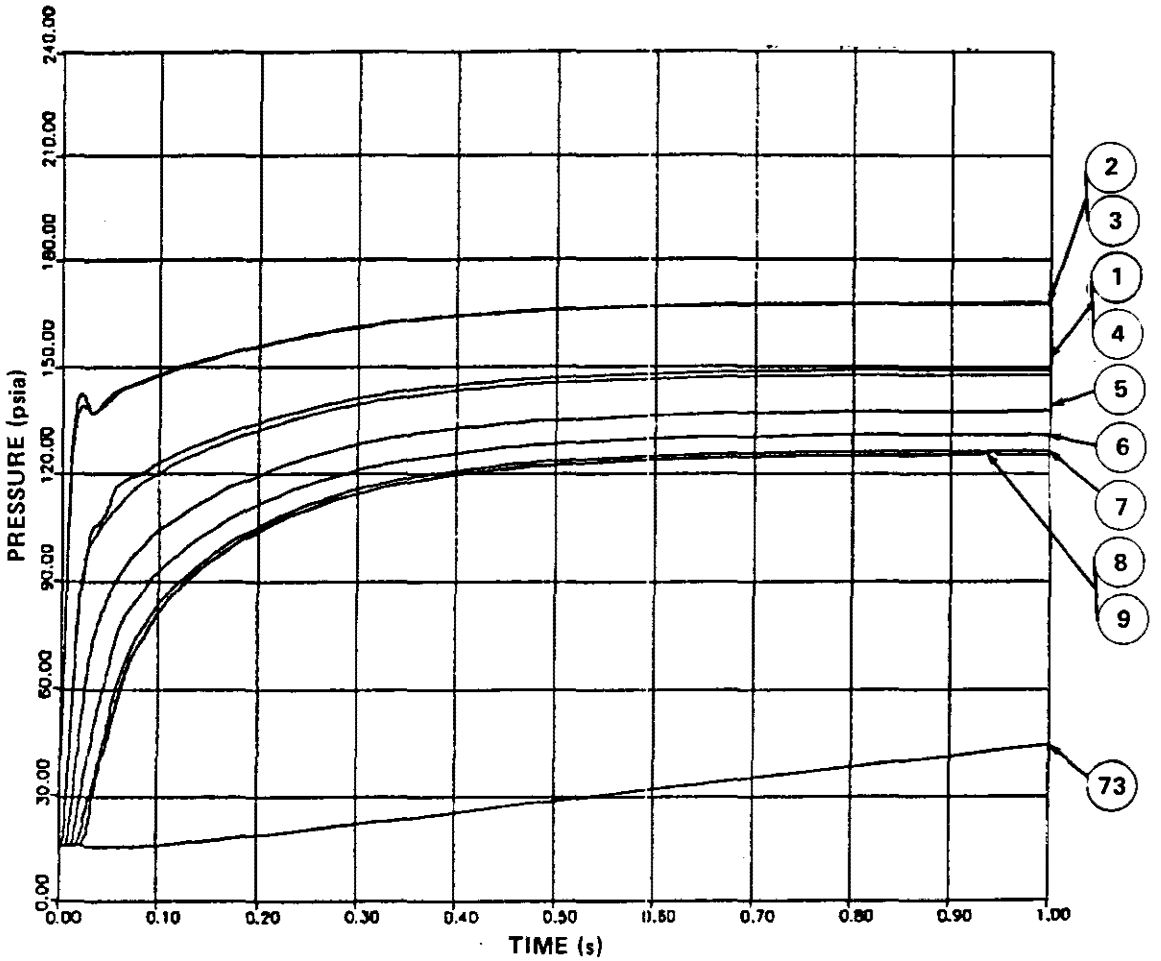

REVISION 0
APRIL 11, 1988

PUBLIC SERVICE ELECTRIC AND GAS COMPANY
HOPE CREEK NUCLEAR GENERATING STATION

PRESSURE TRANSIENT IN SHIELD ANNULUS FOR STRUCTURAL ANALYSIS CASE C

UPDATED FSAR

Sheet 1 of 8
FIGURE 6B-7

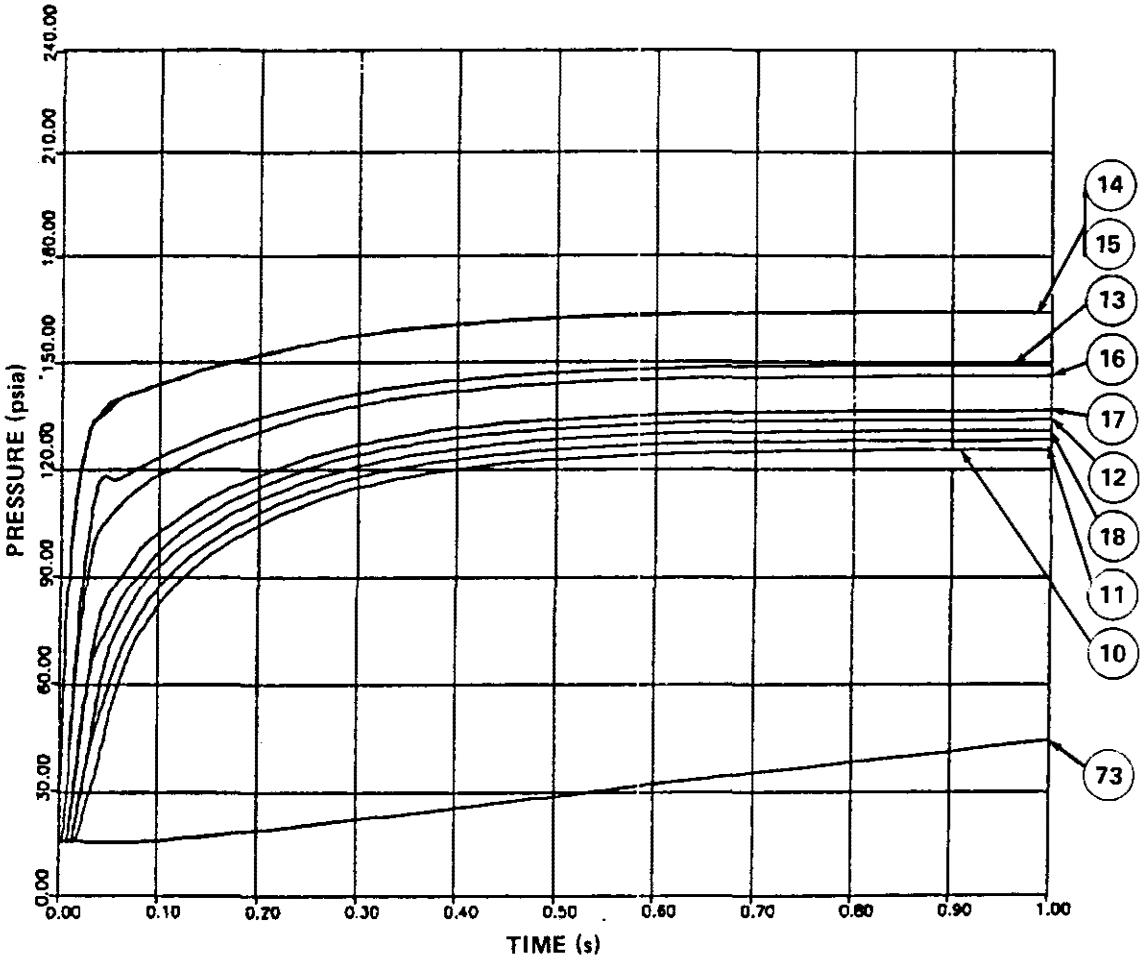

REVISION 0
APRIL 11, 1988

PUBLIC SERVICE ELECTRIC AND GAS COMPANY
HOPE CREEK NUCLEAR GENERATING STATION

PRESSURE TRANSIENT IN SHIELD ANNULUS FOR STRUCTURAL ANALYSIS CASE C

UPDATED FSAR

Sheet 2 of 8
FIGURE 6B-7

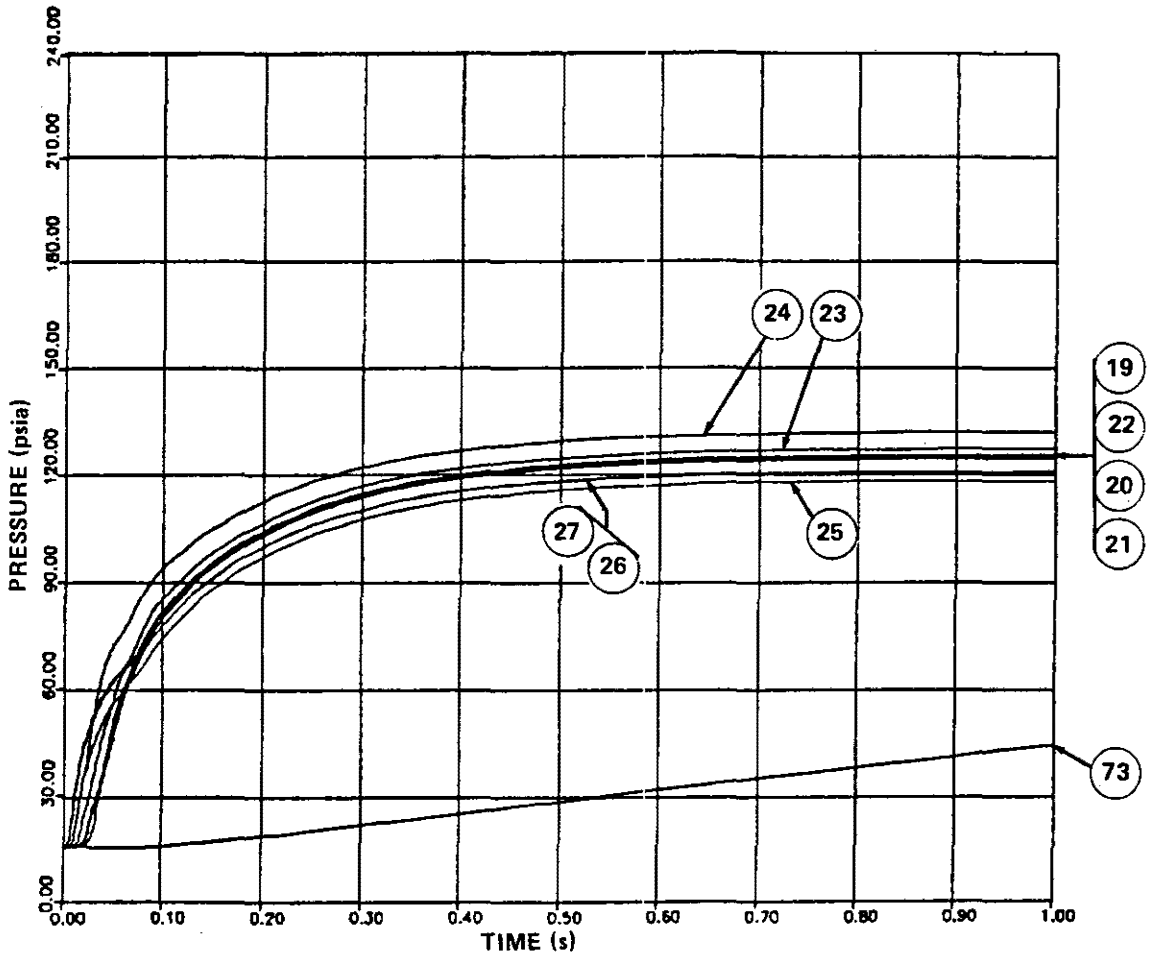

REVISION 0
APRIL 11, 1988

PUBLIC SERVICE ELECTRIC AND GAS COMPANY
HOPE CREEK NUCLEAR GENERATING STATION

PRESSURE TRANSIENT IN SHIELD ANNULUS FOR STRUCTURAL ANALYSIS CASE C

UPDATED FSAR

Sheet 3 of 8
FIGURE 6B-7

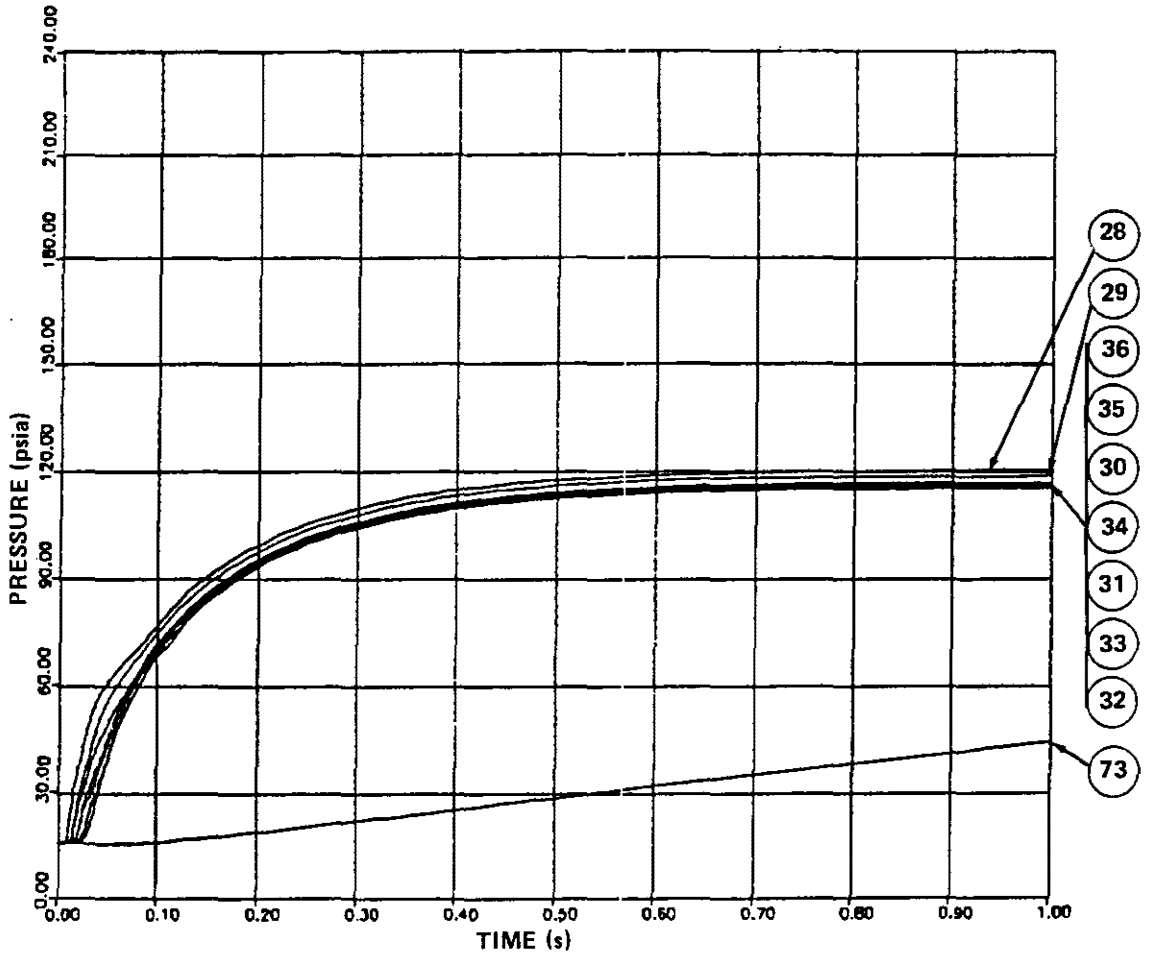

REVISION 0
APRIL 11, 1988

PUBLIC SERVICE ELECTRIC AND GAS COMPANY
HOPE CREEK NUCLEAR GENERATING STATION

PRESSURE TRANSIENT IN SHIELD ANNULUS FOR STRUCTURAL ANALYSIS CASE C

UPDATED FSAR

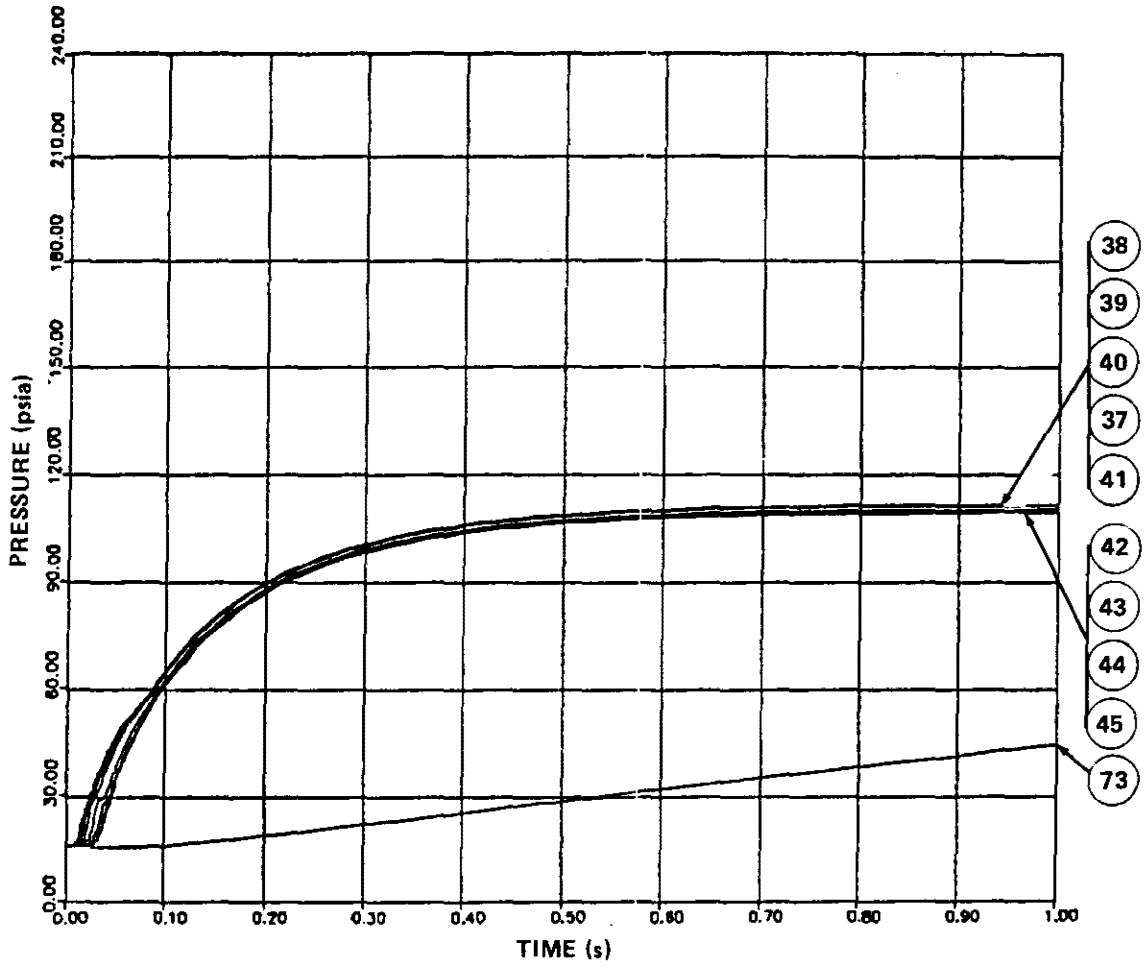

REVISION 0
APRIL 11, 1988

PUBLIC SERVICE ELECTRIC AND GAS COMPANY
HOPE CREEK NUCLEAR GENERATING STATION

PRESSURE TRANSIENT IN SHIELD ANNULUS FOR STRUCTURAL ANALYSIS CASE C

UPDATED FSAR

Sheet 5 of 8
FIGURE 6B-7

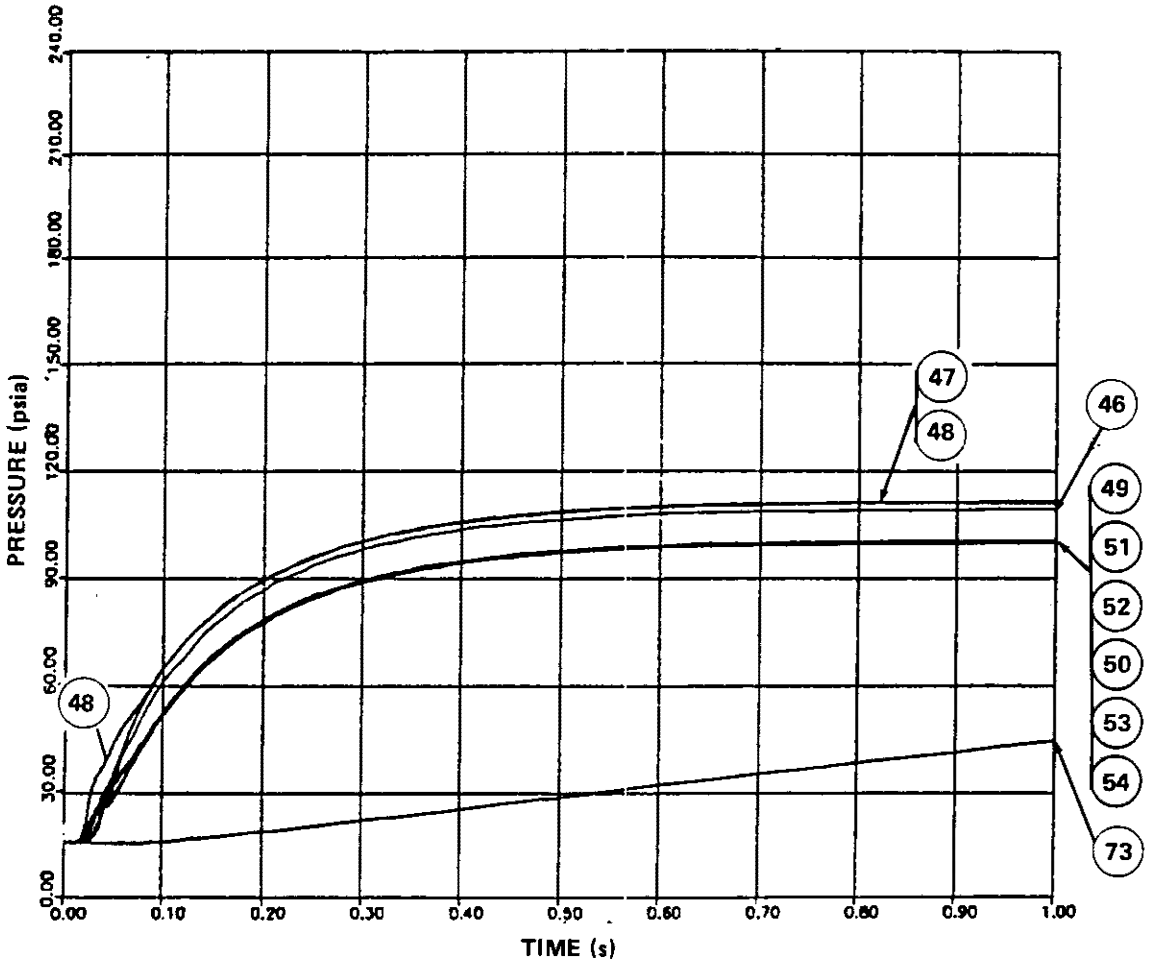

REVISION 0
APRIL 11, 1988

PUBLIC SERVICE ELECTRIC AND GAS COMPANY
HOPE CREEK NUCLEAR GENERATING STATION

PRESSURE TRANSIENT IN SHIELD ANNULUS FOR STRUCTURAL ANALYSIS CASE C

UPDATED FSAR

Sheet 6 of 8
FIGURE 6B-7

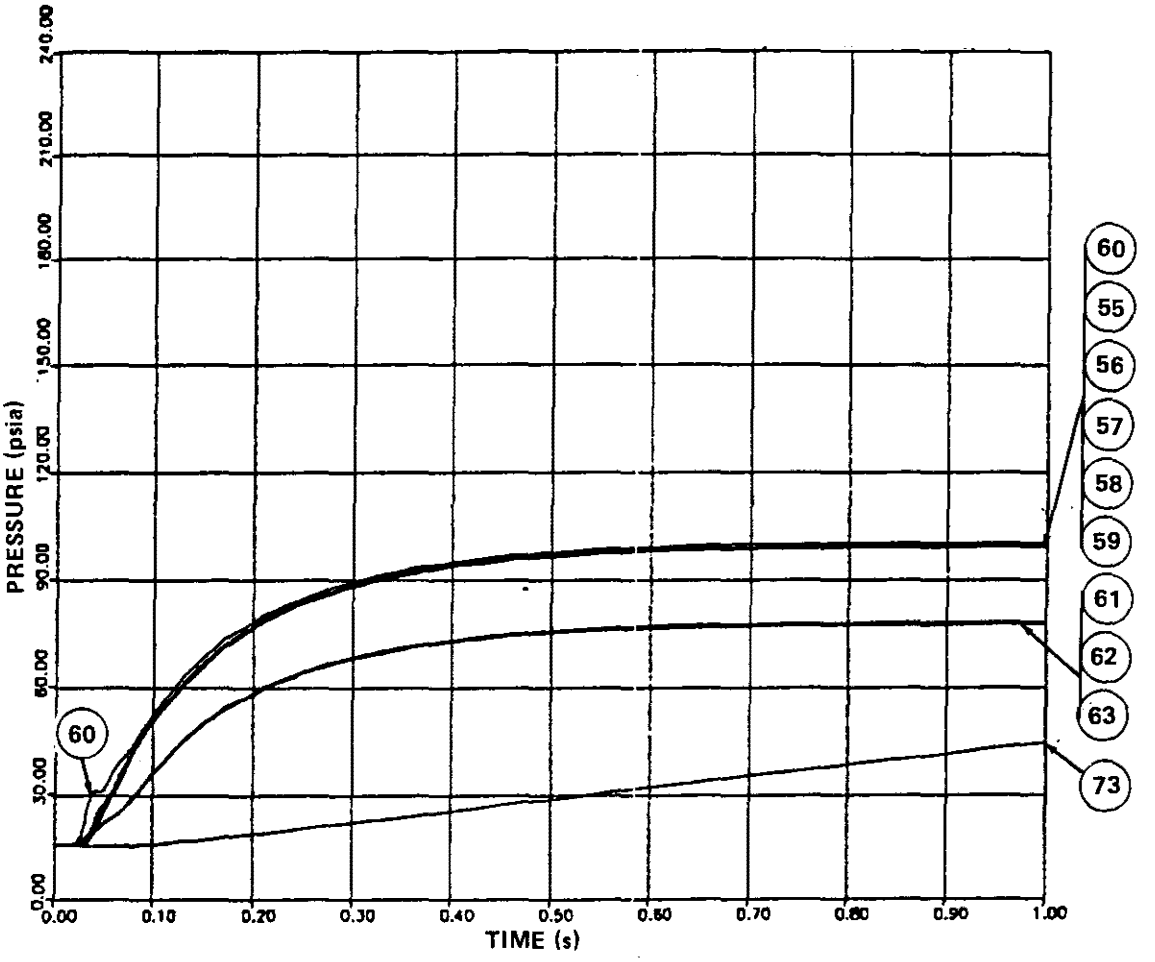

REVISION 0
APRIL 11, 1988

PUBLIC SERVICE ELECTRIC AND GAS COMPANY
HOPE CREEK NUCLEAR GENERATING STATION

PRESSURE TRANSIENT IN SHIELD ANNULUS FOR STRUCTURAL ANALYSIS CASE C

UPDATED FSAR

Sheet 7 of 8
FIGURE 6B-7

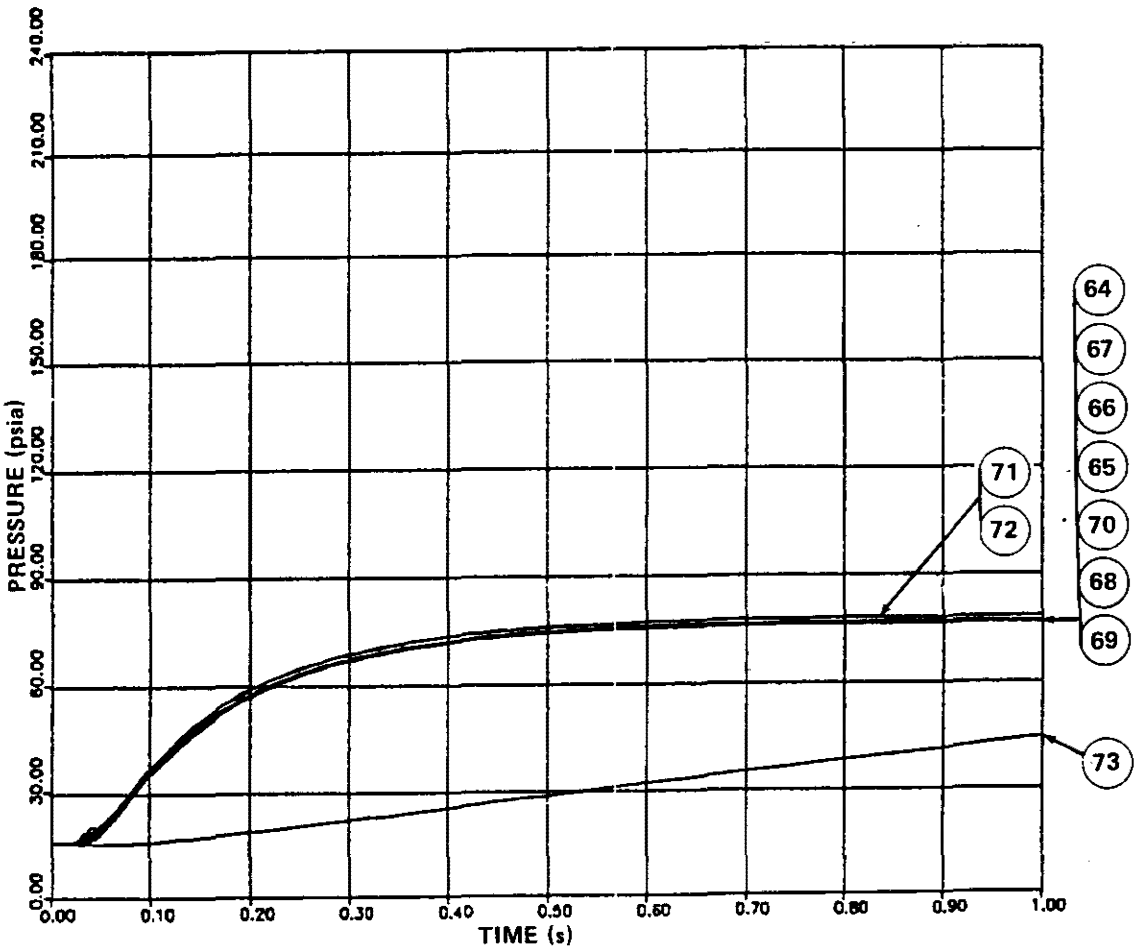

REVISION 0
APRIL 11, 1988

PUBLIC SERVICE ELECTRIC AND GAS COMPANY
HOPE CREEK NUCLEAR GENERATING STATION

PRESSURE TRANSIENT IN SHIELD ANNULUS FOR STRUCTURAL ANALYSIS CASE C

UPDATED FSAR

Sheet 8 of 8
FIGURE 6B-7

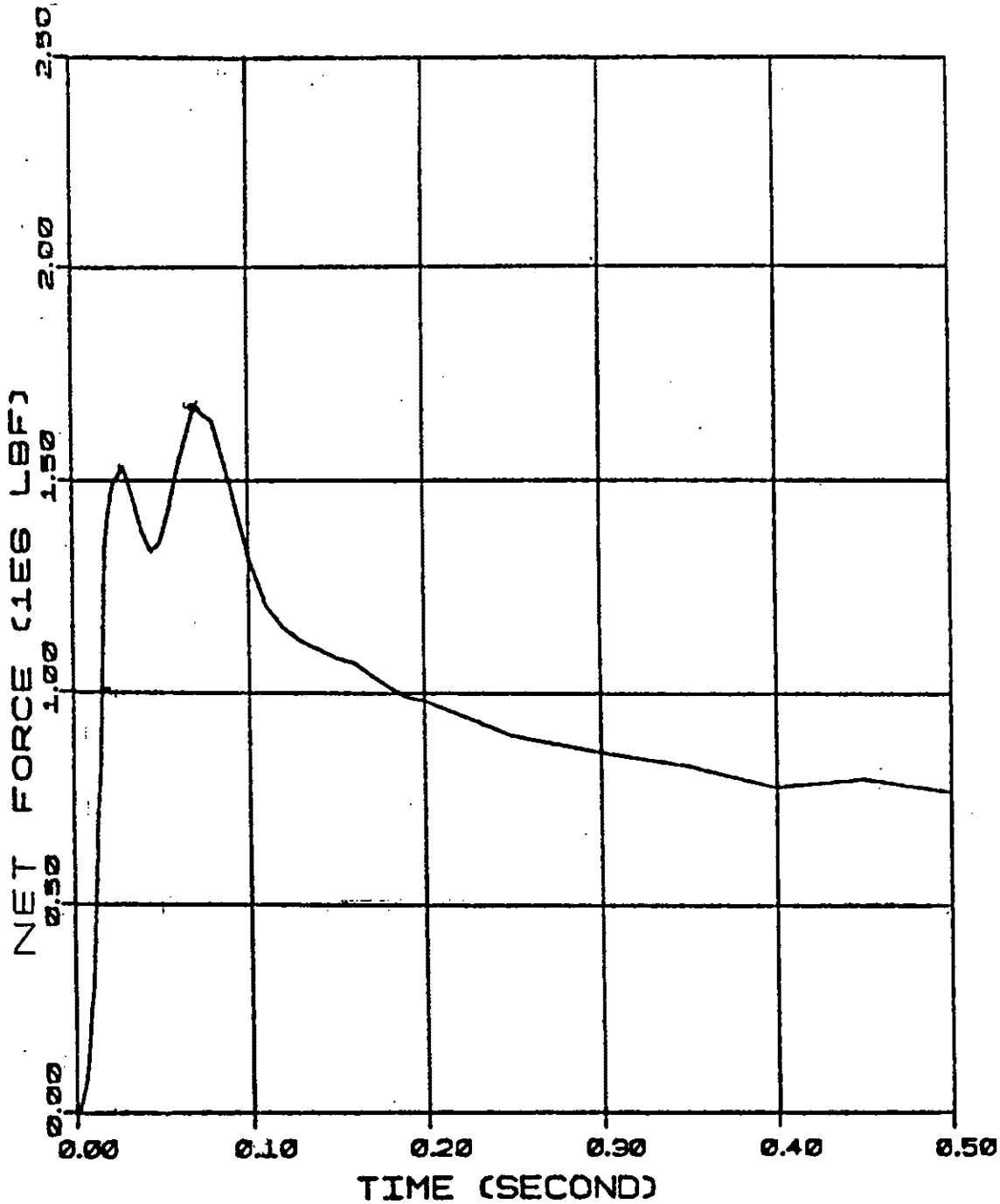

REVISION 0
APRIL 11, 1988

PUBLIC SERVICE ELECTRIC AND GAS COMPANY
HOPE CREEK NUCLEAR GENERATING STATION

FORCE TRANSIENT ON REACTOR PRESSURE VESSEL FOLLOWING A RECIRCULATION LINE BREAK AT THE NOZZLE SAFE END

UPDATED FSAR

FIGURE 6B-8

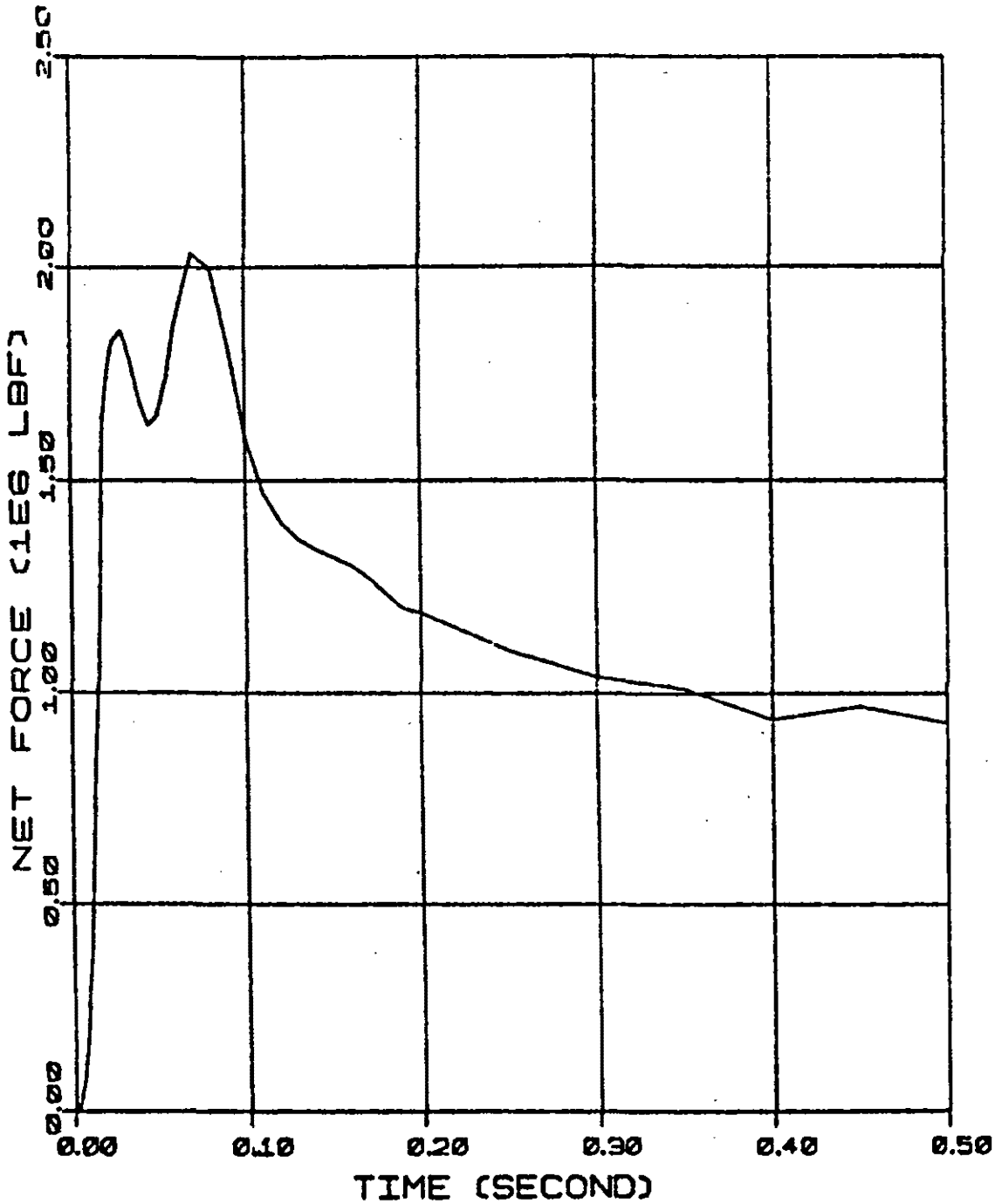

REVISION 0
APRIL 11, 1988

PUBLIC SERVICE ELECTRIC AND GAS COMPANY
HOPE CREEK NUCLEAR GENERATING STATION

FORCE TRANSIENT ON REACTOR SHIELD WALL FOLLOWING A RECIRCULATION LINE BREAK AT THE NOZZLE SAFE END

UPDATED FSAR

FIGURE 6B-9

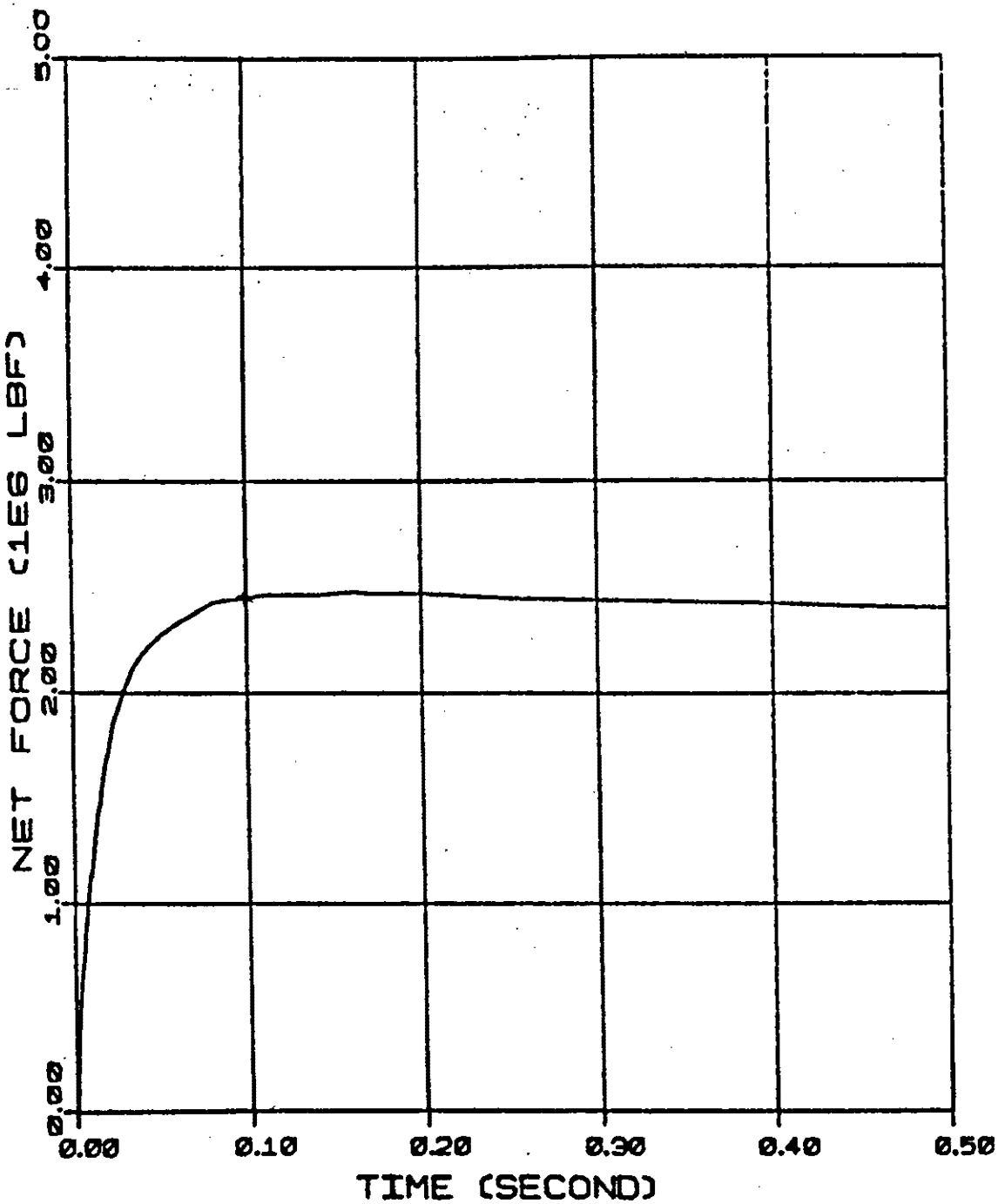

REVISION 0
APRIL 11, 1988

PUBLIC SERVICE ELECTRIC AND GAS COMPANY
HOPE CREEK NUCLEAR GENERATING STATION

FORCE TRANSIENT ON REACTOR PRESSURE VESSEL FOLLOWING A FEEDWATER LINE BREAK

UPDATED FSAR

FIGURE 6B-10

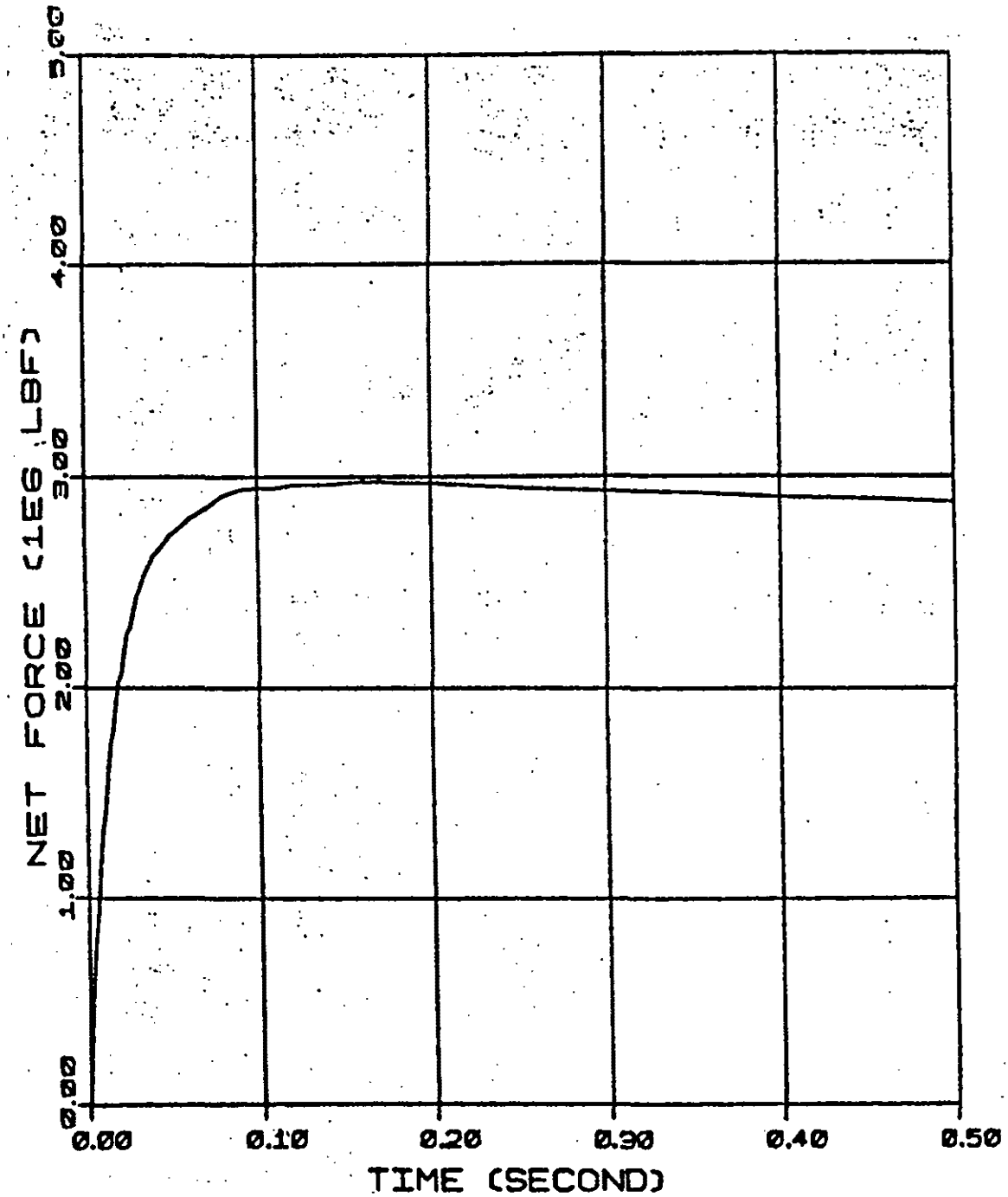

REVISION 0
APRIL 11, 1988

PUBLIC SERVICE ELECTRIC AND GAS COMPANY
HOPE CREEK NUCLEAR GENERATING STATION

FORCE TRANSIENT ON REACTOR SHIELD WALL FOLLOWING A FEEDWATER LINE BREAK

UPDATED FSAR

FIGURE 6B-11

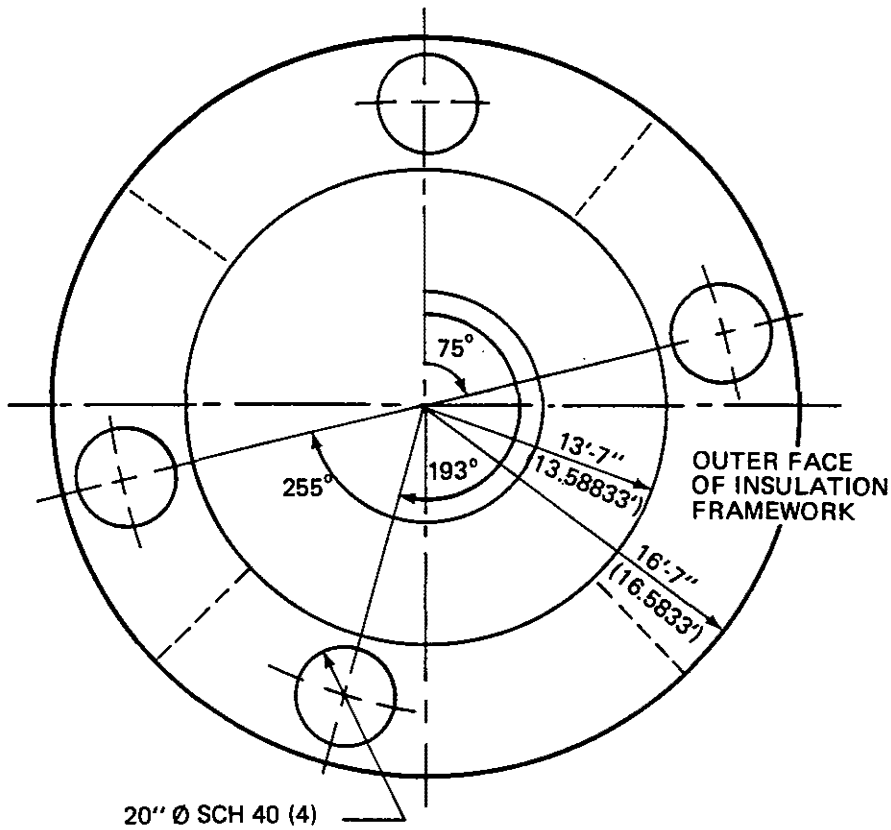

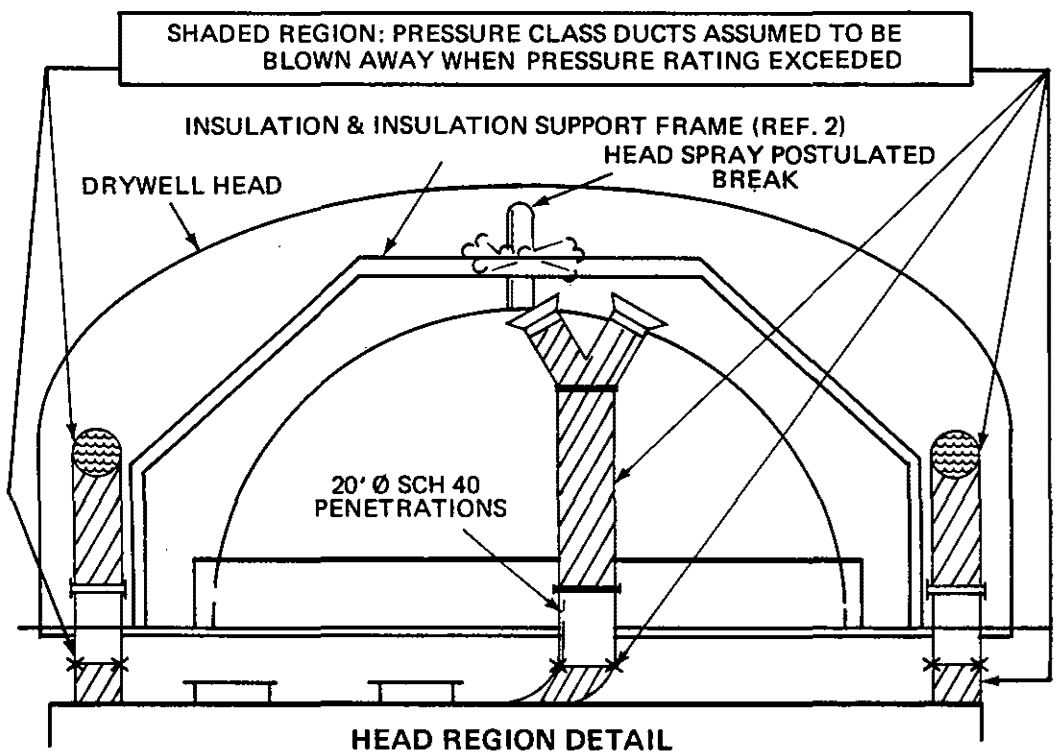

HEAD REGION DETAIL

REVISION 0
APRIL 11, 1988

PUBLIC SERVICE ELECTRIC AND GAS COMPANY
HOPE CREEK NUCLEAR GENERATING STATION

DRYWELL HEAD ARRANGEMENT

UPDATED FSAR

FIGURE 6B-12

THIS FIGURE HAS BEEN DELETED

PSEG NUCLEAR L.L.C.
HOPE CREEK GENERATING STATION

THIS FIGURE HAS BEEN DELETED

PSEG NUCLEAR L.L.C.
HOPE CREEK GENERATING STATION

APPENDIX 6C

STRUCTURAL DESIGN CRITERIA FOR SEISMIC CATEGORY I HVAC DUCTS AND DUCT SUPPORTS

Seismic Category I HVAC ducts are fabricated from sheet metal and/or plate steel. Stiffener plates are provided at 48-1/2 inch maximum spacing. Maximum allowable stiffener plate spacing is based on analysis and tests.

Seismic Category I HVAC duct supports are fabricated from rolled shapes and unistrut members. Transverse bracing is generally provided at every duct support. However, for several duct support types for duct perimeter 150 inches and less, transverse bracing is provided at every alternate duct support. Longitudinal bracing is provided at 32 foot maximum spacing. A minimum of one longitudinal brace is provided in every straight duct run. Duct supports in the control room are attached to a steel liner plate anchored to the concrete ceiling slab (expansion anchor bolts are not used). Expansion anchor bolts are not used to support HVAC equipment with rotating machinery (e.g., fans) attached to walls or ceilings except as follows:

1. Vane axial fans located in service water intake structure.

2. Unit heaters.

Since the above equipment are relatively light in weight, the expansion anchors supporting them provide very large factors of safety relative to the allowable design loads. Vibratory loads on the expansion anchors are insignificant relative to their design capacity.

Seismic analysis of Seismic Category I HVAC ducts and duct supports is performed using the response spectrum method. Damping values used are 2 percent of critical damping for the operating basis earthquake (OBE) and 4 percent of critical damping for the safe shutdown earthquake (SSE) for welded construction. For bolted construction the corresponding damping values are 4 percent and 7 percent in accordance with the NRC Regulatory Guide 1.61. Load combinations and allowable stresses for Seismic Category I HVAC ducts and duct supports are given in Tables 6C-1 and 6C-2, respectively.

TABLE 6C-1

LOAD COMBINATIONS FOR HVAC DUCTS

Loading Combination[1]	Allowable Sheet Corner Stress
D + P	0.6 Fy
D + P + E	0.75 Fy
D + P + E	0.9 Fy
D + P + W	0.9 Fy

(1) Symbols used in load combinations:

- D - Dead weight of duct
- P - Maximum operating pressure inside duct
- E - Operating basis earthquake load
- E_s - Safe shutdown earthquake load
- W_{tp} - Tornado differential pressure
- Fy - Minimum specified yield strength of duct material

TABLE 6C-2

LOAD COMBINATIONS FOR HVAC DUCT SUPPORTS

Load Case	Loading Combination(1)	Allowable Stress(2)(3)
1	D + L	F_s
2	D + E	F_s
3	D + E_s	1.5 F_s or 0.9 Fy whichever is smaller

(1) Symbols used in load combinations:

- D - Dead load including weight of duct, support frame, stiffeners, volume dampers, instrumentation, etc.
- L - Live load = 250 lbs applied to a one square foot area at points of maximum moment and shear (representative of a man walking or crawling on a duct).
- E - Operating basis earthquake load
- E_s - Safe shutdown earthquake load
- F_s - Allowable stress for support material governed by AISC or AISI as applicable
- Fy - Minimum specified yield strength of support material.

(2) Where expansion anchor bolts are used to attach duct supports to concrete structures, 33 percent increase in allowable design loads is permitted for load case 3, for expansion anchors.